PART I.

LOCAL CONVECTIVE THERMAL TRANSFER FROM SPHERICAL SURFACE

PART II.

TEMPERATURE GRADIENTS IN TURBULENT GAS STREAMS

MEASUREMENT OF TEMPERATURE, ENERGY AND PRESSURE GRADIENTS

PART III.

TEMPERATURE GRADIENTS IN TURBULENT GAS STREAMS

BEHAVIOR NEAR BOUNDARY IN TWO-DIMENSIONAL FLOW

Thesis by

Nan-Teh Hsu

In Partial Fulfillment of the Requirements

For the Degree of

Doctor of Philosophy

California Institute of Technology

Pasadena, California

1956

ACKNOWLEDGMENTS

In connection with the research work reported herein, I wish to express my sincere gratitude to Dr. B. H. Sage for his stimulating interest and general guidance throughout the entire program; to K. Sato for his constant cooperation in carrying out all the measurements; to H. H. Reamer for his many suggestions in the operation of the equipment; to W. M. DeWitt, L. T. Carmichael, G. A. Griffith and P. C. Kraft for their contributions in the construction of the equipment; to J. R. Bowden for his help in the taking of data and to H. E. Smith for his conscientious effort in the routine operation of the equipment.

Thanks are also due to Dr. W. H. Corcoran for his constructive criticism and to Evelyn Anderson, June Gray and Lawson Miller for their assistance in the preparation of this manuscript.

Further, I am grateful to the Fluor Corporation, Ltd. for its financial support through the Peter E. Fluor Fellowship awarded me from 1952-55, and to Dean W. N. Lacey for his valuable counsel during my study at the California Institute of Technology.

ABSTRACT

I.

The local convective thermal transfer from a spherical surface in an air stream was experimentally investigated by measuring the temperature distribution in the air stream surrounding the sphere. The investigation was carried out in an air stream of known turbulence level at bulk velocities of 8 and 16 feet per second using two different half-inch spheres. The local thermal flux over the spherical surface was calculated from the detailed measurements of temperature distribution in the air close to the surface. These results are compared with available experimental results obtained at higher velocities with larger spheres.

In the forward region of the sphere from the stagnation point up to an angle of about 80°, the experimental radial temperature distributions are correlated empirically in terms of the displacement thickness of the thermal boundary layer. Over this region the experimental and correlated results are compared in terms of the Nusselt and Reynolds numbers with the results of theoretical analyses based on the laminar boundary layer theory. There is satisfactory agreement with the theoretical results obtained by the method of Drake and the application of the solutions of Eckert.

The integrated values of thermal transfer are in agreement with the gross values obtained from simultaneous over-all measurements. There is also fair agreement between the integrated results and available published information on the gross thermal transfer from a sphere.

II.

A detailed knowledge of the distribution of temperature, thermal flux, and the pressure gradients associated with the turbulent flow of fluids is of importance in creating a background of experimental facts from which it is possible to predict the transfer characteristics for a particular physical situation.

Special methods and equipment employed in the measurement and control of temperature and thermal flux in an investigation of thermal transfer in turbulent gas streams are described. Measurements of the thermal flux and the pressure gradient are presented as a function of the imposed temperature distribution and macroscopic flow rate. They extend from gross velocities of 10 to 90 feet per second and to average temperature gradients as high as 1000° F. per foot.

The results represent a contribution to the knowledge of the shear and the thermal flux associated with the nonisothermal flow of air between parallel plates. As expected, the thermal transfer coefficients for nonuniform transfer are larger than those obtained in this work under conditions of uniform transfer.

III.

The region near the boundary of a turbulently flowing fluid accounts for the greater part of the resistance to thermal transfer to or from the stream. An understanding of the influence of conditions of flow upon the temperature distribution near the boundary of turbulently flowing streams is required in order to permit the recent advances in fluid mechanics to be applied to the prediction of thermal transfer in steady flow.

The detailed temperature distribution near the boundary of a turbulent air stream flowing between parallel plates was measured at gross velocities from 10 to 90 feet per second and for average temperature gradients as high as 1000° F. per foot. The corresponding value of thermal flux was determined directly, and from these primary measurements the temperature gradient and eddy conductivity were established as a function of flow conditions.

The eddy conductivity was correlated with the position in the stream and the gross conditions of flow. The measurements permit estimation of the thermal transfer to a turbulently flowing air stream in conduits of large radius to be made with accuracy adequate for some engineering purposes for a variety of uniform and nonuniform conditions of thermal transfer.

TABLE OF CONTENTS

PART I.

LOCAL CONVECTIVE THERMAL TRANSFER FROM SPHERICAL SURFACE

INTRODUCTION

The study of thermal transfer between a spherical surface and the fluid which is flowing over the sphere is of interest to many problems in chemical engineering. It is also of interest in connection with material transfer because in many instances the processes involved in these two types of transfer are considered to be analogous.

The prediction of thermal transfer from a spherical or blunt-nosed body is also important in the design of supersonic air vehicles. Information from incompressible flow can be modified and applied to the subsonic region around the blunt nose behind the detached shock wave.

Experimental measurement of gross thermal transfer at a spherical surface in a fluid stream over a wide range of flow conditions has been carried out by many investigators. However, most of such experimental work is concerned with the over-all thermal transfer from the entire surface; information regarding local conditions provides a more complete understanding of the processes involved in connection with thermal transfer from a sphere.

At present there is only limited experimental information available on the local thermal transfer for a sphere. Cary (3) reported experimental results of local thermal transfer from a 5-inch iron sphere in air at Reynolds numbers between 4.4×10^4 to 1.5×10^5. Lautman and Droege (16) measured the local thermal transfer from a 9-inch copper sphere in air in the Reynolds number range of 1.3×10^5 to 1×10^6.

Xenakis and coworkers (35) repeated the work of Lautman and Droege with the 9-inch sphere along with two other spheres 6 and 12 inches in diameter. In all these investigations hollow spheres were used, and the entire spherical surface with the exception of a small isolated plug was heated with steam. The isolated plug was made flush with the surface and was independently heated. The sphere was rotated so that the plug took up different angular positions around a great circle. The local rate of thermal transfer was then given by the energy required to maintain the plug at the same temperature as the steam-heated surface.

In the present study the rates of local thermal transfer for half-inch spheres in an air stream of known turbulence level were determined at Reynolds number from about 1500 to 4200. A method different from that mentioned above was used. A 0.0003-inch thermocouple was employed to measure the temperature distribution in the air stream around the sphere with special emphasis on the region close to the surface. The local thermal flux was calculated from the limiting radial temperature gradient at the surface and the thermal conductivity of the air. Two different spheres were used. One was a porous sphere with liquid evaporating from its surface and the other a silver sphere with an internal electric heater. When the porous sphere was used, heat was transferred from the air stream to the surface; in the case of the heated silver sphere heat transfer took place from the surface to the surrounding air. The total rate of evaporation from the porous sphere and the total energy input to the silver sphere were also measured so

that the over-all thermal transfer obtained by integrating the local thermal flux could be checked.

The present experimental investigation covers one phase of a long-range program of study on the effect of turbulence on thermal and material transfer of the Chemical Engineering Laboratory of the California Institute of Technology.

THEORETICAL CONSIDERATIONS

In general, theoretical treatments of local thermal transfer characteristic of immersed bodies are based on the solution of the Prandtl boundary layer equations using a variety of approximations. As applied to a sphere these equations are valid only for the region between the forward stagnation point and the point of separation of the boundary layer. The complex nature of the flow beyond the separation point has so far prevented satisfactory analysis concerning the velocity and temperature distributions in that region. Most of the available analytical solutions are for two-dimensional situations. Mathematical analyses dealing with a rotationally symmetric blunt-nosed body applicable to a sphere are relatively few; exact solutions are limited to a neighborhood of the stagnation point under special conditions. This experimental study was carried out at relatively low velocity corresponding to a Mach number of less than 0.1; the ratio of the surface temperature to the stream temperature ranged from 0.93 to 1.1, and the variation of surface temperature was about 2° F. over the front half of

the sphere. Recent calculations of Reshotko and Cohen (26) show that in the range of ratio of surface to stream temperature mentioned, the effect of compressibility of the fluid on thermal transfer is less than 1%. Under these conditions, the flow encountered in this investigation is comparable to constant-property, incompressible laminar flow. Therefore, available analyses applicable to a sphere under these specified conditions will be outlined and their solutions compared later with the experimental results of this study.

Sibulkin (31) presented an exact solution for the thermal transfer at the stagnation point of a sphere under the above-prescribed conditions. The pertinent boundary layer equations given in the coordinate system of Figure 1 are:

Continuity:

$$\frac{\partial(zu)}{\partial s} + \frac{\partial(zv)}{\partial n} = 0 \qquad (1)$$

Momentum:

$$u\frac{\partial u}{\partial s} + v\frac{\partial u}{\partial n} = u_1\frac{du_1}{ds} + \nu\frac{\partial^2 u}{\partial n^2} \qquad (2)$$

Energy:

$$u\frac{\partial t}{\partial s} + v\frac{\partial t}{\partial n} = K\frac{\partial^2 t}{\partial n^2} \qquad (3)$$

with the boundary conditions:

$$n = 0: \quad u = 0, \quad v = 0, \quad t = t_s .$$

$$n = \infty: \quad u = u_1, \quad t = t_\infty .$$

The velocity field is obtained by solving Equations 1 and 2, and the temperature field, from the velocity field and Equation 3. The local thermal flux is calculated from the normal temperature gradient and the thermal conductivity of the fluid as follows:

$$\dot{q} = -k_s \left(\frac{\partial t}{\partial n} \right)_{n=0} \tag{4}$$

In solving the equations, Sibulkin (31) used velocity distribution in the boundary layer given by Homann (10) together with a linear velocity profile along s.

Approximate solutions using the Karman-Pohlhausen integral method have been obtained for the thermal transfer of the stagnation point and the forward region of a sphere by several investigators. To simplify calculation the integral method does not attempt to satisfy the differential boundary layer equations for every particle of fluid, but instead it solves the momentum and energy integral equations by the judicious choice of plausible expressions for the velocity and temperature distributions in the flow and the thermal boundary layers. The momentum integral equation is obtained by equating the net exchange of momentum flux for an elemental length of the flow boundary layer to the forces

acting on the surface of the element, and the energy integral equation is similarly arrived at by writing the energy balance over the region included in an elemental length of the thermal boundary layer. This integral method was first devised by Karman (14) and applied by Pohlhausen (24) in the solution of flat-plate flow problems. Applicable to a sphere in steady incompressible laminar flow where the fluid properties are assumed constant the momentum integral equation (22) and the analogous energy equation are:

Momentum:

$$\frac{\partial}{\partial s}\int_0^{\delta} u^2 dn - u_1 \frac{\partial}{\partial s}\int_0^{\delta} u\,dn - \frac{1}{z}\frac{\partial z}{\partial s}\left(u_1\int_0^{\delta} u\,dn - \int_0^{\delta} u^2 dn\right) = \delta u_1 \frac{du_1}{ds} - \nu\left(\frac{\partial u}{\partial n}\right)_{n=0} \quad (5)$$

Energy:

$$\frac{\partial}{\partial s}\int_0^{\delta_t} u(t - t_\infty)\,dn + \frac{1}{z}\frac{\partial z}{\partial s}\int_0^{\delta_t} u(t - t_\infty)\,dn = -K\left(\frac{\partial t}{\partial n}\right)_{n=0} \quad (6)$$

where δ is the flow boundary layer thickness and δ_t the thermal boundary layer thickness. The expressions for the velocity and temperature distributions are usually assumed to be polynomials in $\frac{n}{\delta}$ and $\frac{n}{\delta_t}$ respectively:

$$\frac{u}{u_1} = \varphi_1\left(\frac{n}{\delta}\right) \quad (7)$$

and

$$\frac{t - t_\infty}{t_s - t_\infty} = \theta = \varphi_2\left(\frac{n}{\delta_t}\right) \tag{8}$$

The coefficients of the functions φ_1 and φ_2 are fixed by the appropriate boundary conditions. The knowledge of the velocity profile along s is required to solve for δ as a function of s from Equations 5 and 7. An expression for the ratio of $\frac{\delta}{\delta_t}$ involving u_1 and the Prandtl number defined as $\frac{\nu}{K}$ is obtained from Equations 5 and 8. After δ_t as a function of s is evaluated the local thermal flux is calculated from the derivative of the function φ_2 at $n = o$ and the temperature difference $t_s - t_\infty$ by the following expression:

$$\mathring{q} = -k_s\left(\frac{\partial t}{\partial n}\right)_{n=o} = -k_s \frac{t_s - t_\infty}{\delta_t} \varphi_2'(o) \tag{9}$$

Korobkin (15) reported results from his unpublished work in which he computed the local thermal transfer at the stagnation point by the integral method using Tomotika's distribution (34) for both the velocity and temperature distribution in the boundary layer. The Tomotika expression is a quartic form with coefficients depending on the velocity gradient along s. Korobkin (15) also presented results from unpublished work of Sibulkin who calculated the local thermal transfer over the front half of a sphere by the integral method using parabolic expressions for both the velocity and temperature distribution in the boundary layer.

Another approximate method for calculating thermal transfer over the surface of a rotationally symmetric body is comprised of the work of Eckert (8) and that of Drake (7). Eckert (8) obtained an exact solution for the energy equation of incompressible laminar boundary layer flow over a wedge-shaped body of variable vertex angle and applied the results to the forward region of a cylinder by assuming that each point on the surface of the cylinder could be replaced by an equivalent wedge which had equal stream velocity and thermal boundary layer thickness as well as identical velocity gradient in the stream and thermal boundary layer thickness gradient along the direction of flow over the surface. An approximate expression for the exact solution was given. Drake (7) applied the Mangler transformations (18) to the energy equation and obtained relations enabling the use of Eckert's two-dimensional solutions for a rotationally symmetric body. Korobkin (15) reported such results for the forward region of a sphere.

The parameter $\frac{\eta u}{\sqrt{Re}}$ is generally used in comparing results of thermal transfer because solutions based on the laminar boundary layer theory for thermal transfer in a given fluid medium can be expressed in the form:

$$\eta u = C_1 (Re)^{\frac{1}{2}} \tag{10}$$

For example, the thermal flux given by the analysis of Sibulkin (31) is

$$\dot{q} = k_s \, g(Pr) \, (t_s - t_\infty) \left(\frac{\beta}{\nu}\right)^{\frac{1}{2}} \tag{11}$$

where β is the velocity gradient $\frac{du_i}{ds}$, and $g(Pr)$ a function depending on the Prandtl number. As the definition of Nusselt number is

$$Nu = \frac{h D}{k_s} \tag{12}$$

where the thermal transfer coefficient is given by the relationship:

$$h = \frac{\dot{q}}{t_s - t_\infty} \tag{13}$$

the combination of Equations 11, 12 and 13 gives

$$Nu = g(Pr) \left(\frac{\beta D}{\nu}\right)^{\frac{1}{2}} \tag{14}$$

According to the potential theory, $\beta = \frac{3U}{D}$ for a sphere. Then Equation 14 becomes

$$Nu = C_2 \, g(Pr) \left(\frac{D U}{\nu}\right)^{\frac{1}{2}} = C_2 \, g(Pr) \left(Re\right)^{\frac{1}{2}} \tag{15}$$

as the Reynolds number Re is defined by

$$Re = \frac{D U}{\nu_s} \tag{16}$$

For constant-property analysis there is no question as to the value of ν_s ; for situations where the surface temperature is different from the stream temperature, the kinematic viscosity is evaluated at the surface temperature to be consistent with the use of thermal conductivity at the surface temperature in the definition of the Nusselt number. The function $g(Pr)$ in Equation 15 can usually be approximated by an expression in the form $C_3(Pr)^m$ over a limited range of Prandtl number. Then Equation 15 becomes

$$\eta u = C_4(Pr)^m(Re)^{\frac{1}{2}} \tag{17}$$

For a given fluid, the Prandtl number is constant over a moderate range of temperature; therefore Equation 17 is identical with Equation 10 where C_1 depends on $\frac{du_1}{ds}$ and the Prandtl number.

The analyses considered so far have been for flow over a surface with zero normal velocity as given by the boundary condition of $v = 0$ at $n = 0$. For the porous sphere used in this investigation there is a small normal velocity at the surface due to evaporation. The effect of the normal velocity at the surface on the velocity and temperature distribution in the boundary layer can be taken into account by specifying the boundary condition at $v = v_s$, at $n = 0$ in solving the boundary layer equations. Exact solutions for two-dimensional flow over a flat plate with the new boundary condition have been obtained by Schlichting and Bussmann (30) for both positive and negative values of v_s .

Mickley and his coworkers (21), by using similarity considerations, extended these solutions for the prediction of thermal and material transfer. Spalding (32) solved similar equations for material transfer at the stagnation point of a sphere by the integral method. At the evaporation rates encountered in this study using the porous sphere, the normal velocity at the surface amounted to about 0.005 foot per second compared to a stream velocity of 8 feet per second and the concentration of n-heptane at the surface was 0.05 mole fraction. Under these conditions, estimates based on the results of the above analyses showed that when the porous sphere was used in this investigation the effect of material transfer on the temperature gradient, hence the thermal transfer, was negligible.

EQUIPMENT AND MATERIALS

The measurements of the temperature distribution in the air around the sphere were carried out with the spheres supported one at a time over an air stream emerging from a rectangular jet. The arrangements of the air supply, the porous and silver spheres, and the thermocouple probe will be described.

A. Air Supply

Figure 2 shows schematically the arrangement of air supply to the jet. The same arrangement was used in an earlier study on the evaporation of drops (11). The primary object was to obtain a uniform velocity and temperature at the opening of the jet where the sphere was located.

Outside air brought in by a centrifugal blower A passed through the venturi meter C and a series of sections of square ducting and elbows on to the converging section H which formed the jet. The square duct measured 12 x 12 inches and the jet opening, 3 x 12 inches. All the sections were constructed from steel and joined by flanges with neoprene gaskets. The air was heated to the desired temperature by heaters B, E, F and G. Energy to the control heater G was supplied by a thyratron unit which was regulated by a sensing resistance thermometer through a Wheatstone bridge; light reflected from the mirror of the bridge galvanometer and directed at a photoelectric cell controlled the thyratron output. Details of this temperature control system have been described by Corcoran and his coworkers (4). The walls of the sections were insulated with magnesia from point E on to the end of the jet. Heaters K, L, M and N located underneath the insulations kept the walls essentially at air-stream temperature. The venturi air temperature was measured at D. Wall temperatures were measured with 40-gage copper-constantan thermocouples at five different cross sections. Heater unit F which consisted of five individual heaters strung across the channel supplied a variable amount of heat to different portions of the air stream to give a more uniform temperature at the jet opening. Two 0.003-inch copper-constantan thermocouples located across the jet opening measured the air temperature.

A steel plate 3/16 inch thick with 7/8 inch holes was inserted at I between the converging section and the straight section J of the

jet. The purpose of this grid was to provide a known turbulence level for the air stream at the cross section where the temperature measurement was made. Information on the changes of turbulence level with grid size and downstream distance was obtained from a study by Davis (5). With the 7/8-inch grid a range of turbulence levels could be obtained by using different lengths of straight sections (28). The present study was made at an essentially constant turbulence level of about 5.4%.

B. Porous Sphere

The half-inch porous sphere was made from processed diatomaceous earth commercially identified as "Allen filter material" which was obtained through the courtesy of the Union Oil Company. A 3/16-inch glass tubing which tapered down to a 0.030-inch capillary provided the feed-tube for the liquid and the support for the sphere as shown in Figure 3. The glass feed-tube was connected to a copper feed line which passed through an air-foil section to the injector. The air-foil section was attached to a traversing mechanism so the porous sphere could be moved into the desired position in the air stream. The capillary end of the glass tube was fitted in a hole drilled into the center of the sphere; a thin film of sodium silicate solution was used to cement the porous sphere to the glass capillary. The temperature at the center and at a point in the tube 3/4 inch from the center of the sphere was measured with small copper-constantan thermocouples connected as shown in one part of Figure 3. The 0.002-inch bare constantan wire common to

both junctions, together with the two 0.003-inch insulated copper wires were brought out of the feed line through a neoprene seal. The common reference junction kept at melting-ice temperature was formed by an extension of the constantan wire and a third copper wire.

A glass capillary U-tube manometer with one end open to the atmosphere was attached to the feed-tube at a point about 4 inches from the center of the sphere. The liquid level in the manometer served to indicate the attainment and maintenance of a steady condition of liquid feed rate.

Liquid to the sphere was fed by an injector. The plunger of the injector was driven through a series of reduction gears by a direct current motor. The speed of the motor, hence the injection rate, was controlled by a strobo-synchronizing system schematically shown in Figure 4. This system has been described in detail by Reamer and Sage (25). It included: (a) a quartz oscillator as the time standard, (b) a predetermined counter which produced a pulse at the desired time interval to be synchronized by the rotation of the shaft that worked the plunger in the injector, (c) a photoelectric cell which received light from an incandescent source through a spiral disk mounted on the rotating shaft, so the output of the photoelectric cell depended on the angular position of the shaft, (d) an electronic switch which transmitted the output from the photoelectric cell to a voltage amplifier only at the instant when the pulse arrived from the counter; furthermore, this output was maintained until the arrival of the next pulse,

and (e) a thyratron modulating circuit one half of which was actuated by the output of the voltage amplifier connected with the electronic switch and the other half by manual control; this circuit supplied power to the armature of the direct current motor whose shunt field was provided by a steady 110-volt direct current source. During operation, when the rotation of the shaft and the counter pulse were synchronized, the output to the photoelectric cell remained constant and there was no change in the power to the motor. When the speed of rotation became out of phase with the counter pulse, the position of the disk at the time of the pulse caused a change in the amount of light transmitted to the photoelectric cell thereby affecting its output in such a manner as to bring the rotation speed back in synchronization with the pulse. This control was effective over a range such that the rotation might lead or lag the pulse by as much as 30°; within this range, the change in output of the photoelectric cell with respect to the angular position of the disk was linear. The manual control of the thyratron circuit helped to bring the motor speed within the control range. The possibility of having the speed of the motor controlled at some multiple of the desired speed was eliminated by comparing the frequency of the light signals from the counter with that of the light flashes operated by a contact on the rotating shaft.

The injector was immersed in a constant-temperature bath. To prevent temperature fluctuations in the liquid, the feed line from the injector was jacketed up to the feed-tube, and oil from the constant-

temperature bath was circulated through the jacket. The jacket was in turn insulated with asbestos coverings. Fluctuations in the liquid temperature would cause the level in the capillary manometer to give a false indication of too fast or too slow a rate of evaporation due to the expansion or contraction of the liquid.

The liquid used was research-grade n-heptane obtained from the Phillips Petroleum Co. Its purity was given as 99.99 mole %. Before use, the n-heptane was allowed to stand in contact with sodium ribbons for a period of about a week. The specific weight of the dried n-heptane was found to be 42.429 pounds per cubic foot at 77° F. and its index of refraction relative to the D-lines of sodium was 1.3877 at 68° F. Rossini (27) reported respective values of 42.417 pounds per cubic foot at 77° F. and 1.3864 at 68° F.

The n-heptane was deaerated under vacuum and redistilled twice in a glass system before it was loaded into the evacuated injector. The feed line and the porous sphere were similarly filled with the liquid. The porous sphere was immersed in a beaker of n-heptane when it was not in use.

C. Silver Sphere

The half-inch silver sphere consisted of an outer silver shell D 0.016-inch thick and an inner copper sphere E as shown in Figure 5. This same sphere was used in an earlier study (1). A heater of silk-insulated chromel wire was wound in a spiral groove K on the copper sphere. This core was then covered by soft-soldering together two

silver hemispherical shells each of which was provided with a 0.096-inch stainless steel tube B at point C. A steel wire A passing through the inner sphere was used as the horizontal support for the whole assembly. The ends of the wire were anchored on two supporting blocks located outside the jet opening. Slight tension was applied to the wire through retaining nuts to keep the sphere in place. Leads for four copper-constantan thermocouples and the heater circuit were brought out through the steel tube at each end. The four thermocouple junctions on the inside surface were located on one half of a great circle at F, G, H and J with azimuth angles of -45, 0, $22\frac{1}{2}$ and $67\frac{1}{2}^{o}$ from the lead point so that when the sphere was rotated about the horizontal support through ball bearings, the thermocouple junctions traversed along four circles of different diameters perpendicular to the support. At the ends of the tube two disks graduated in degrees indicated the angular position of the sphere. Two small guard heaters wound around the tube about $\frac{1}{4}$ inch from the surface compensated for the conduction loss along the supporting tube.

The internal heater was supplied by a 6-12 volt direct current source while the external guard heaters were supplied individually by a variac with a 6.3 volt alternating current source from a filament transformer.

D. Thermocouple Probe

A differential thermocouple consisting of platinum and platinum-rhodium wires was used in measuring the temperature distribution in the

air stream surrounding the sphere. The platinum-rhodium alloy contained 10% rhodium. The measuring junction was made by carefully fusing 0.0003-inch wires of platinum and platinum-rhodium while the reference junction was constructed by silver-soldering together 0.010-inch platinum and platinum-rhodium wires. The two junctions were put together and supported on a probe as shown in Figure 6. The tips of the two electrically insulated stainless steel needles provided rigid supports for the 0.010-inch wires; the platinum lead was soldered on one tip and the platinum-rhodium wire of the reference junction, on the other. The 0.0003-inch wires of the measuring junction were then soft-soldered on the respective heavier wires. The needle tips were one inch apart and the reference junction was located about one inch behind the measuring junction, so the tips of the needles and the reference junction were all in the region at free stream temperature during measurements around the sphere. The two platinum leads were brought to a constant-temperature junction box, and copper leads were used between the junction box and the potentiometer. The needles were so imbedded in the bakelite fork that a slight tension could be applied to the fine wire by adjusting small screws on one arm of the bakelite fork. It was important to keep the fine wire taut in the air stream to allow an accurate positioning of the junction and to prevent the delicate wire from vibrating and breaking.

The probe assembly was attached to a traversing unit which was made up of a jeweller's milling head mounted on a slide rest. Precision

dial gages with 0.001-inch divisions were incorporated in this unit to measure the vertical and horizontal distances. This arrangement permitted the thermocouple to be traversed along any of the three directions in the cartesian coordinate system given in Figure 1.

Figure 7 is a photograph showing the thermocouple probe with the silver sphere over the air stream and the porous sphere immersed in n-heptane in the foreground.

MEASUREMENTS

A. Flow Conditions

The present study included four tests using the porous and silve spheres at bulk air velocities of 8 and 16 feet per second corresponding to Reynolds numbers of about 1500 to 4200. The experimental flow conditions are summarized in Table I. The bulk velocity of the air stream was calculated from venturi measurements of the weight rates of flow and the dimensions of the jet opening. The turbulence level of the air stream, defined as the ratio of the root-mean-square value of velocity fluctuation to the bulk velocity, was obtained from information on grid size, downstream distance from the grid, and the bulk air velocity (5,28). All four tests were conducted at essentially one constant level of turbulence using a 12-inch straight section over the grid; the actual values of turbulence level were at 5.2 to 5.6%. This variation was due to the difference in the bulk air velocity. The free stream temperature was controlled at 100° F. The uncertainty in the

velocity measurement was not more than 0.5% and the air temperature was known to $\pm$ 0.2° F.

B. Temperature Distribution

The reference coordinate system used in this study is given in Figure 1. The origin of the cartesian coordinates was taken to be at the center of the sphere. The X-coordinate was along the direction of flow of the main air stream and the Y- and Z-coordinates were along the width and the length of the jet opening, respectively. Horizontal and vertical temperature traverses were made in one half of the X-Z or Y = 0 plane. The locations of these traverses are indicated in Figure 8. The top vertical traverse was not made for the porous sphere because of the location of the feed-tube.

In order to orient the thermocouple junction with respect to the sphere two preliminary horizontal traverses were made. The first was made along the Y-direction near the equator (X = 0), and the other along the Z-direction at Y = 0 near the south pole (X = -.250 inch). These traverses were made close enough to the surface, usually about 0.005 inch from it, so that a plot of thermocouple readings versus traverse distance would indicate a definite peak denoting the center line of the sphere in that direction. These "peaks" could usually be determined within 0.001 inch.

After establishing the points Y = 0 and Z = 0, the regular traverses were made beginning with the vertical traverse at the south pole. Every traverse was started from a point at which free stream temperature was indicated and then the thermocouple junction was moved toward the surface

at small enough intervals to give a well-defined temperature distribution. Usually, intervals of 0.005 to 0.025 inch were used in regions where the temperature gradient was gentle and intervals of 0.002 or 0.001 inch were taken in regions having steep temperature gradients as the surface was approached. The locations of the surface were taken to be the points at which no further change in thermocouple reading was observed with a small change in traverse distance. These points could be located within half a division (0.0005 inch) on the dial gage. A measure of the accuracy of this method for the determination of the surface points was given by fitting a half-inch circle drawn to scale on a plot through these experimental surface points. In each of the four tests of this study, the largest deviation from the theoretical circle was not more than 0.002 inch.

Calibration of the platinum and platinum-rhodium thermocouple was obtained by constructing a similar thermocouple with wires from the original spools of materials and comparing it against a platinum resistance thermometer at four points in the temperature range of 70 to 220° F.; the 0.0003-inch junction was placed close to the resistance thermometer in an agitated oil bath and the 0.010-inch junction was kept at melting-ice temperature. A quadratic equation was fitted to the experimental points by the least squares method. The standard deviation between the experimental points and the calibration curve was 0.13° F. As the calibration was made with the reference junction at 32° F. and the traverses taken with the reference junction at 100° F., the slopes of the calibration

equation at the temperature level involved were used in converting the traverse thermocouple readings to temperature. The measuring junction was at temperature lower than 100° F. when used with the porous sphere and at temperature higher than 100° F. in the case of the heated sphere. Uncertainty associated with these experimental temperatureswas not more than 0.5° F.

C. Porous Sphere

After the desired flow conditions had been established, the injection of liquid to the porous sphere was started. The porous sphere was then raised from the beaker of n-heptane in which it had been immersed, and was maneuvered into position over the air stream. The steady evaporation rate was determined by adjusting the speed of the injector motor until a constant level was maintained in the capillary manometer. The liquid level in the manometer was observed through a telescope mounted on a cathetometer. It was found that the indication was most sensitive with the constant level at a height of one-half to one inch below the sphere, although the same result was obtained when the height of the constant level was varied over the range of three inches above to two inches below the sphere. The evaporation rate could usually be established within one-half hour, but a period of 6-10 hours was required to complete all the temperature traverses for a given set of flow conditions. During the traverses the porous sphere was rinsed from time to time with fresh n-heptane to keep any adsorbed material or impurity from concentrating on the surface liquid film.

At the end of the run, the porous sphere was re-immersed in n-heptane before the injector motor was stopped.

The injector bath was kept at 115° F. The over-all weight rate of evaporation was calculated from the volumetric rate and the specific weight of n-heptane at the injector temperature. The volumetric rate was established from the preset counter reading, the reduction gear ratio, and the dimensions of the injector. The principal source of uncertainty in the determination of evaporation rate was the fluctuation in the liquid temperature. The values of evaporation rate are believed to have a probable error of 0.5%.

The temperature at the center of the sphere and at a point in the feed-tube 3/4 inch from the center were measured so that the amount of heat conducted through the tube could be estimated.

D. Silver Sphere

In the tests using the heated sphere, the total energy input and the surface temperature were measured in addition to the temperature distribution in the surrounding air. The accuracy of the energy input measurement depended largely on how exactly the conduction loss along the stainless steel tube could be compensated. The two guard heaters were individually controlled, and the voltages applied were determined by having the four thermocouples on the inside surface lined up in the horizontal X = 0 plane and then regulating the input to the external heaters until the four thermocouples readings were nearly equal. From axial symmetry with respect to the air flow, the four thermocouples

should give the same reading in these positions; in the two tests a temperature difference of 0.4 to 0.5° F. between the highest and lowest readings was observed. The total energy input to the internal heater of the sphere was determined by measuring the electrical potentials across the heater and a series resistor of accurately known resistance. Due to conduction through the leads for the heater and the thermocouples, the probable error associated with the values of energy input may be as high as 2%. The local surface temperature was given by the four thermocouples when the sphere was rotated about its horizontal support at 30° intervals as indicated by the graduated disks.

TREATMENT OF DATA AND RESULTS

A. Temperature Distribution

The measured temperature given by the thermocouple readings indicated that a steep temperature gradient existed along the length of the thermocouple amounting to a maximum value of about 5×10^3 °F. per foot for the porous sphere and 8×10^3 °F. per foot in an opposite direction for the heated sphere. The temperature at the thermocouple junction was either the lowest or the highest depending on whether the porous or the silver sphere was involved, and a temperature difference existed between the junction and the air surrounding it so that the heat conducted along the wire was balanced by the heat exchange between the junction and the air. Consequently, all the thermocouple temperature

were corrected to give the true air temperature. The correction was based on a heat balance as mentioned above over an elemental length of the thermocouple. The relationship between the true air temperature and the measured temperature is given by the following differential equation:

$$t_a - t_w = - \frac{D\,k}{4\,h} \frac{\partial^2 t_w}{\partial Y^2} \qquad (18)$$

Due to the complex variation of the heat transfer coefficient h with Y and the difficulty in expressing the temperature distribution mathematically, a simple analytical solution for Equation 18 was not possible. However, an electric analog computer consisting of a network of variable resistances was set up to give an approximate solution. The details of the electric analog method as applied to this particular problem have been described by Sato (28) and Meldau (20).

The largest correction was about 2° F. for points close to the surface of the sphere. The biggest uncertainty in the analog solution was due to the point values of the heat transfer coefficient which were estimated from calculated velocity distributions. It is believed that the corrected temperature is within 1° F. of the true air temperature. A complete list of the experimental and corrected temperatures for the four tests is given in Tables II to V. Figures 10 and 11 show the isotherms in the region of flow that is affected by the presence of the sphere. The details of the isotherms in the wake of the sphere were obtained by cross-plotting and interpolating the data at the experimental points.

B. Radial Temperature Gradient and Local Thermal Flux

Of all the temperature traverses given in Figure 8, only the ones at X = 0 and those at Z = 0 are in the radial directions. In order to obtain radial temperature distribution at other locations on the sphere, the points on each horizontal traverse were projected through concentric arcs on to a radial line as shown in Figure 9. The angle α of each radial line was measured from a traverse point which was at a radial distance of 0.005 inch from the surface. The points used in the direct determination of radial temperature gradients were within a radial distance of 0.010 inch from the surface and the maximum arc angle involved in the projection of the traverses ranged from about 0.8 to 2°, the extreme cases at X = $\pm$ 0.250 inch were projected through about 9°. It was assumed that within this thin shell around the sphere, the isotherms followed the contour of the surface over the short arc lengths involved. The radial distances obtained for the experimental points through the above operation are given in Tables II to V, and the corresponding angle α of the radial line for each traverse is also included.

Plots of temperature versus radial distance indicated that a linear distribution existed close to the surface of the sphere, so the radial temperature gradient at the surface could simply be obtained from the slope of the straight line through these points near the surface. The least squares method was applied in determining the best straight line, and the distance over which this linear distribution persisted was established by inspection of the plots. On an average, 6 points were

usually involved in the least-squares computation for each line. The standard deviation for each line ranged from 0.03 to 1.0° F. except in three cases out of a total of forty when the standard deviation was as high as 1.5° F. The radial temperature distributions and the fitted straight lines for two complete tests are given in Figures 12 and 13.

The local thermal flux was calculated from Equation 4 using the thermal conductivity of air at the surface temperature. The concentration of n-heptane at the surface of the porous sphere was about 5 mole %. There is no simple method of predicting the thermal conductivity for a mixture of polyatomic gases from data of the individual components (9). According to an expression developed by Lindsay and Bromley (17) the thermal conductivity for the air-heptane mixture at the surface of the porous sphere was about 1.5% lower than that for pure air. As the uncertainty involved in the given expression was of the same order of magnitude as the correction, no correction was made for the thermal conductivity for air. Values for the physical properties of air are given in Table VI. The results of local thermal flux are given in Table VII and are shown also in polar coordinates in Figures 10 and 11.

C. Gross Thermal Transfer

The gross thermal transfer for each test was obtained by two independent methods: (a) by integrating the local thermal flux over the entire surface of the sphere:

$$\underline{\dot{Q}} = -\oint_{o}^{A} k_s \left(\frac{\partial t}{\partial n}\right)_{n=o} dA \tag{19}$$

and (b) from over-all measurements. In the case of the silver sphere where radiation transfer was negligible the only thermal transfer was by convection, so the measured gross thermal transfer was simply the total energy input to the internal heater. The measured gross thermal transfer for the porous sphere was obtained by considering an energy balance over the surface of the sphere. In the energy balance, the enthalpy associated with the incoming liquid heptane and the outgoing vapor, the convective thermal transfer through the air, the heat conducted through the supporting tube, and the transfer by radiation were taken into account. Conduction through the supporting tube included contributions from the glass tube, liquid n-heptane, and the thermocouple wires. The quantities involved in the energy balance are shown in Figure 14. The gross convective thermal transfer through the air was then given by

$$\begin{aligned}
\underline{\dot{Q}} &= -\left(u_g \sigma_g H_g - u_\ell \sigma_\ell H_\ell\right) - \Sigma k_i A_i \left(\frac{\partial t}{\partial x}\right)_{n=o} - \underline{\dot{Q}}_r \\
&= -\underline{\dot{m}}\left(H_g - H_\ell\right) - \Sigma k_i A_i \left(\frac{\partial t}{\partial x}\right)_{n=o} - \underline{\dot{Q}}_r \qquad (20) \\
&= -\underline{\dot{m}}\left[L + C_{p,\ell}\left(t_g - t_\ell\right)\right] - \Sigma k_i A_i \left(\frac{\partial t}{\partial x}\right)_{n=o} - \underline{\dot{Q}}_r
\end{aligned}$$

Values of heat of vaporization and isobaric heat capacity for the liquid n-heptane were taken from Rossini (27) and Douglas and coworkers (6)

respectively, and the thermal conductivity values were from the International Critical Tables (12). These properties of liquid n-heptane are included in Table VI. The conduction term in the right-hand side of Equation 20 amounted to about 1% of the total convective transfer, with most of it contributed by the copper thermocouple wires. The radiation term was calculated from:

$$\dot{Q}_r = A \sigma_r \left(T_{sp}^4 - T_{sr}^4\right) \frac{1}{\left(\frac{1}{\epsilon_{sr}} + \frac{1}{\epsilon_{sp}} - 1\right)} \qquad (21)$$

where a value of 0.8 based on unglazed silica was assigned for the emissivity of the wetted surface and a value of 0.85 for that of the painted walls and surroundings.

Values of integrated and measured gross convective transfer are compared in Table VIII.

D. Generalized Correlations

As given by Equation 8, the non-dimensional temperature ratio θ was assumed to be a function of $\frac{n}{\delta_t}$ in the approximate method of solution mentioned earlier. The temperature measurements of this study were correlated on this basis over the forward region of the sphere. The displacement thickness of the thermal boundary layer defined as

$$\delta_t^* = \int_0^\infty \theta \, dn \qquad (22)$$

was used because it was more conveniently determined from the experimental data. The displacement thickness δ_t^* so defined is analogous to the displacement thickness for the flow boundary layer which is

$$\delta^* = \int_0^\infty \left(1 - \frac{u}{u_1}\right) dn \tag{23}$$

By comparing the momentum and energy equations (Equations 2 and 3) it can be shown that if $\frac{du_1}{ds} = 0$ and $Pr = 1$,

$$1 - \frac{u}{u_1} \equiv \frac{t - t_\infty}{t_s - t_\infty} \tag{24}$$

The values of δ_t^* were obtained graphically from the experimental data according to Equation 22 and they are presented in Table IX and Figure 15. When the values of θ are plotted against $\frac{n}{\delta_t^*}$ as shown in Figure 16 A - D, it is seen that θ is essentially a single function of $\frac{n}{\delta_t^*}$ regardless of angle position for the data of both spheres. In the attempt to fit an empirical function to the data, a form of the Blasius velocity distribution (2) was found to fit best when the Blasius parameter η was modified by dividing by an empirical constant, C = 1.75:

$$\theta = 1 - f'\left(\frac{\eta}{C}\right) = 1 - f'\left(\frac{\eta}{1.75}\right) \tag{25}$$

where $f'(\eta)$ is the Blasius distribution which consists of a power

series development near the surface and an asymptotic development near the edge of the boundary layer, and the two expressions are joined at an appropriate point. The Blasius function and its derivative are tabulated by Schlichting (29).

The radial temperature gradient at the surface was obtained by differentiating Equation 25:

$$\left(\frac{\partial t}{\partial n}\right)_{n=0} = - \frac{1.75\ (t_s - t_\infty)}{\delta_t^*}\ f''(0) \qquad (26)$$

where $f''(0)$ is the derivative of $f'(\eta)$ at $\eta = 0$, and is equal to 0.332 numerically. Hence the thermal flux could be calculated when δ_t^* and the temperature difference are known.

The experimental values of δ_t^* were correlated in terms of D, U and ν_s by considering that δ_t^* is a function of $\sqrt{\frac{D\nu_s}{U}}$ and α. The correlation as shown in Figure 17 is good up to an angle α of about 80°. The values of $\delta_t^*\sqrt{\frac{U}{D\nu_s}}$ are given in Table X. The standard deviation of $\delta_t^*\sqrt{\frac{U}{D\nu_s}}$ for the four tests from the smoothed curve is 0.04. Applying this correlation and Equation 26 to the experimental flow conditions and surface temperature of this study, local thermal flux was calculated. The results are compared with those obtained from experimental temperature gradients in Table XI.

An expression for the parameter $\frac{\eta u}{\sqrt{Re}}$ is given by the combination of Equations 12, 13, 16 and 26:

$$\frac{Nu}{\sqrt{Re}} = \frac{1.75 \times 0.332}{\delta_t^* \sqrt{\frac{U}{D\nu_s}}} = \frac{1.75 \times 0.332}{\phi(\alpha)} \qquad (27)$$

where the function $\phi(\alpha)$ is given by the values of $\delta_t^* \sqrt{\frac{U}{D\nu_s}}$ in Figure 17. The results of Equation 27 are included in Figures 18 and 19.

E. Comparison of Results

Experimental values of local thermal transfer over the surface of the sphere from this investigation are plotted in Figure 18 in terms of $\frac{Nu}{\sqrt{Re}}$ and the angle from the forward stagnation point. The slight increase of $\frac{Nu}{\sqrt{Re}}$ with angle position near the stagnation point as shown by the average curve is probably not significant as the uncertainty involved in assuming that the isotherms follow the contour of the surface is greatest in that region. The variations in the region beyond 100° are believed to be due to the difference in the supports of the two spheres. The correlated curve according to Equation 27 included in the same plot is similar to the average curve for the experimental data.

The experimental results of Cary (3) and Xenakis and coworkers (35) are also included in Figure 18, each curve representing the average of their reported values. Cary's results include five sets of values for a 6-inch sphere at Reynolds numbers between 4.4×10^4 to 1.5×10^5 and those of Xenakis are made up of 4 sets of values for the three spheres used at Reynolds numbers from 8.7×10^4 to 1.8×10^5 which are

below the critical Reynolds number for spheres. The temperature used for the thermal conductivity and kinematic viscosity in establishing the Nusselt and Reynolds numbers was not given by Cary. It is believed that he used thermal conductivity at surface temperature and kinematic viscosity at free stream temperature. Xenakis used thermal conductivity at the average temperature between the surface and free stream values and probably used kinematic viscosity at free stream temperature. The actual free stream temperature was not indicated in either of the two reports, therefore no adjustment was made to the reported values. If the surface temperature is taken to be 240° F. and the free stream temperature 70° F., Cary's results should be about 10% higher and those of Xenakis about 5% higher than those shown in Figure 18 to be on a common basis with the experimental results of this study. Cary's data are somewhat lower and those of Xenakis are higher than the results of this investigation. As pointed out by Korobkin (15) the values of Cary may be too low because of internal heat exchange in the sphere between the presumably isolated plug and the steam which heated the rest of the surface; it is likely that the isolated plug was partly heated by the steam. The high values of Xenakis may be due to the way the spheres were supported; according to the photographs presented in his report (35) the guy wires used in steadying the "cross wind" support appear to be located very close to the sphere.

In Figure 19 the experimental and correlated results of this study

are compared with theoretical results for the forward region of the sphere up to an angle of about 80°. The Prandtl number for the air stream in this investigation is 0.71 whereas a Prandtl number of 0.7 has been used in the theoretical considerations. It is seen that at the stagnation point the experimental value of $\frac{Nu}{\sqrt{Re}}$ is lower than that given by Sibulkin (31); in the rest of the forward region there is good agreement between the experimental results and the Eckert-Drake curve (15). The theoretical curve of Sibulkin as reported by Korobkin (15) is somewhat higher, the difference may be due to the choice of parabolic expressions for the velocity and temperature distributions in the integral method of solution.

As shown in Table VIII the integrated values of gross thermal transfer for the whole sphere are in fair agreement with those obtained from simultaneous over-all measurements. The higher measured values for the silver sphere may be due to the presence of the horizontal support which tends to cause local increase in thermal transfer in the downstream half of the sphere. The gross thermal transfer was not measured in the studies by Cary (3) and Xenakis (35).

The integrated values of gross thermal transfer of this study are compared with available information on the gross thermal transfer from a sphere in terms of the Nusselt and Reynolds numbers in Figure 20. The correlation of Williams as given by McAdams (19), the theoretical line of Johnstone and coworkers (13) and the experimental results of Tang and coworkers (33) are included as these results represent the extremes of published results in the Reynolds number range concerned.

CONCLUSIONS

The thermal transfer of direct concern here is that which takes place as the result of a temperature difference between a spherical surface and the flowing air stream. The local thermal flux has been calculated from the measured temperature gradients at the surface and the thermal conductivity of the air. The validity of the values of local thermal flux of this study is substantiated by the satisfactory agreement between the integrated gross values and those obtained from simultaneous over-all measurements. This validity is also supported by the fact that the integrated values are in fair agreement with available published data.

In convective thermal transfer the effect of the turbulence level of the fluid stream is significant. Results of a recent study of the effect of turbulence on gross thermal transfer from a sphere (28) indicated that for an air stream having a turbulence level of 13% at a Reynolds number of 3600 the over-all Nusselt number was 11% higher than that of an undisturbed air stream at the same Reynolds number. The present study was made in an air stream with a turbulence level of 5.2 to 5.6%. The intensity of turbulence of the air stream in the investigations cited was not given and the effect of turbulence was not considered in the theoretical treatments. The influence of turbulence in the air stream might account for some of the difference in the results presented.

The measurements of the temperature distribution within the

thermal boundary layer are plotted in Figures 16 A-D, using the non-dimensional variable $\Theta = \frac{t - t_\infty}{t_s - t_\infty}$ versus $\frac{n}{\delta_t^*}$. The results indicate that these experimental data may be described with reasonable accuracy by the following semi-empirical equation:

$$\Theta = 1 - f'\left(\frac{\eta}{C}\right)$$

where $f'(\eta)$ is the Blasius theoretical velocity distribution in the flow boundary layer (2,29) and C, a constant pure number, lies between 1.6 and 1.9 . In viewing these results, it seems quite conclusive that the value C = 1.75 provides good agreement with the data.

The empirical correlations of temperature distribution and displacement thickness of the thermal boundary layer resulting from this experimental study provide a simple means of calculating the local thermal flux over the surface of the leading half of a sphere. The uncertainty involved is probably not more than ± 8%. As the size of the spheres used in this investigation has been constant, further studies using spheres of different diameters are necessary to confirm the effect of sphere diameter as given in the correlation of displacement thickness.

In comparing the gross thermal transfer from the leading half of the sphere with that of the trailing hemispherical surface by integrating the experimental local thermal flux, it is interesting to note that over the range of Reynolds number involved in this study the contribution

of the leading half is essentially constant at about 75% of the total value. It is expected that as the Reynolds number is increased the contribution of the trailing half may gradually become more significant due to the increase of turbulence in the wake.

The results of this investigation are not sufficient to establish the thermal transfer over the trailing half of the sphere on a local basis. The complex nature of the flow in this region makes it difficult to analyze and interpret the results. There is definite need for more experimental as well as theoretical studies on the fluid dynamics in the region close to the surface in the wake of a sphere.

NOMENCLATURE

A	area, ft^2
C	constant
C_p	isobaric heat capacity, Btu/(lb)(^oF)
D	diameter, ft
h	local thermal transfer coefficient, Btu/(ft^2)(sec)(^oF)
H	specific enthalpy, Btu/lb
k	thermal conductivity, Btu/(ft^2)(sec)(^oF/ft)
K	thermometric conductivity, ft^2/sec
L	latent heat of vaporization, Btu/lb
m	constant
$\dot{\underline{m}}$	transport rate, lb/sec
Nu	Nusselt number, $\frac{h D}{k_s}$
n	radial or normal distance from surface, inch or ft
Pr	Prandtl number, $\frac{\nu}{K}$
$\dot{q}$	local thermal flux in direction n, Btu/(ft^2)(sec)
$\dot{\underline{Q}}$	gross thermal transfer from surface, Btu/sec
r	radial distance from center of sphere, inch or ft
Re	Reynolds number, $\frac{D U}{\nu_s}$
s	distance parallel to surface in direction of main flow, ft
t	temperature, ^oF
T	thermodynamic temperature, ^oR
u	local velocity along s, ft/sec
u_1	local velocity at the edge of flow boundary layer, ft/sec
U	bulk or free stream velocity, ft/sec

v	local velocity along n, ft/sec
X,Y,Z	coordinate axes with zero at center of sphere, inch or ft
α	angle from forward stagnation point, degree
β	velocity gradient along s, sec^{-1}
δ	flow boundary layer thickness, ft
δ_t	thermal boundary layer thickness, ft
δ^*	displacement thickness of flow boundary layer, ft
δ_t^*	displacement thickness of thermal boundary layer, ft
θ	non-dimensional temperature ratio, $\frac{t - t_\infty}{t_s - t_\infty}$
ϵ	emissivity
η	Blasius parameter
ν	kinematic viscosity, ft^2/sec
σ	specific weight, lb/ft^3
σ_r	Stefan-Boltzman constant, 0.1713×10^{8} $Btu/(ft^2)(hr)(^oR^4)$

Subscripts

a	air
g	gas phase
l	liquid phase
r	radiation
s	surface
sp	sphere
sr	surrounding
w	thermocouple wire
∞	free stream condition

REFERENCES

1. Baer, D. H., Schlinger, W. G., Berry, V. J., and Sage, B. H., J. Appl. Mech., 20, 407 (1953).

2. Blasius, H., Z. f. Math. u. Phys., 56, 1 (1908).

3. Cary, J. R., Trans. Am. Soc. Mech. Engrs., 75, 483 (1953).

4. Corcoran, W. H., Page, F., Jr., Schlinger, W. G., and Sage, B. H., Ind. Eng. Chem., 44, 410 (1952).

5. Davis, L., Jet Propulsion Laboratory, Calif. Inst. of Technology, Report No. 3-17, (1952).

6. Douglas, T. B., Furukawa, G. T., McCoskey, R. E., and Ball, A. F., J. Research, Nat. Bur. Stds., 53, 139 (1954).

7. Drake, R. M., Jr., J. of Aero. Sci., 20, 309 (1953).

8. Eckert, E., Forschungsh. Ver. dtsch. Ing., No. 416 (1942).

9. Hirschfelder, J. O., Curtiss, C. F., and Bird, R. B., "Molecular Theory of Gases and Liquids," John Wiley and Sons, Inc., New York, 1954.

10. Homann, F., Z. angew. Math. u. Mech., 16, 153 (1936).

11. Hsu, N. T., Sato, K., and Sage, B. H., Ind. Eng. Chem., 46, 870 (1954).

12. International Critical Tables, V (1929).

13. Johnstone, H. F., Pigford, R. L., and Chapin, J. H., Trans. Am. Inst. Chem. Engrs., 37, 95 (1941).

14. von Karman, Th., Z. angew. Math. u. Mech., 1, 244 (1921).

15. Korobkin, I., "Duscussion of Local Laminar Heat Transfer Coefficients for Spheres and Cylinders in Incompressible Flow," Paper No. 54-F-18 presented at 1954 Fall Meeting of ASME, Milwaukee, Wisconsin, Sept., 1954.

16. Lautman, L. G., and Droege, W. C., Air Material Command, AIRL A6118, 50-15-3, Aug. 1950.

17. Lindsay, A., and Bromley, L. A., Ind. Eng. Chem., 42, 1508-11 (1950).

18. Mangler, W., Z. angew. Math. u. Mech., 28, 97 (1948).

19. McAdams, W. H., "Heat Transmission," McGraw-Hill Book Co., New York, 1954.

20. Meldau, R. F., Department of Chemical Engineering, Calif. Inst. of Technology, Student Report No. 621, June 1955.

21. Mickley, H. S., Ross, R. C., Squyers, A., and Stewart, W. E., NACA TN 3208, July 1954.

22. Millikan, C. B., Trans. Am. Soc. Mech. Engrs., 54, 29 (1932).

23. Page, F., Jr., Corcoran, W. H., Schlinger, W. G., and Sage, B. H., Ind. Eng. Chem., 44, 419 (1952).

24. Pohlhausen, K., Z. angew. Math. u. Mech., 1, 252 (1921).

25. Reamer, H. H., and Sage, B. H., Rev. Sci. Inst., 24, 362 (1953).

26. Reshotka, E., and Cohen, C. B., NACA TN 3513, July 1955.

27. Rossini, F. D., Pitzer, K. S., Arnett, R. L., Braun, R. M., and Pimentel, G. C., "Selected Values of Physical and Thermodynamic Properties of Hydrocarbons and Related Compounds," Carnegie Press, Pittsburgh, 1953.

28. Sato, K., Calif. Inst. of Technology, thesis, 1955.

29. Schlichting, H., "Boundary Layer Theory," translated by J. Kestin, McGraw-Hill Book Co., New York, 1955.

30. Schlichting, H., and Bussmann, K., Schriften, Deutsche Akad. Luftfahrtforschung, 7B, 25 (1943).

31. Sibulkin, M., J. of Aero. Sci., 19, 570 (1952).

32. Spalding, D. B., Proc. Roy. Soc. (London) A221, 78 (1954).

33. Tang, Y. S., Duncan, J. M., and Schweyer, H. E., NACA TN 2867, March 1953.

34. Tomotika, S., Brit. Aero. Res. Comm., R & M No. 1678, 1936.

35. Xenakis, G., Amerman, A. E., and Michelson, R. W., Wright Air Development Center Rep. 53-117, Apr. 1953.

LIST OF FIGURES

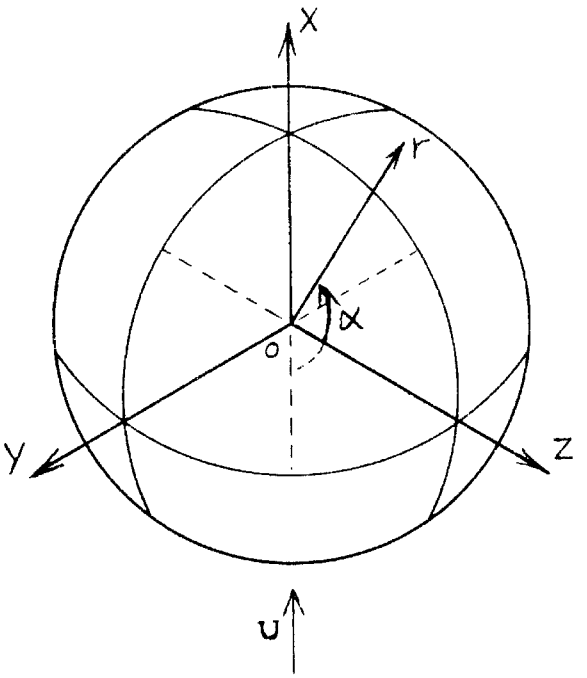

(A) Three - Dimensional

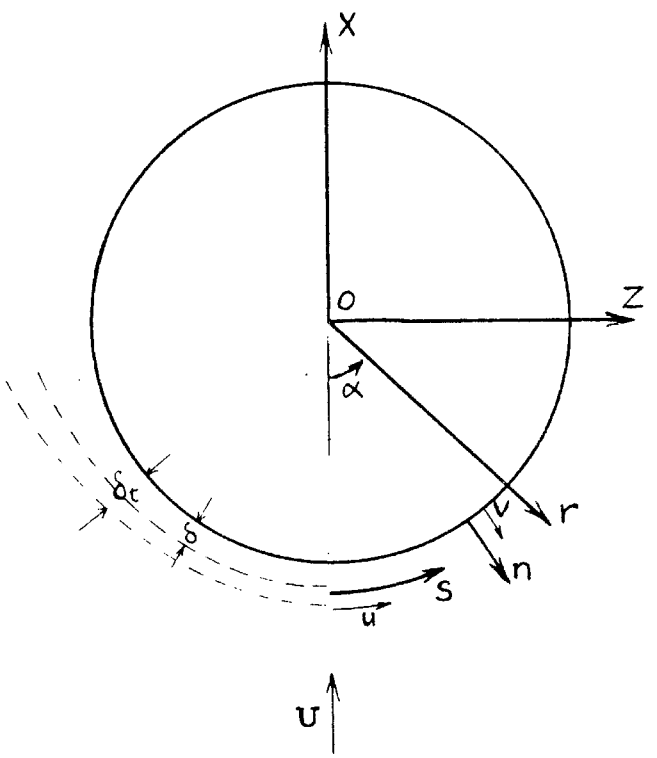

(B) X-Z (Y = 0) Plane

Fig. 1 Coordinate System

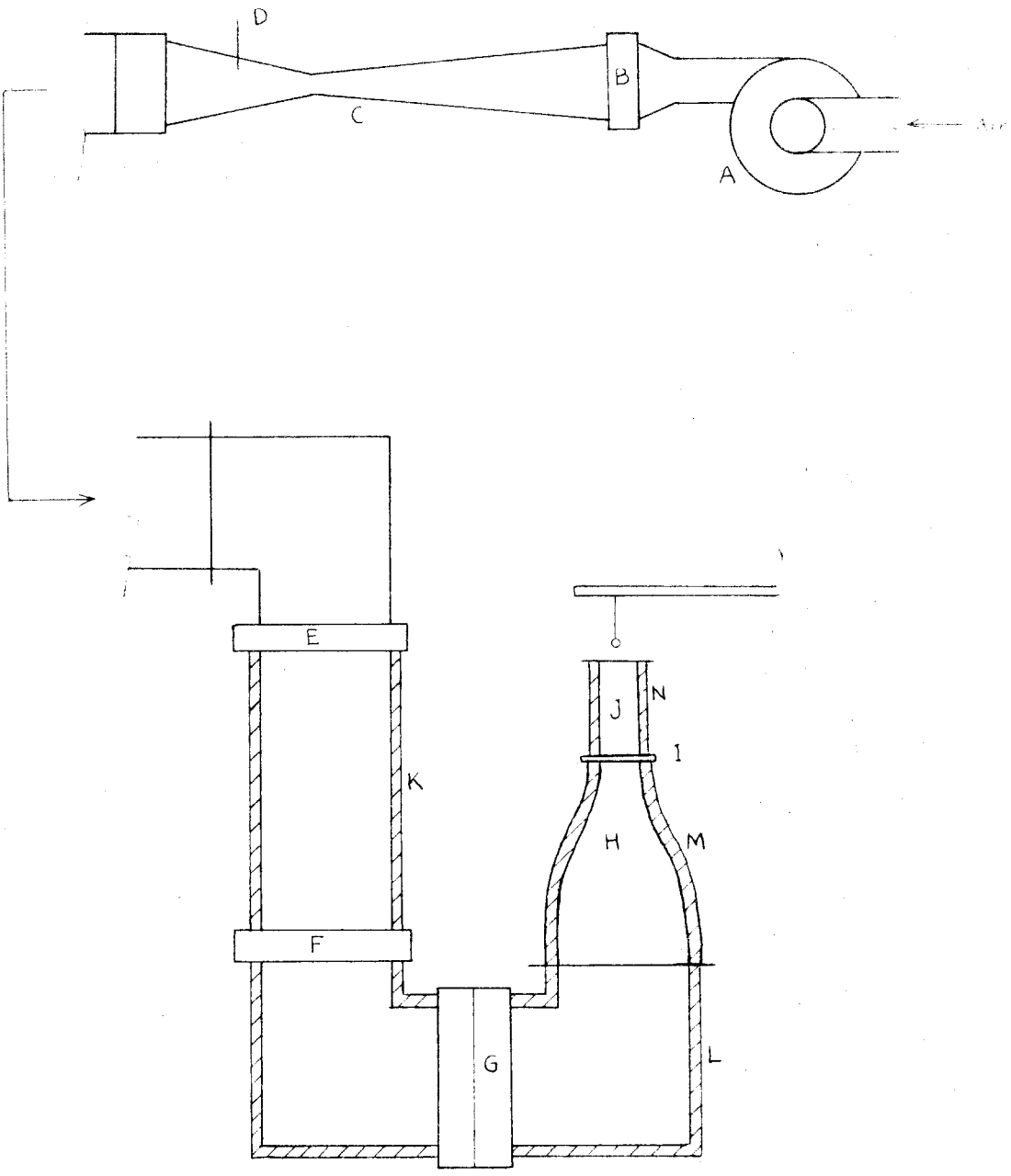

Fig. 2 Arrangement of Air Supply

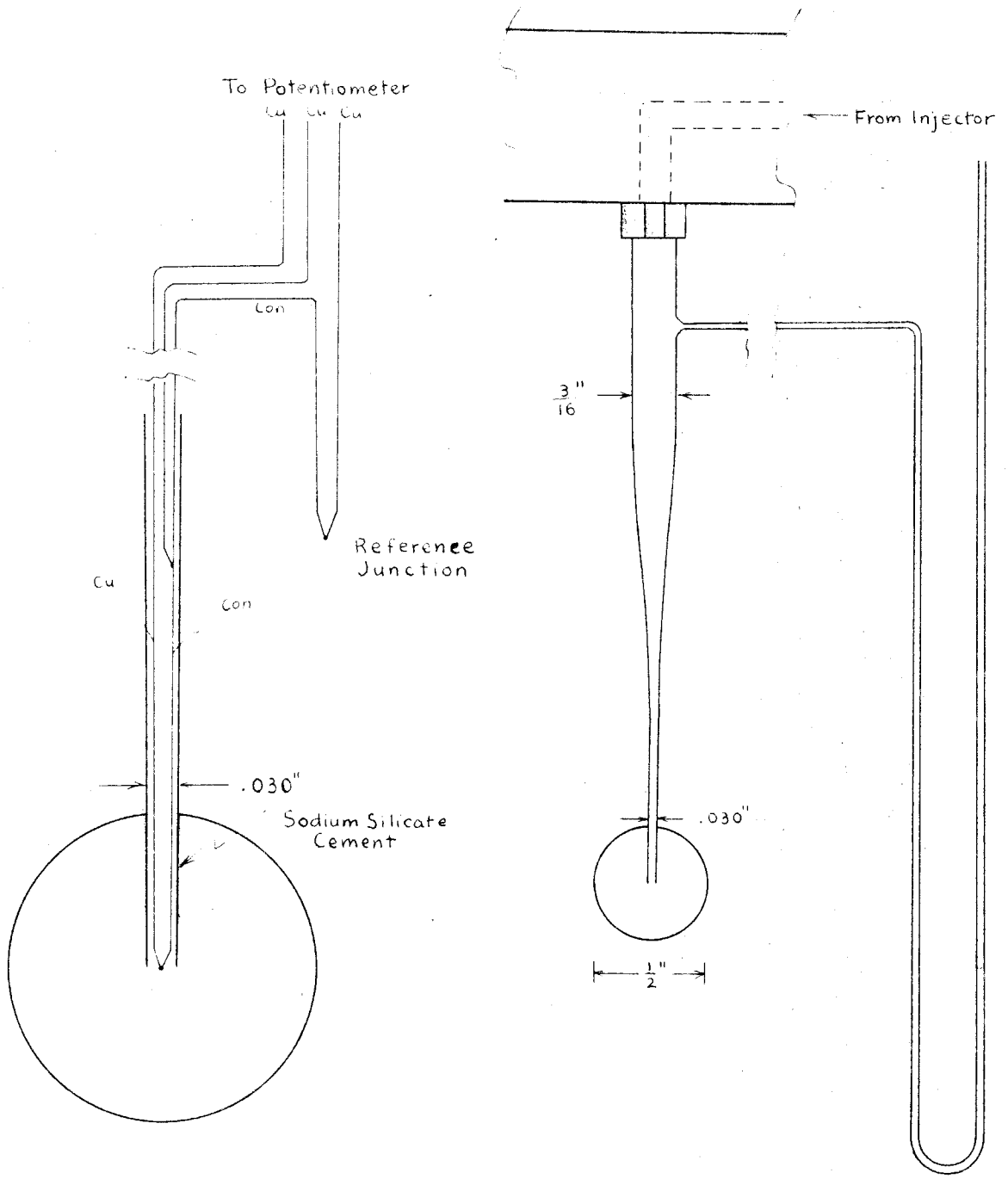

(A) Thermocouples (B) Sphere with Capillary Manometer

Fig. 3 Porous Sphere Assembly

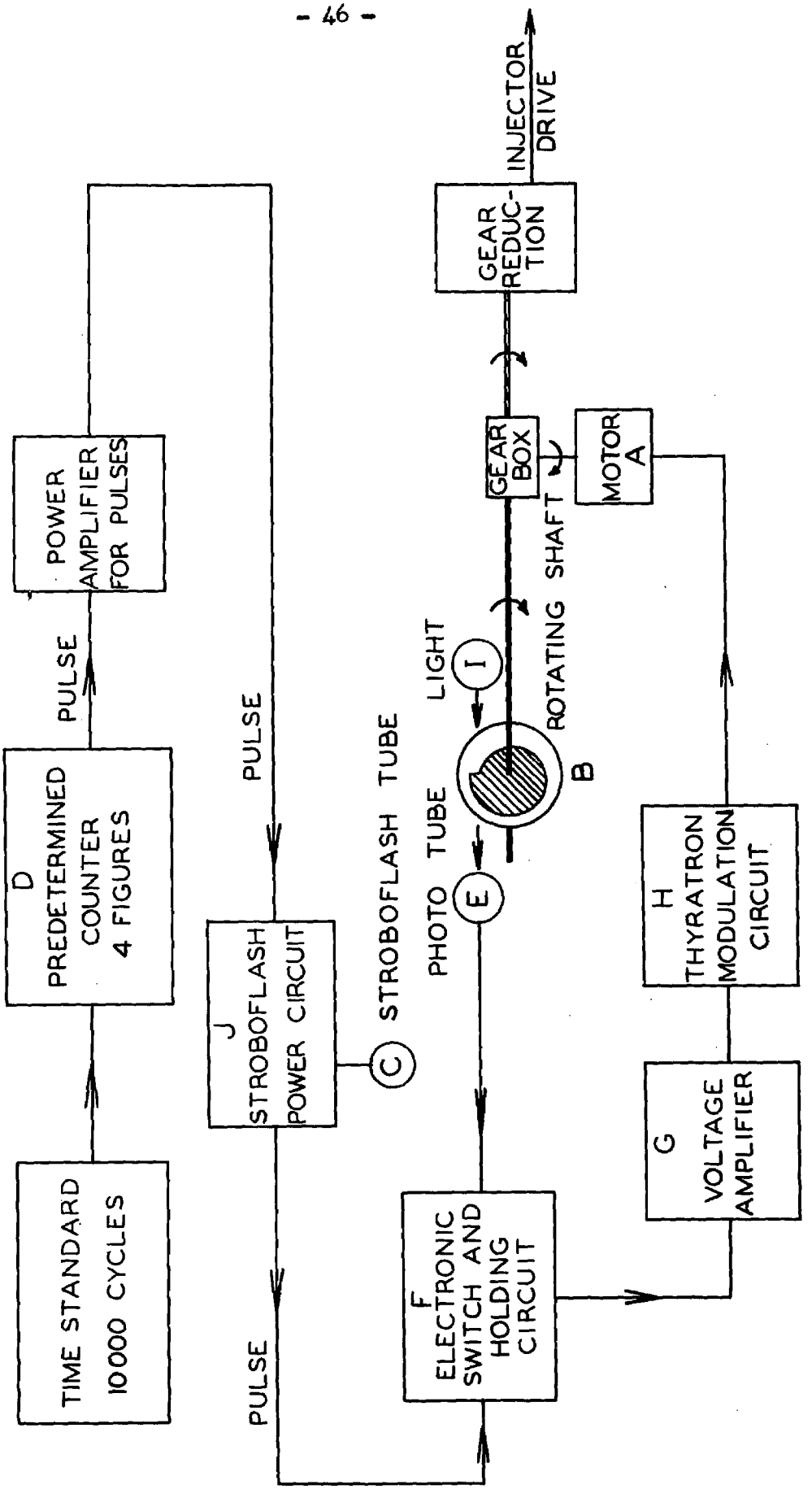

Fig. 4 Injection System

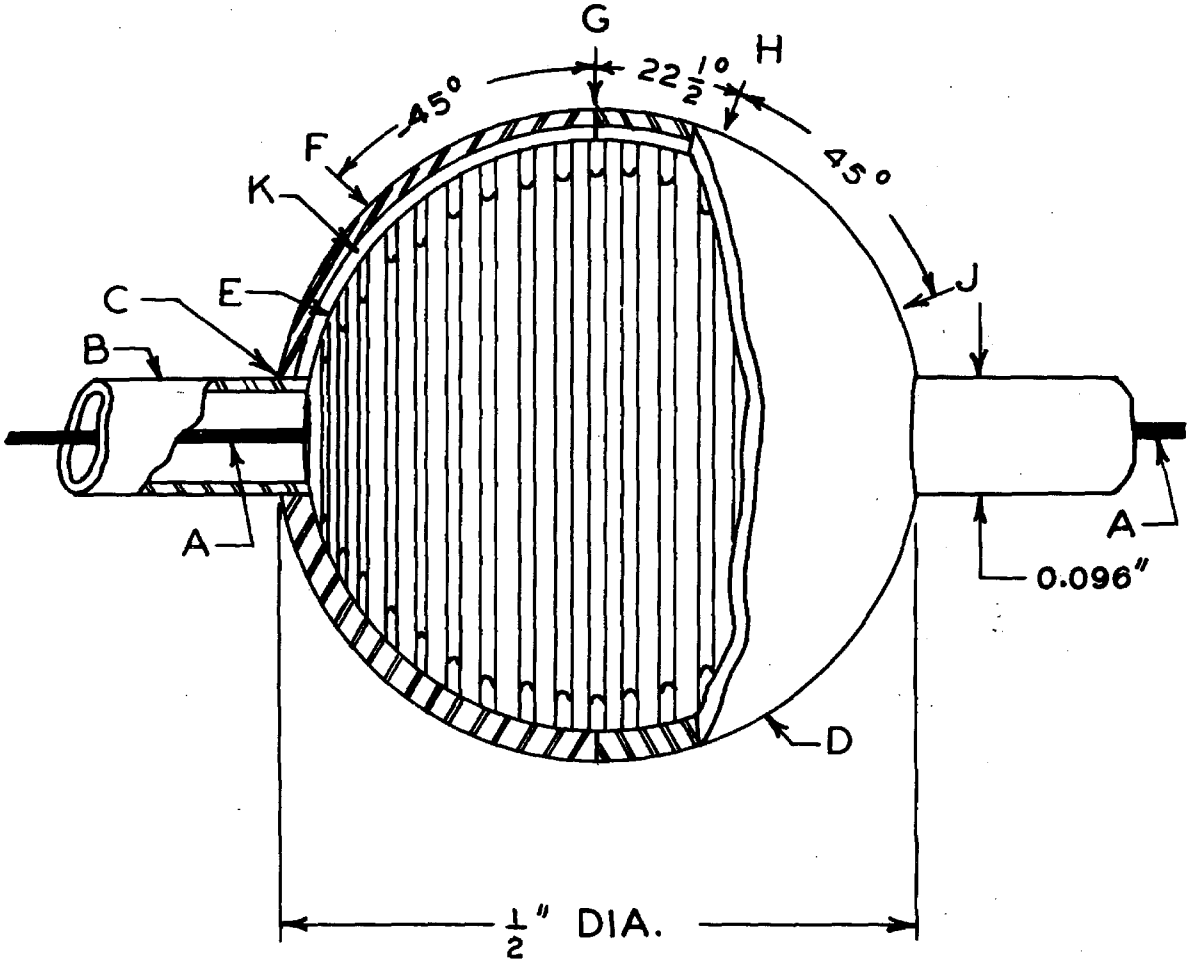

Fig. 5 Silver Sphere Assembly

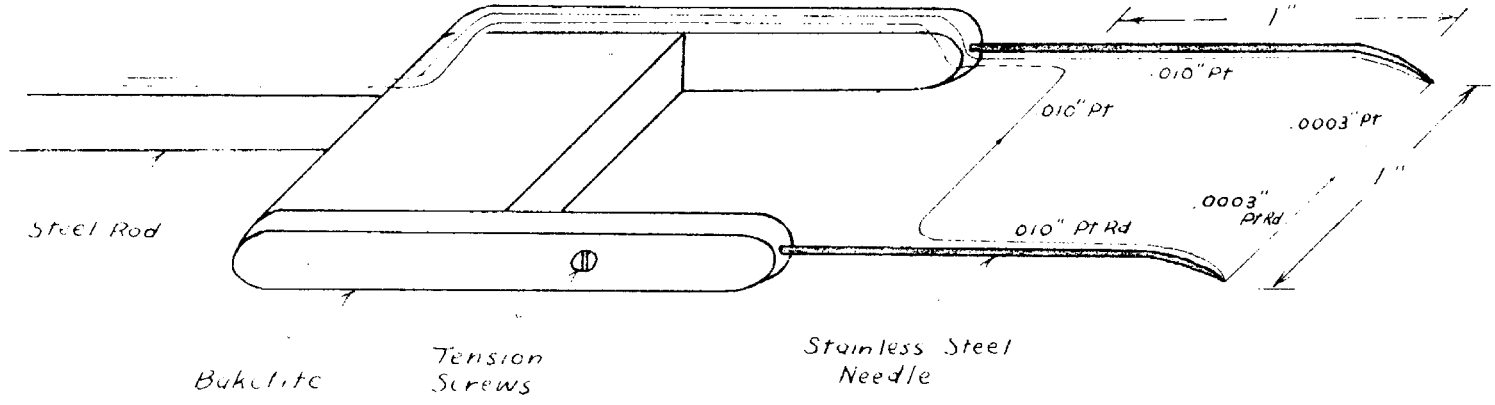

Fig. 6 Thermocouple Probe

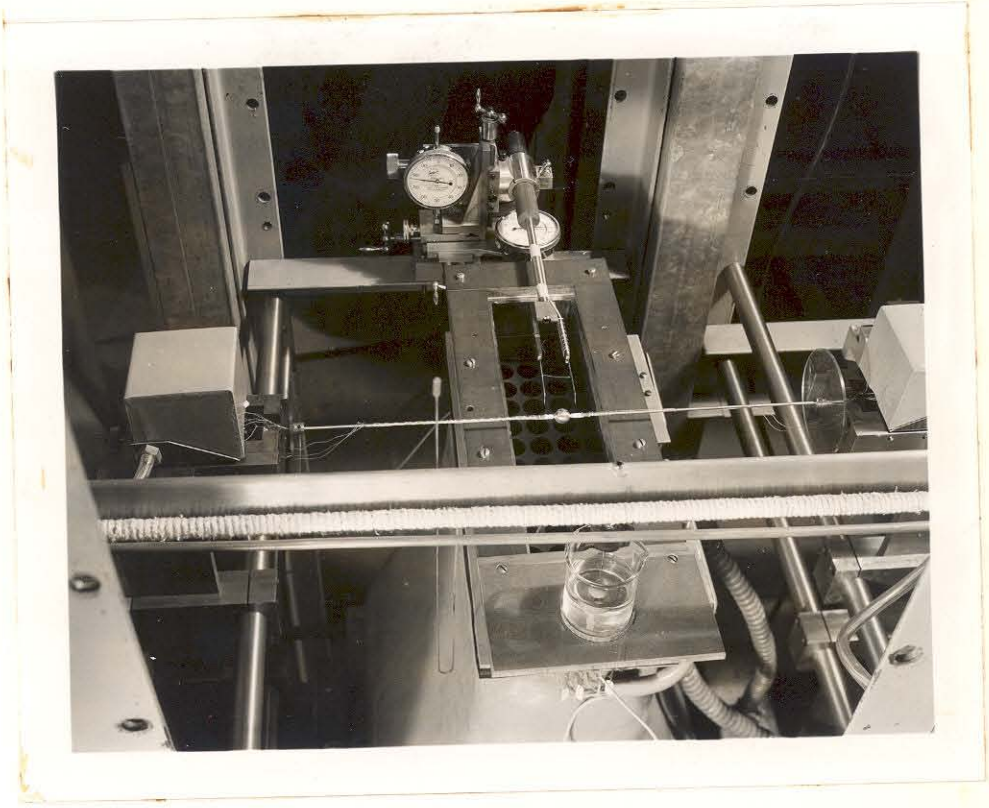

Fig. 7. Photograph of Spheres and Thermocouple Probe over Air Jet

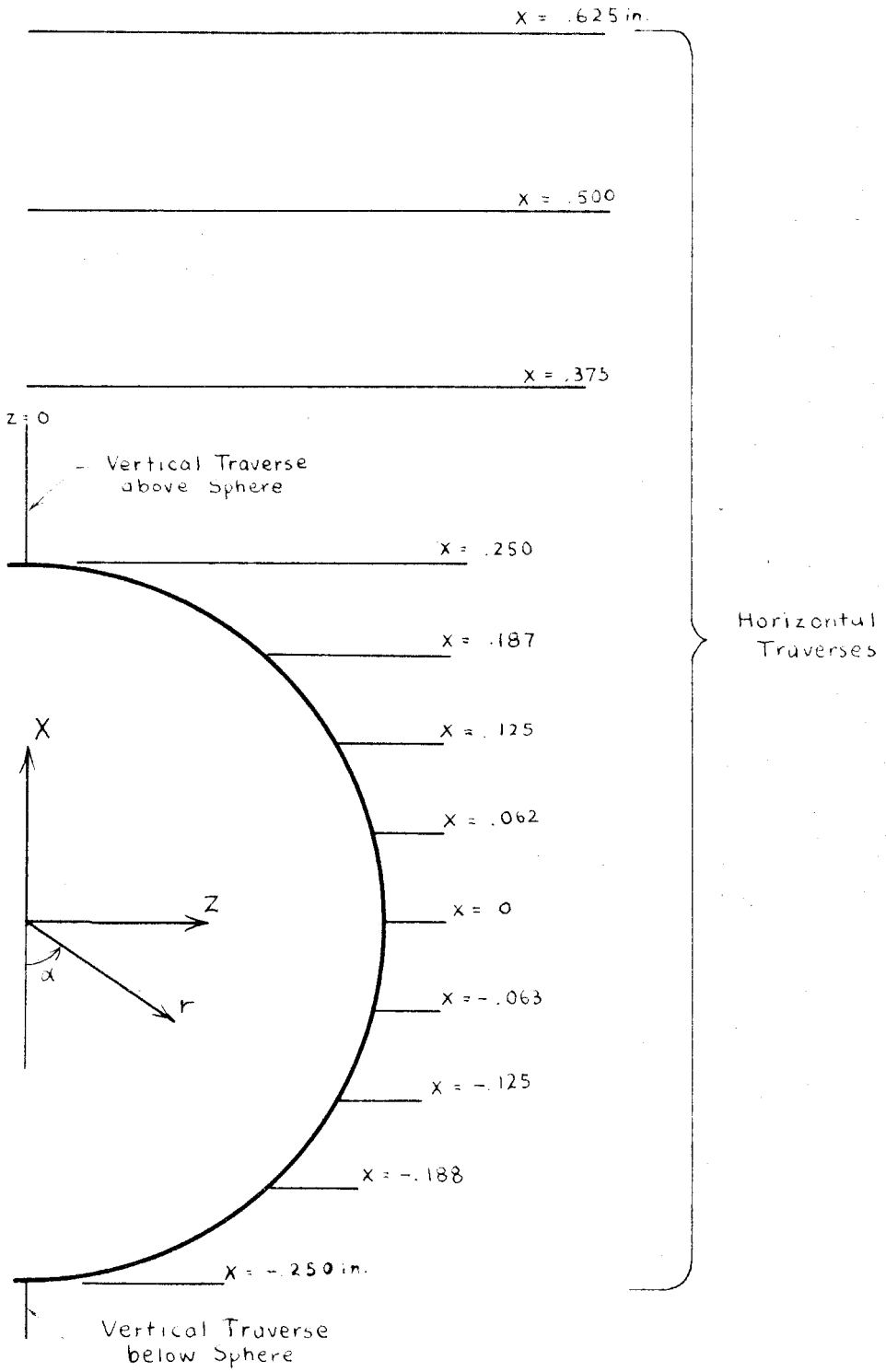

Fig 8 Traverse Locations

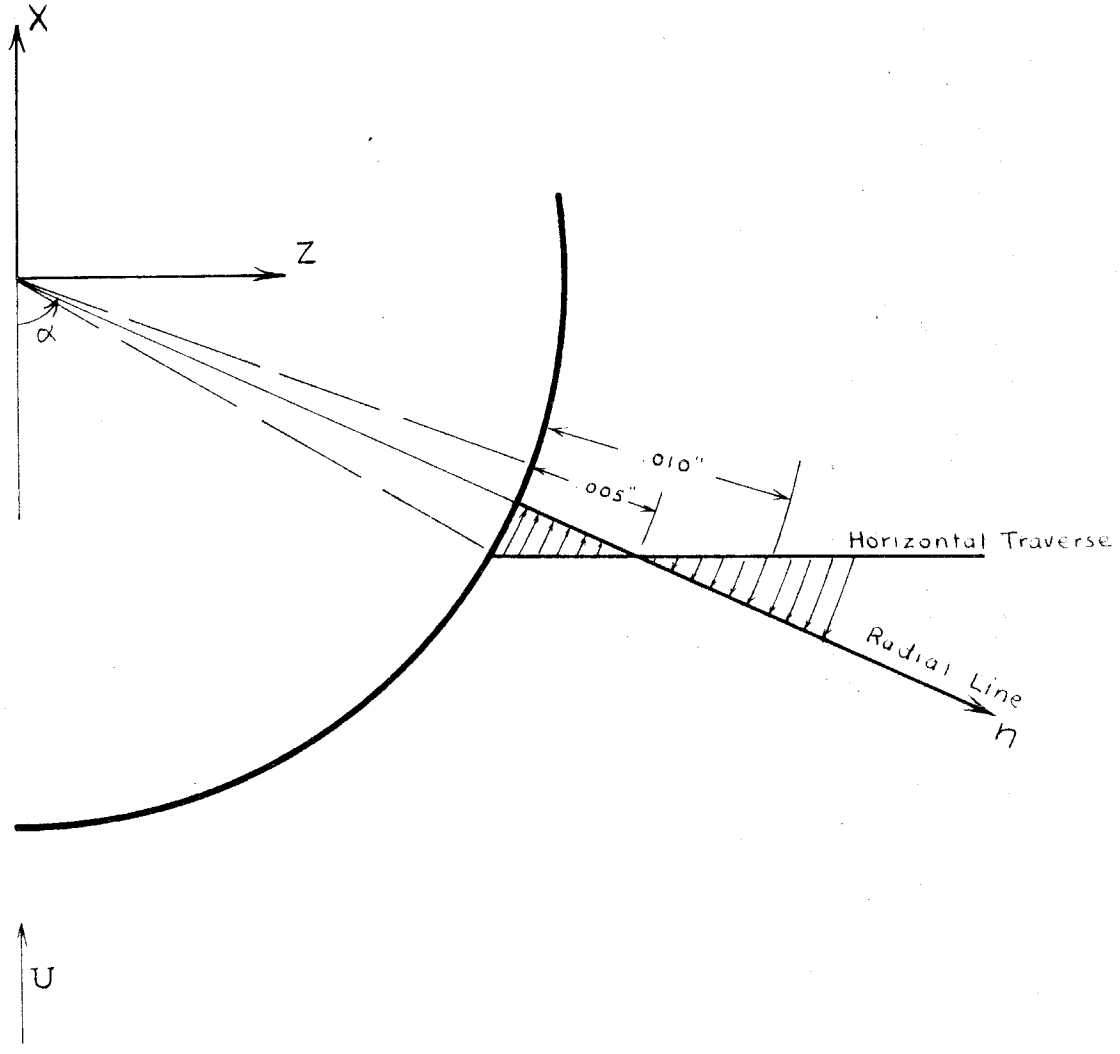

Fig. 9 Projection of a Horizontal Traverse

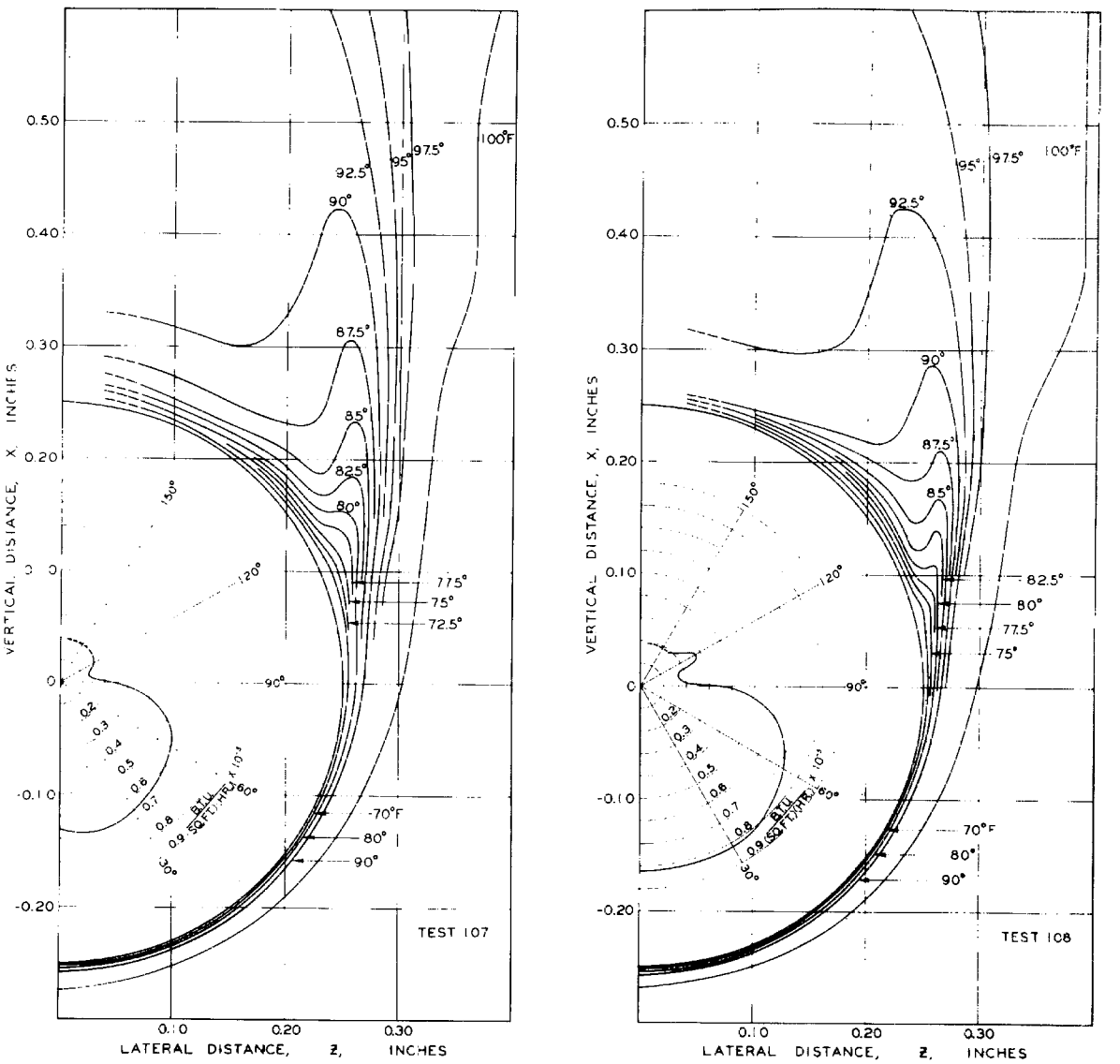

Fig. 10 Temperature Distribution and Local Thermal Flux around Porous Sphere

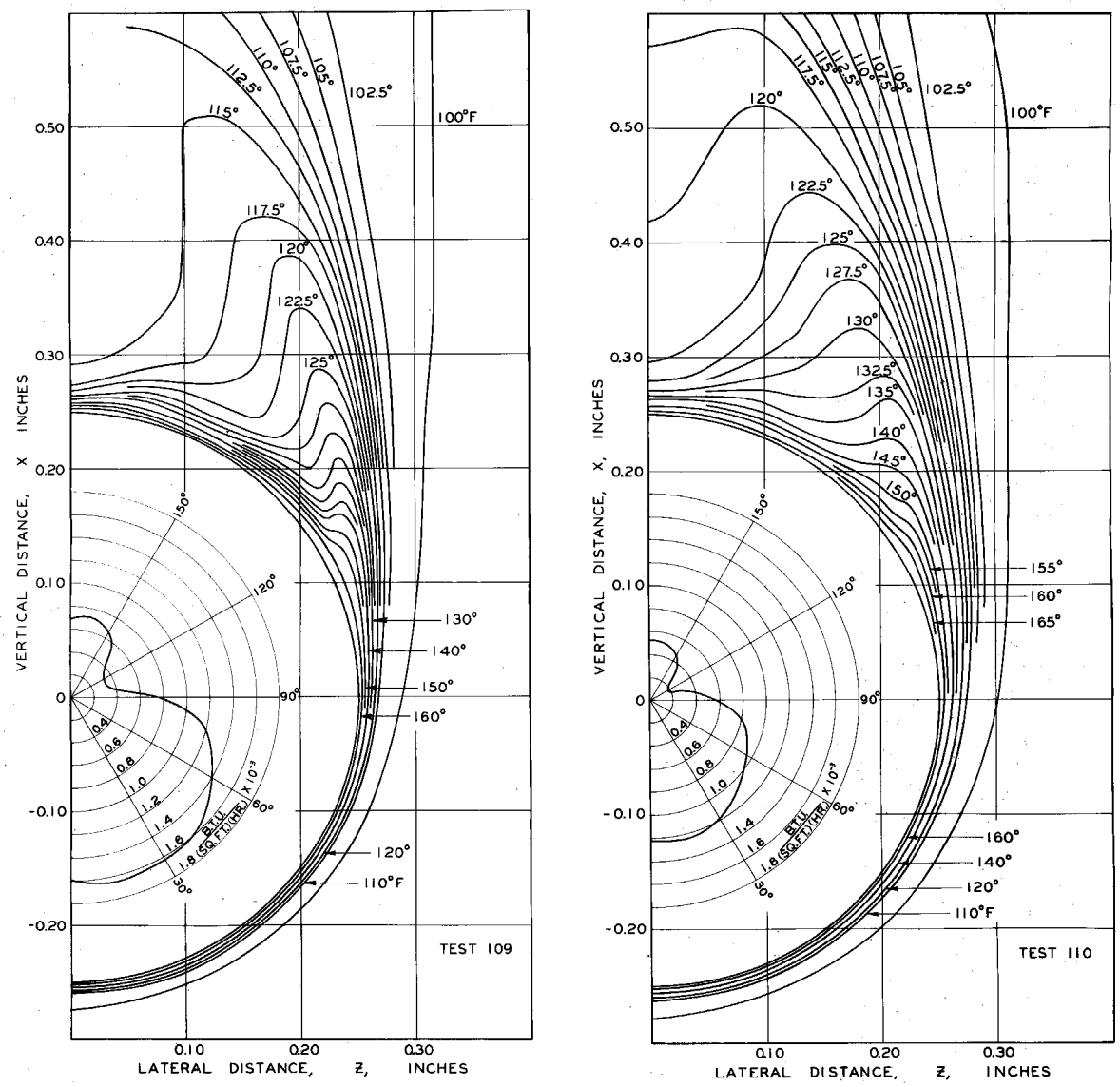

Fig. 11 Temperature Distribution and Local Thermal Flux around Silver Sphere

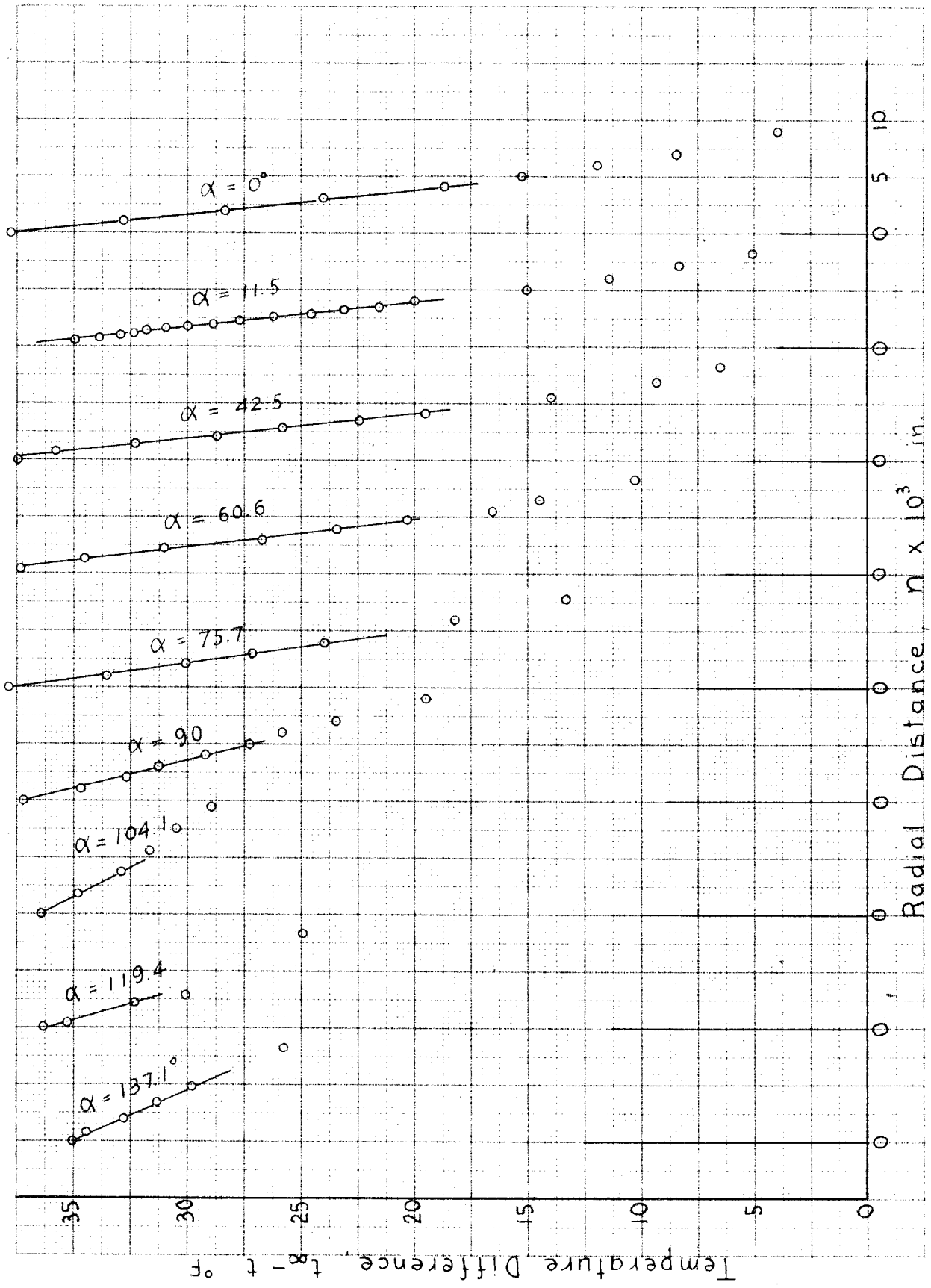

Fig. 12 Radial Temperature Distribution - Test 108

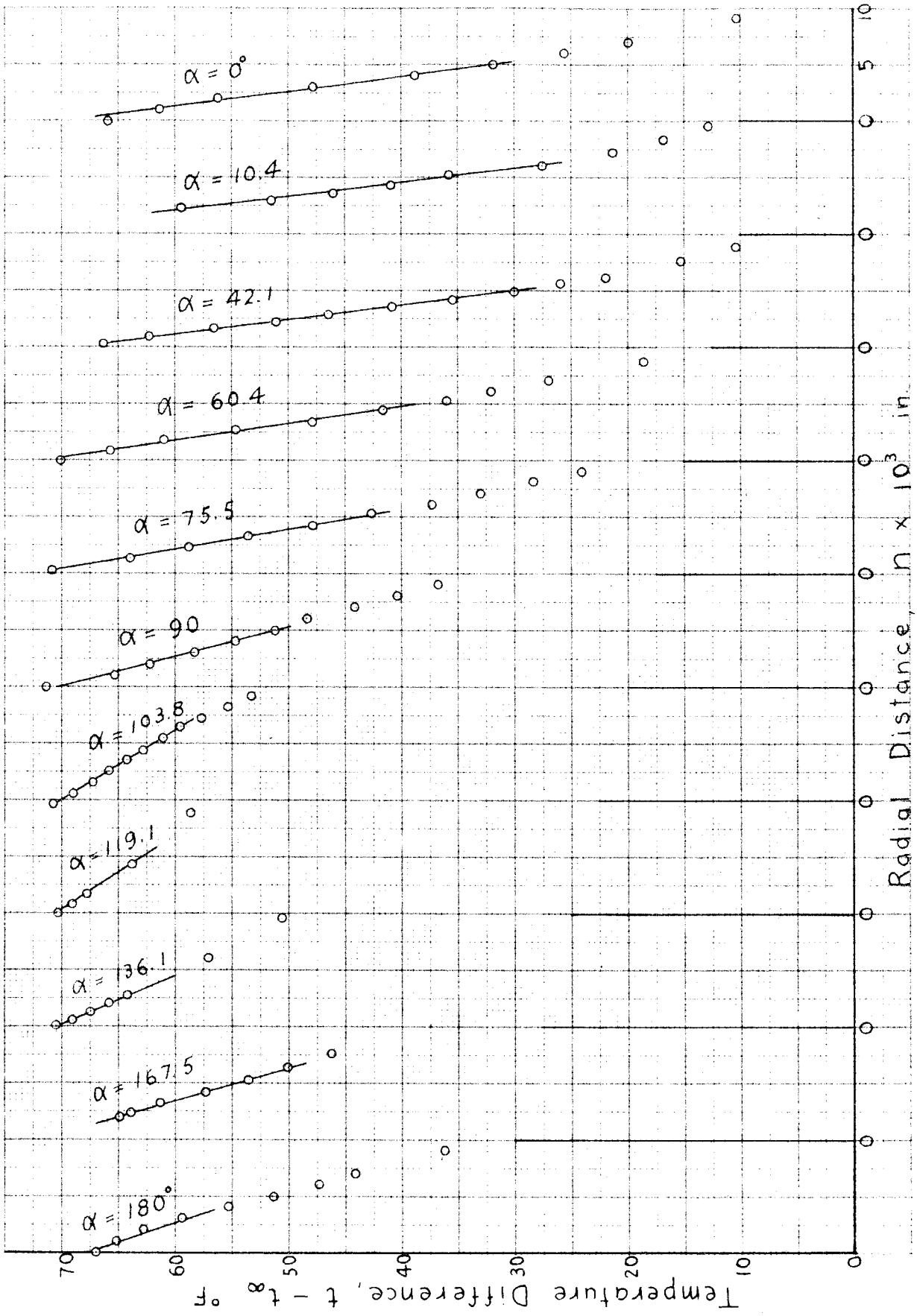

Fig. 13 Radial Temperature Distribution - Test 109

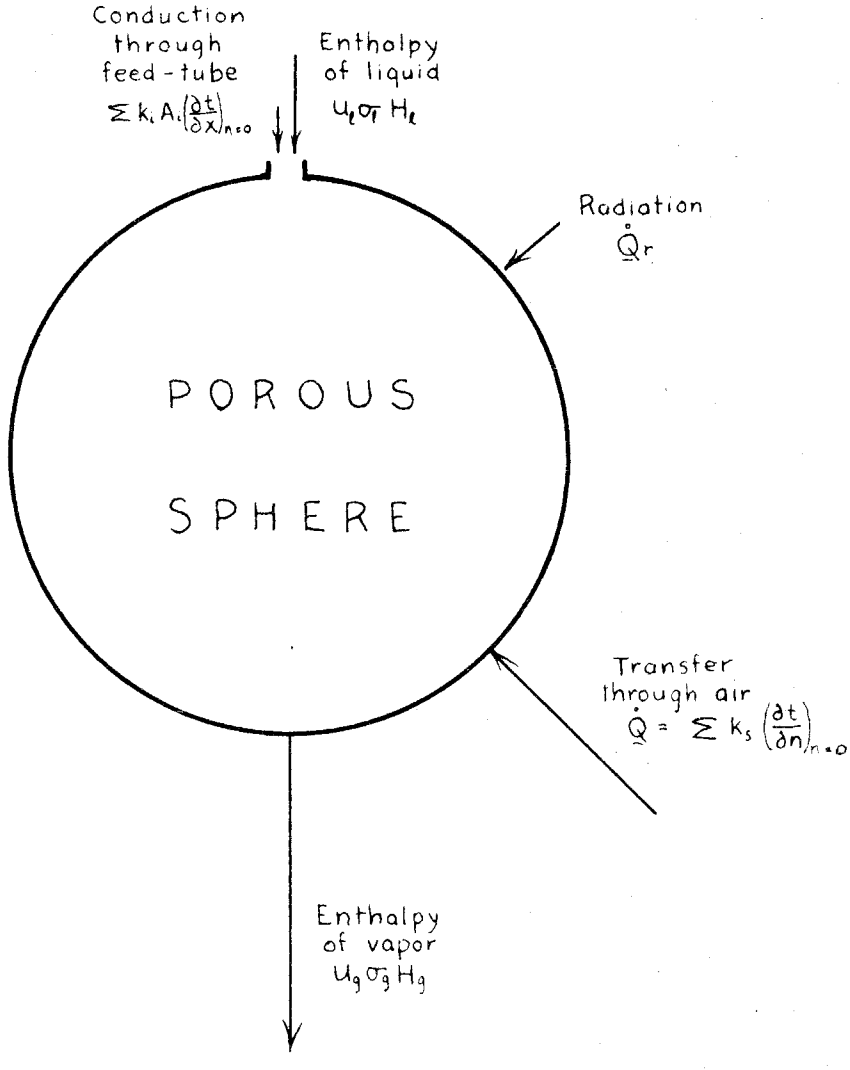

Fig 14 Energy Balance over Porous Sphere

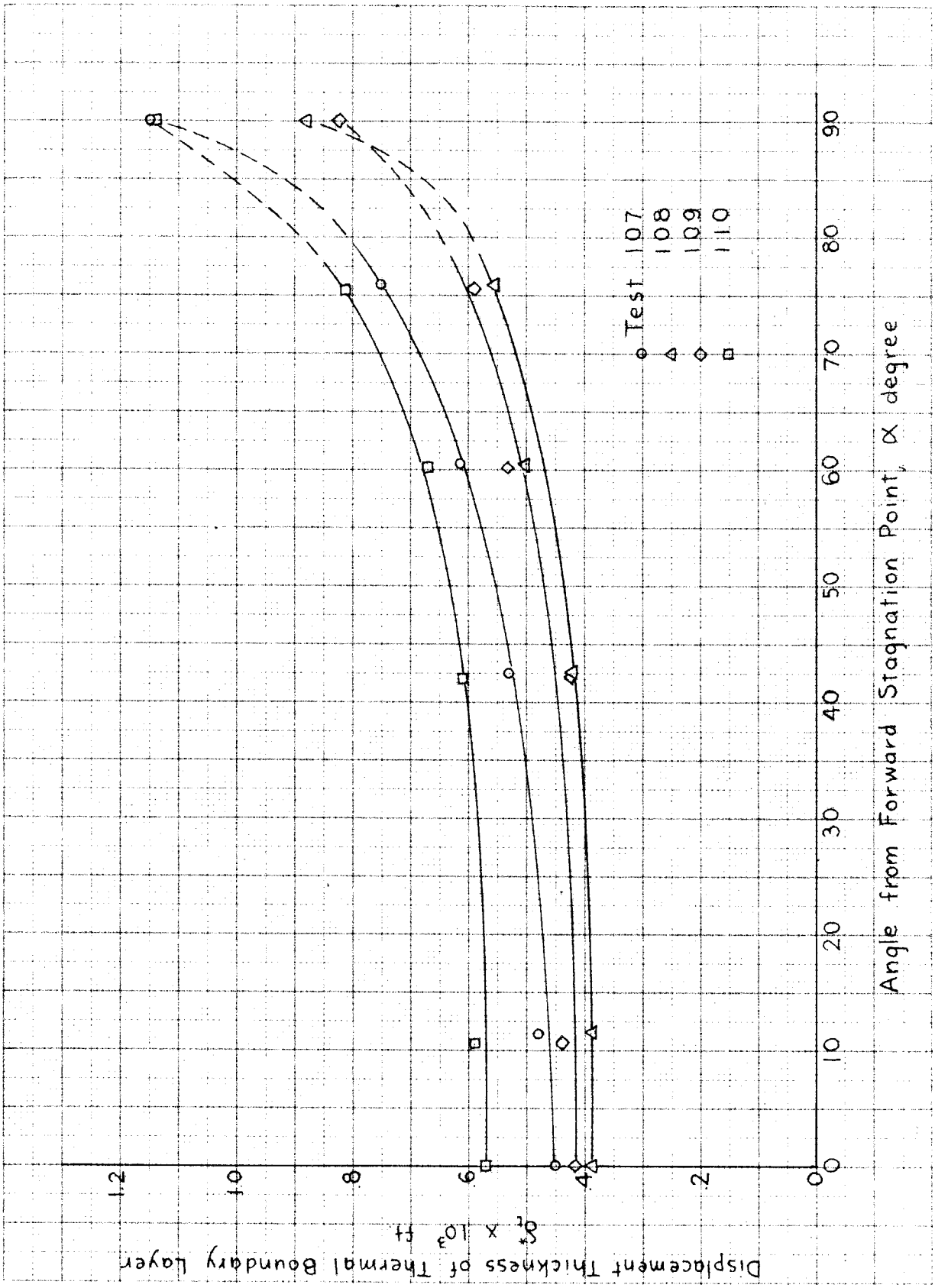

Fig. 15 Displacement Thickness as Function of Angular Position

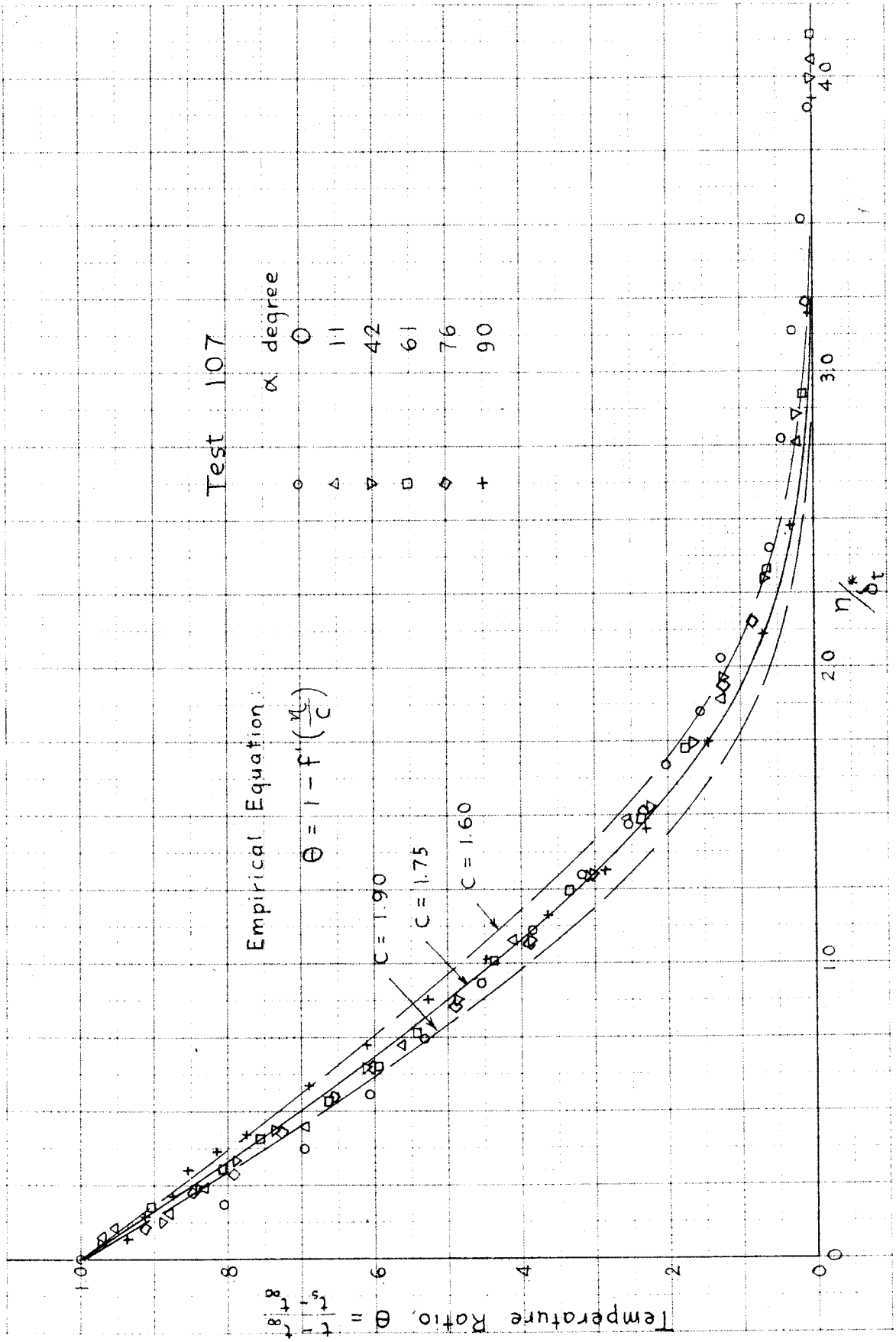

Fig. 16 - A Temperature Distribution in the Thermal Boundary Layer - Test 107

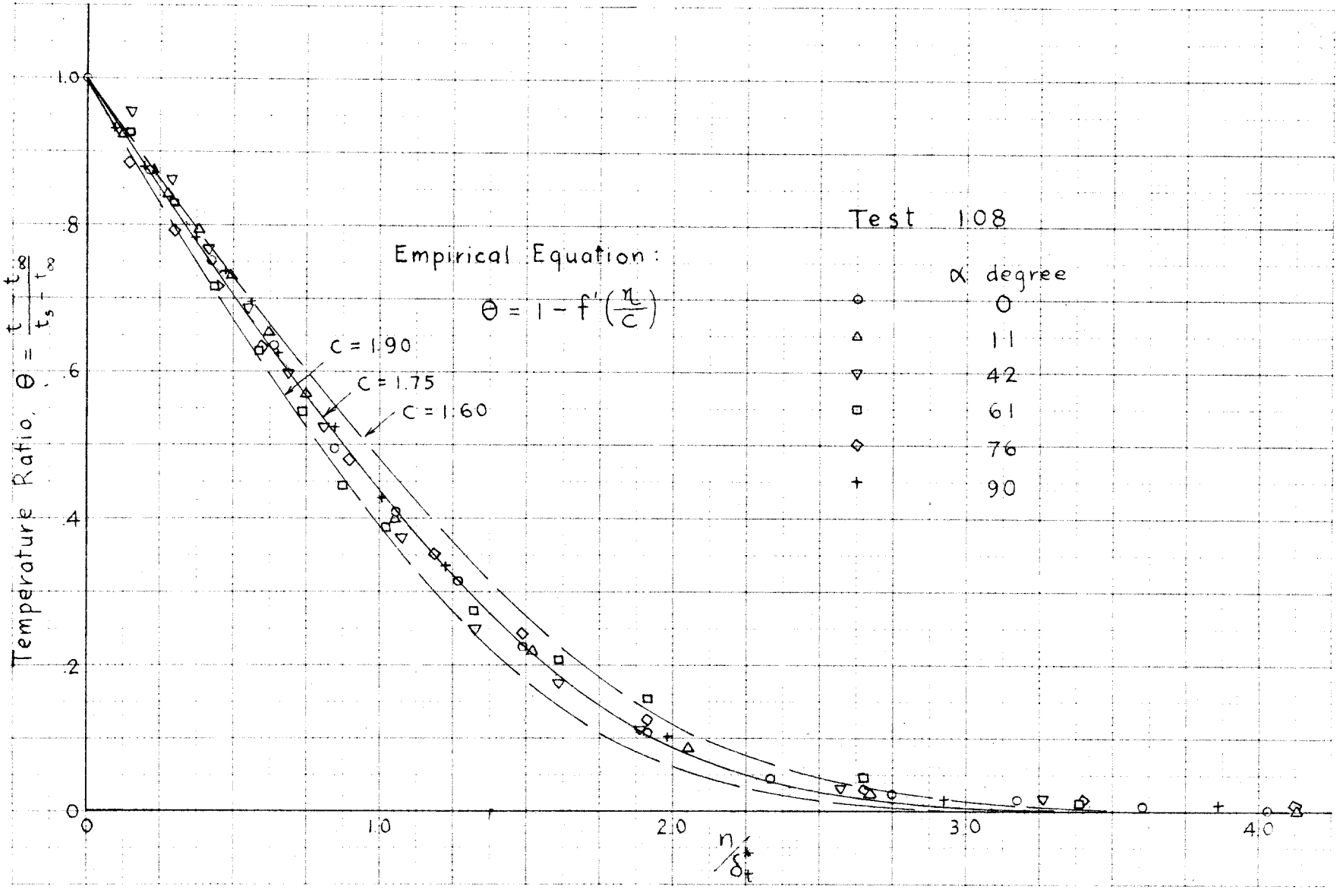

Fig. 16-B Temperature Distribution in the Thermal Boundary Layer - Test 108

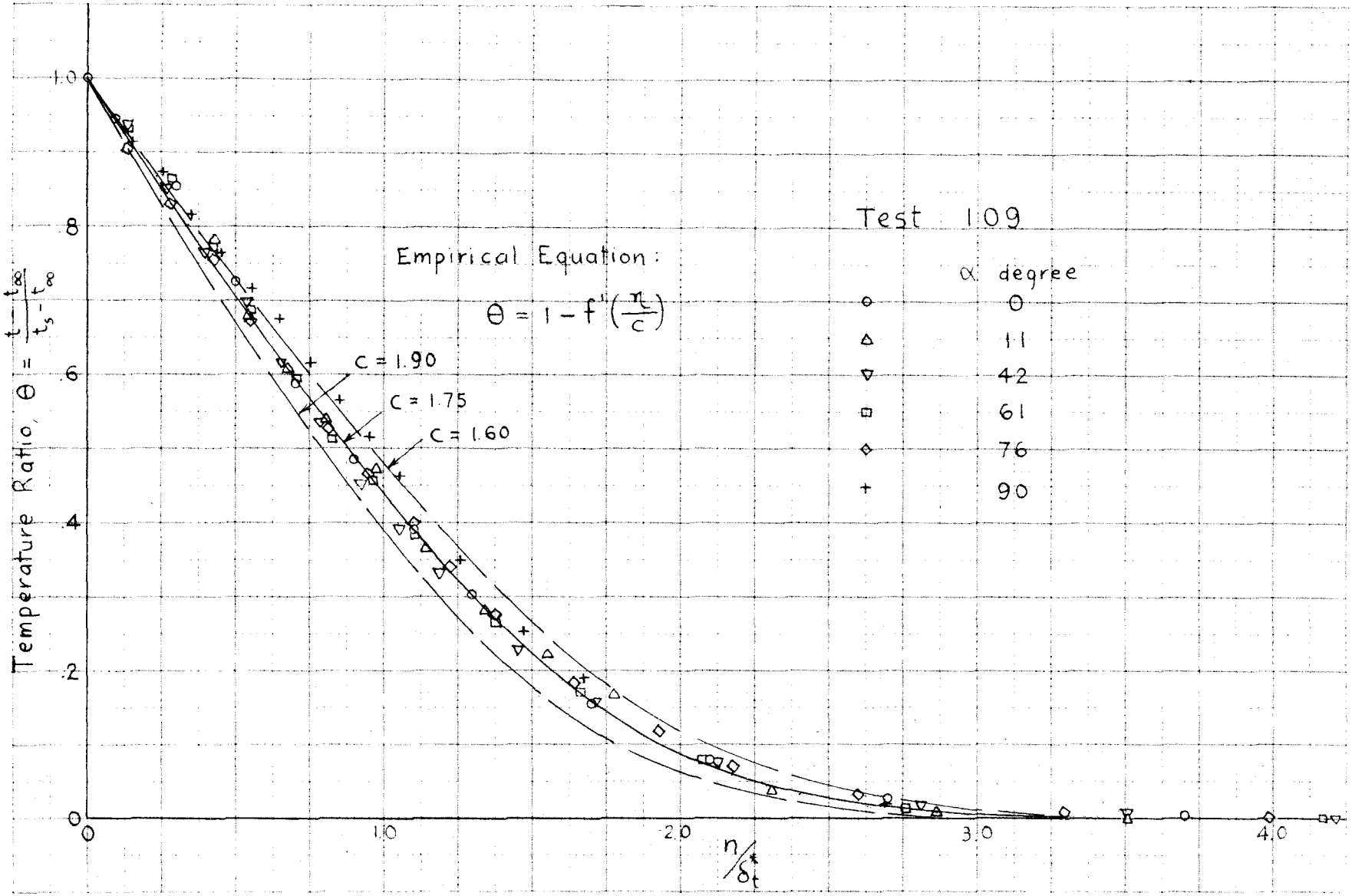

Fig. 16 - C Temperature Distribution in the Thermal Boundary Layer - Test 109

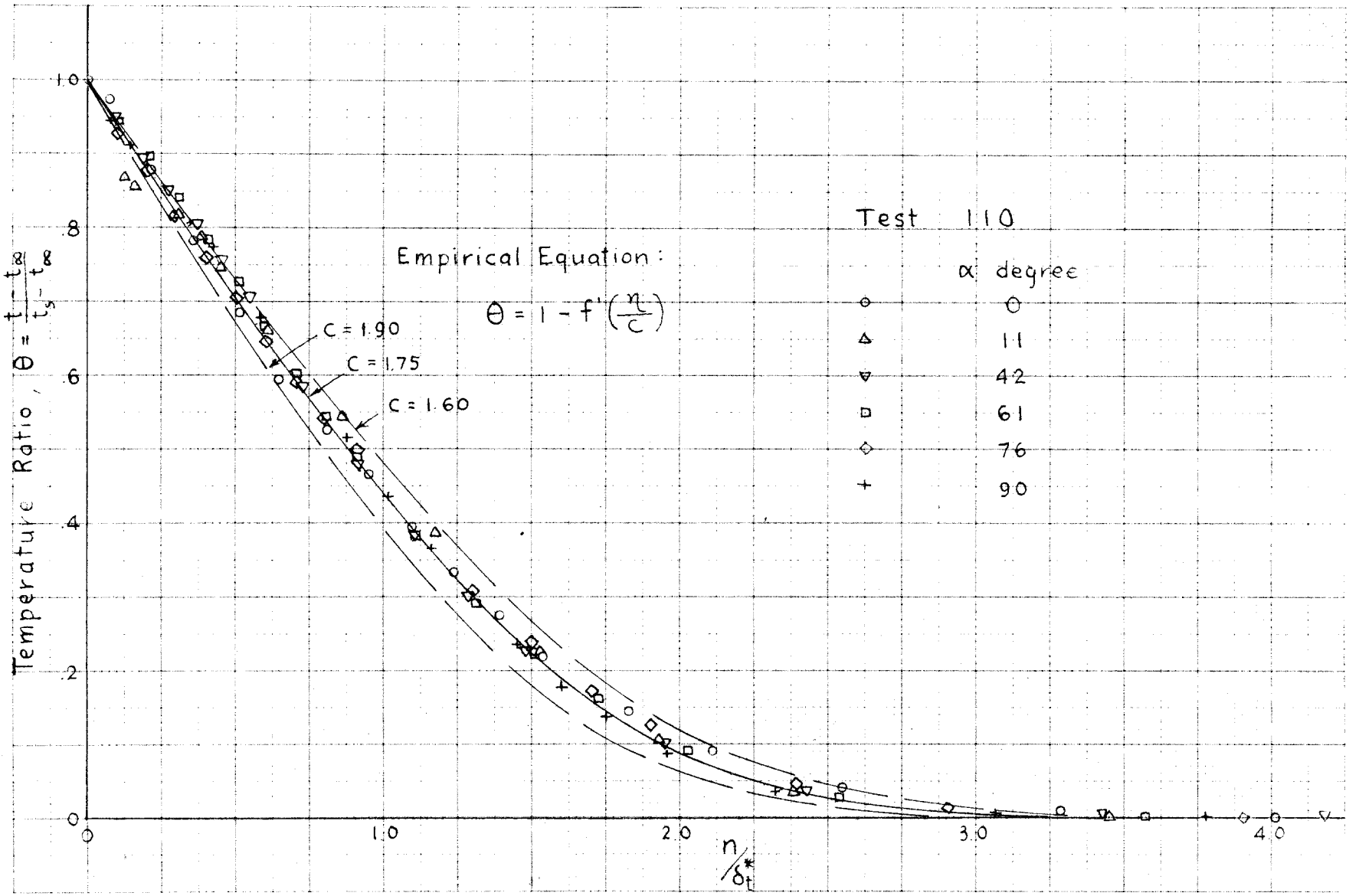

Fig. 16 - D Temperature Distribution in the Thermal Boundary Layer - Test 110

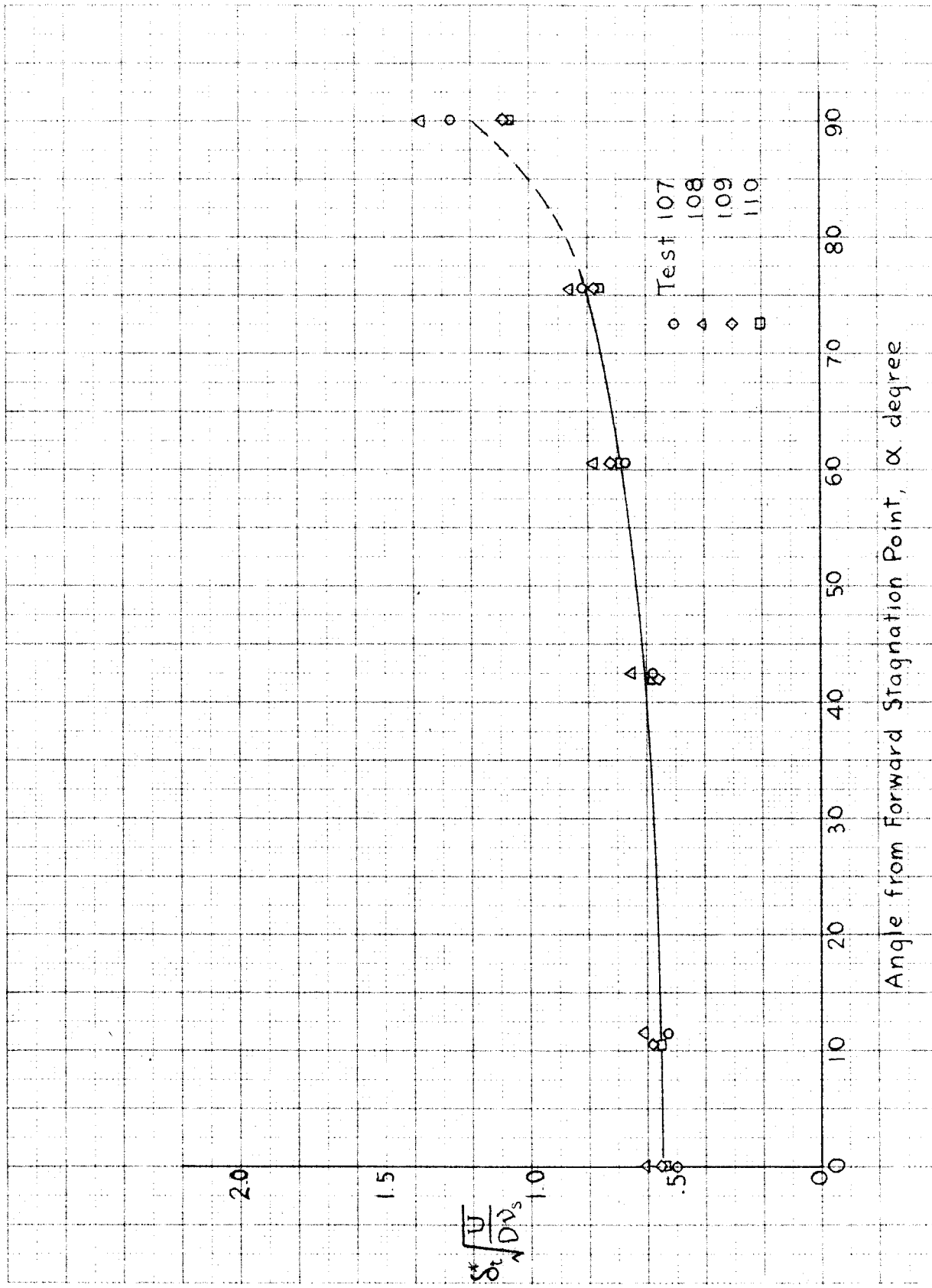

Fig 17 $\delta_t^* \sqrt{\frac{U}{D\nu_s}}$ as Function of Angular Position

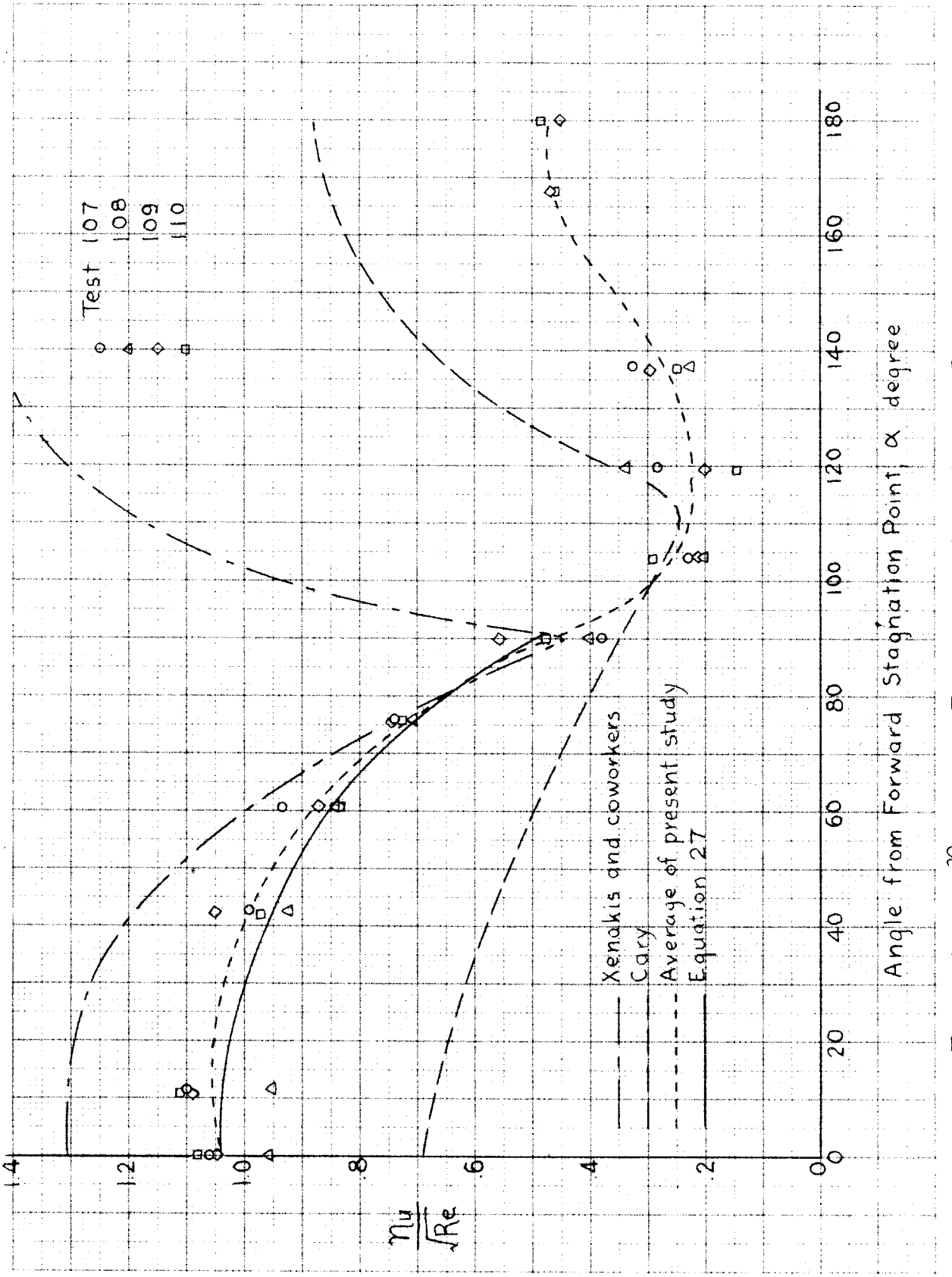

Fig. 18 $\frac{Nu}{\sqrt{Re}}$ as Function of Angular Position

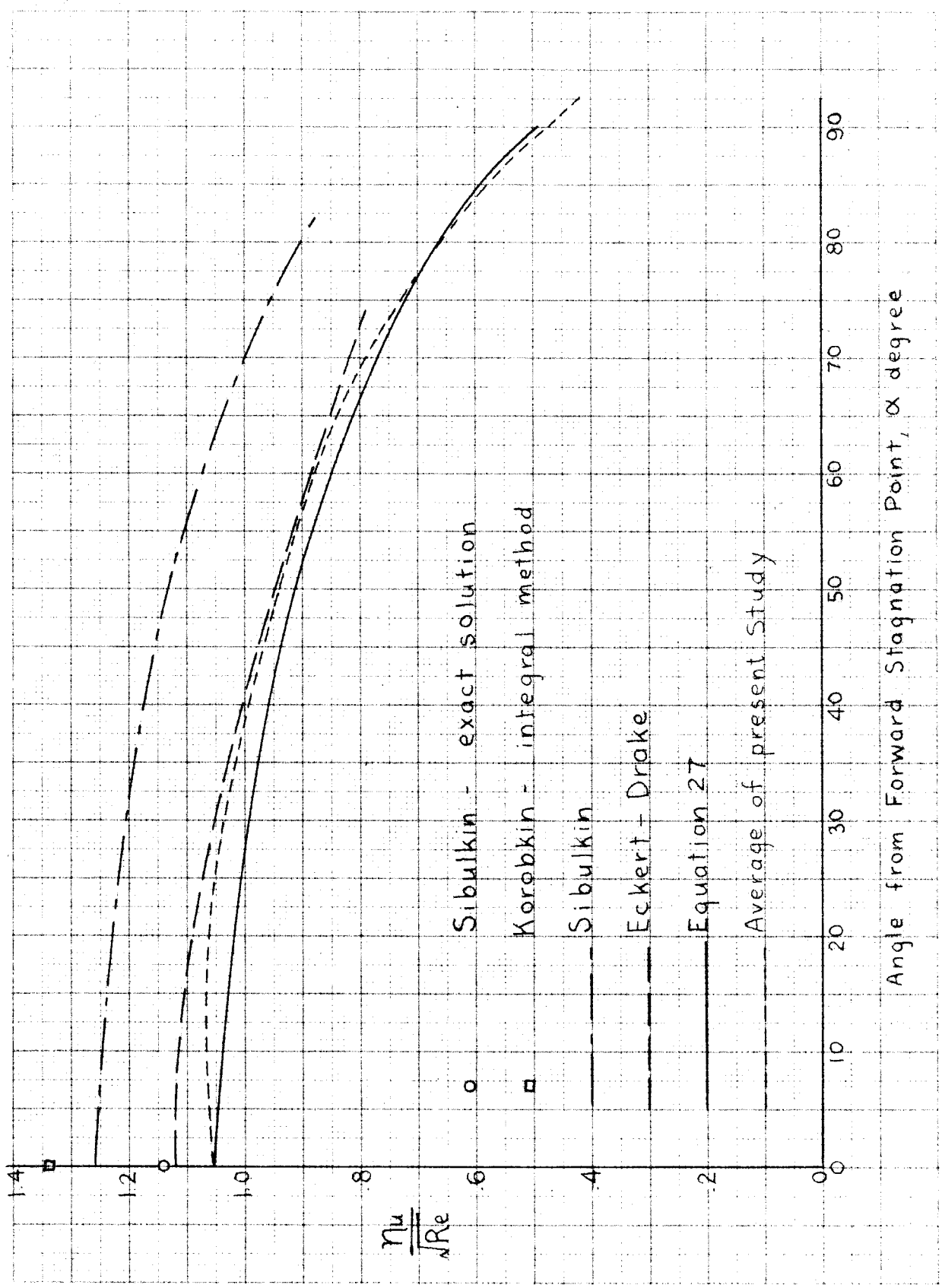

Fig 19 $\frac{Nu}{\sqrt{Re}}$ as Function of Angular Position

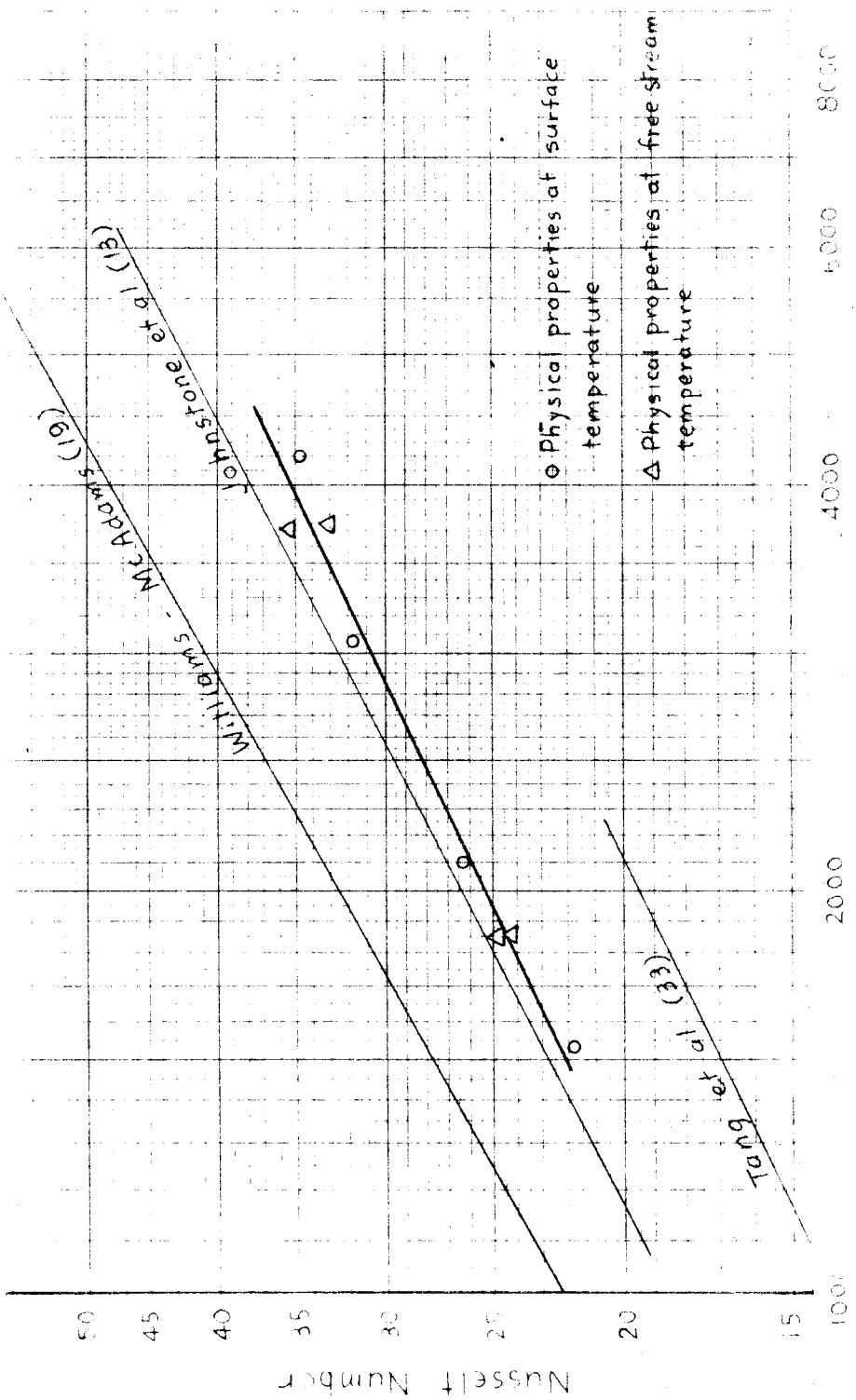

Fig. 20 Comparison of Gross Thermal Transfer

LIST OF TABLES

Table I

Experimental Conditions

	Test Number			
	107	108	109	110
Sphere				
Type	porous	porous	silver	silver
Diameter, in	0.500	0.500	0.500	0.500
Total heptane evap. rate x 10^6 lb/sec	3.878	5.515	-	-
Total energy input x 10^3 Btu/sec	-	-	1.533	1.094
Average surface temperature, ^oF	63.2	63.4	169.7	170.2
Temp. of liq. heptane entering sphere, ^oF	96.9	97.9	-	-
Air Stream				
Bulk velocity, ft/sec	8.04	16.23	16.13	8.06
Bulk temperature, ^oF	100.1	100.1	100.1	100.1
Pressure, lb/sq. in. abs.	14.349	14.308	14.369	14.277
Weight fraction water	0.0065	0.0061	0.0030	0.0042
Turbulence level, %	5.6	5.2	5.2	5.6
Reynolds number, $\frac{DU}{\nu_s}$	2100	4200	3060	1530

Table II

Measurements of Temperature Distribution - Test 107

Vertical traverse below sphere at Z = 0 in. ($\alpha = 0^\circ$)

X	t_{expt}	t_{corr}	r_{calc}
in.	°F	°F	in.
-.274	100.1	100.1	
-.271	99.8	99.8	
-.269	99.5	99.5	
-.267	98.9	98.9	
-.265	98.4	98.4	
-.263	97.8	97.8	"
-.261	95.2	95.2	"
-.260	94.0	94.0	"
-.259	92.3	92.3	
-.258	90.5	90.3	
-.257	88.5	87.8	
-.256	86.2	85.3	
-.255	83.5	82.5	
-.254	80.6	79.6	
-.253	77.6	76.7	
-.252	74.4	73.3	
-.251	70.5	69.1	
-.250*	63.6	61.6	

Horizontal traverse at X = -.250 in. ($\alpha = 11.5^\circ$)

Z	t_{expt}	t_{corr}	r_{calc}
in.	°F	°F	in.
.111	100.1	100.1	.2735
.101	99.8	99.8	.2696
.091	99.2	99.2	.2660
.081	97.2	97.2	.2628
.076	95.5	95.2	.2609
.071	93.4	93.1	.2599
.066	90.8	90.3	.2586
.061	87.9	87.4	.2573
.056	85.0	84.3	.2562
.051	82.0	81.2	.25515
.046	79.4	78.5	.2542
.041	76.7	75.8	.2533
.036	74.4	73.4	.2526
.031	72.0	70.9	.2519
.026	69.9	68.6	.25135
.023	68.4	66.9	.2511
.021	67.8	66.3	.2509
.019	66.6	64.9	.2507
.017	65.4	63.5	.2506
.015	64.8	62.8	.25045

*Indicates surface point.

Table II (cont'd)

Horizontal traverse at X = -.188 in. ($\alpha = 42.5^\circ$)

Z in.	t_{expt} °F	t_{corr} °F	r_{calc} in.
.201	100.1	100.1	.2752
.191	99.2	99.2	.2680
.186	97.5	97.5	.2645
.183	95.5	95.3	.2624
.181	94.0	93.7	.2610
.179	91.7	91.4	.2596
.177	88.8	88.4	.2582
.175	85.6	85.1	.2568
.173	81.8	81.3	.2555
.171	77.3	76.6	.2541
.169	72.6	71.6	.2528
.168	70.5	69.6	.2521
.167	68.4	67.5	.2515
.166	66.9	65.8	.2508
.165*	63.0	61.5	.2500

Horizontal traverse at X = -.125 in. ($\alpha = 60.6^\circ$)

Z in.	t_{expt} °F	t_{corr} °F	r_{calc} in.
.251	100.1	100.1	.2804
.241	99.5	99.5	.2715
.236	97.8	97.8	.2671
.231	93.7	93.4	.26265
.229	91.4	91.2	.2609
.227	87.9	87.5	.2591
.225	84.1	83.6	.2574
.223	80.3	79.8	.2556
.222	78.2	77.2	.2548
.221	75.8	75.2	.2539
.220	72.6	71.7	.2530
.219	70.5	69.8	.2522
.218	67.2	66.2	.2513
.217	64.8	63.6	.2504
.2165*	63.9	62.6	.2500

Table II (cont'd)

Horizontal traverse at X = -.063 in. (α = 75.7°)

Z	t_{expt}	t_{corr}	r_{calc}
in.	°F	°F	in.
.282	100.1	100.1	.28895
.272	99.8	99.8	.2792
.262	96.9	96.9	.2695
.260	95.5	95.3	.2675
.258	93.7	93.6	.2656
.256	91.4	91.3	.2636
.254	88.5	88.3	.2617
.252	85.3	85.1	.2598
.250	81.8	81.5	.2578
.248	77.6	77.1	.2559
.247	75.5	75.0	.2549
.246	72.9	72.4	.2539
.245	70.5	69.9	.2530
.244	68.4	67.8	.2520
.243	66.3	65.4	.2510
.242*	63.3	62.1	.2500

Horizontal traverse at X = 0 in. (α = 90.0°)

Z	t_{expt}	t_{corr}	r_{calc}
in.	°F	°F	in.
.304	100.1	100.1	
.294	99.8	99.8	
.284	98.9	98.9	
.279	97.5	97.5	
.274	94.9	94.9	
.270	91.7	91.7	
.268	89.7	89.7	
.266	87.0	86.9	
.264	84.1	83.9	
.262	81.2	80.9	
.260	78.2	77.9	
.258	75.3	75.0	
.256	72.3	72.0	
.255	70.8	70.5	
.254	69.3	69.0	
.253	68.4	68.1	
.252	67.2	66.9	
.251	66.3	65.9	
.250*	64.2	63.7	

Table II (cont'd)

Horizontal traverse at X = .062 in. ($\alpha = 104.1^{\circ}$)

Z	t_{expt}	t_{corr}	r_{calc}
in.	°F	°F	in.
.311	100.1	100.1	
.301	99.8	99.8	
.291	99.2	99.2	
.281	96.3	96.3	
.276	93.4	93.4	
.273	91.1	91.1	
.271	89.4	89.2	
.269	87.9	87.7	
.267	86.5	86.3	
.265	84.7	84.6	
.263	82.6	82.5	
.261	80.6	80.4	
.259	78.8	78.6	
.257	77.0	76.8	
.255	75.3	75.1	
.253	73.2	72.9	.2605
.251	71.7	71.3	.2585
.249	70.2	69.8	.2566
.247	69.0	68.6	.2547
.245	67.8	67.4	.2527
.243	66.3	65.8	.2508
.242*	65.7	65.2	.2500

Horizontal traverse at X = .125 in. ($\alpha = 119.4^{\circ}$)

Z	t_{expt}	t_{corr}	r_{calc}
in.	°F	°F	in.
.323	100.1	100.1	
.313	99.8	99.8	
.303	99.5	99.5	
.293	97.5	97.5	
.288	95.5	95.5	
.283	92.9	92.9	
.278	89.7	89.7	
.273	86.5	86.5	
.268	83.2	83.2	
.263	80.3	80.3	
.258	78.2	78.2	
.253	77.3	77.3	
.243	76.1	76.1	
.238	75.0	75.0	
.233	73.8	73.8	
.228	72.0	71.8	.2600
.223	69.3	69.0	.2556
.221	68.1	67.8	.2539
.219	67.2	66.9	.2522
.217	65.7	65.3	.2504
.216*	63.9	63.4	.2495

Table II (cont'd)

Horizontal traverse at X = .187 in. (α = 137.1°)

Z	t_{expt}	t_{corr}	r_{calc}
in.	°F	°F	in.
.324	100.1	100.1	
.314	99.5	99.5	
.304	98.1	98.1	
.294	95.5	95.5	
.289	93.4	93.4	
.284	91.1	91.1	
.279	88.5	88.5	
.274	85.9	85.9	
.269	84.1	84.1	
.264	82.9	82.9	
.254	82.9	82.9	
.244	83.8	83.8	
.234	85.0	85.0	
.224	85.0	85.0	
.214	84.4	84.3	
.204	82.3	82.3	
.194	78.8	78.7	
.189	77.3	77.2	
.184	75.0	74.7	
.179	73.2	72.9	.2589
.174	70.8	70.5	.2554
.172	69.6	69.3	.2541
.170	68.7	68.3	.2527
.168	67.8	67.4	.2514
.167	67.2	66.8	.2507
.166*	64.8	64.2	.2500

Horizontal traverse at X = .250 in.

Z	t_{expt}
in.	°F
.331	100.1
.321	99.8
.311	98.9
.301	96.9
.291	94.0
.286	92.6
.281	90.5
.276	88.8
.271	87.3
.261	85.9
.251	86.2
.241	87.0
.231	87.7
.221	88.5
.211	88.8
.201	88.5
.191	88.5
.181	88.5
.171	88.2
.161	87.9
.151	87.7
.141	87.3
.121	86.2
.101	84.7
.081	81.8
.071	80.0

Table II (cont'd)

Horizontal traverse at X = .375 in.		Horizontal traverse at X = .500 in.		Horizontal traverse at X = .625 in.	
Z	t_{expt}	Z	t_{expt}	Z	t_{expt}
in.	°F	in.	°F	in.	°F
.366	100.1	.366	100.1	.391	100.1
.341	99.8	.341	99.5	.366	99.8
.316	98.4	.316	98.4	.341	99.5
.291	94.3	.291	95.8	.316	98.7
.266	90.0	.266	92.9	.291	97.2
.241	89.4	.241	91.1	.266	95.2
.216	90.2	.216	90.8	.241	93.7
.191	90.8	.191	91.1	.216	92.6
.166	91.4	.166	91.4	.191	92.0
.141	91.4	.141	91.7	.166	92.3
.116	91.7	.116	91.7	.141	92.3
.091	91.7	.091	91.7	.116	92.3
.066	91.7	.066	92.0	.091	92.3
				.066	92.6

Table III

Measurements of Temperature Distribution - Test 108

Vertical traverse below sphere at Z = 0 in. ($\alpha = 0^\circ$)

X	t_{expt}	t_{corr}	r_{calc}
in.	°F	°F	in.
-.269	100.1	100.1	
-.267	99.8	99.8	
-.265	99.5	99.5	
-.263	99.2	99.2	
-.261	98.4	98.4	
-.259	96.1	96.1	
-.257	92.0	91.7	
-.256	89.1	88.2	
-.255	85.6	84.7	
-.254	82.3	81.4	
-.253	77.6	76.1	
-.252	73.5	71.8	
-.251	69.0	67.3	
-.250*	64.5	62.4	

Horizontal traverse at X = -.250 in. ($\alpha = 11.5^\circ$)

Z	t_{expt}	t_{corr}	r_{calc}
in.	°F	°F	in.
.100	100.1	100.1	.2693
.090	99.8	99.8	.2657
.080	99.2	99.2	.2625
.075	98.4	98.4	.2610
.070	96.9	96.9	.2596
.065	95.2	95.0	.2583
.060	92.3	91.8	.2571
.055	89.4	88.7	.2560
.050	85.9	85.1	.25495
.045	82.3	81.4	.2540
.042	79.7	78.5	.2535
.040	78.2	77.0	.2532
.038	76.7	75.5	.2529
.036	75.3	73.9	.2526
.034	73.8	72.4	.2523
.032	72.6	71.2	.2520
.030	71.4	70.1	.2518
.028	70.5	69.2	.2516
.026	69.6	68.3	.25135
.024	69.0	67.7	.25115
.022	68.4	67.1	.2510
.020	67.5	66.2	.2508
.018	66.6	65.2	.2506

*Indicates surface point.

Table III (cont'd)

Horizontal traverse at X = -.188 in. (α = 42.5°)

Z	t_{expt}	t_{corr}	r_{calc}
in.	°F	°F	in.
.199	100.1	100.1	.2738
.189	99.5	99.5	.2666
.184	98.9	98.9	.2631
.179	96.1	95.9	.2596
.177	93.7	93.5	.2582
.175	91.1	90.8	.2568
.173	86.7	86.2	.2555
.171	81.2	80.5	.2541
.170	78.5	77.7	.2535
.169	75.3	74.3	.2528
.168	72.3	71.4	.2521
.167	68.7	67.9	.2515
.166	65.4	64.3	.2508
.165*	64.2	62.6	.2500

Horizontal traverse at X = -.125 in. (α = 60.6°)

Z	t_{expt}	t_{corr}	r_{calc}
in.	°F	°F	in.
.250	100.1	100.1	.2795
.240	99.8	99.8	.2706
.235	98.4	98.4	.2662
.230	94.6	94.4	.2618
.228	92.6	92.4	.2600
.226	90.0	89.8	.2583
.224	85.9	85.6	.2565
.223	83.8	83.5	.2556
.222	80.3	79.8	.2548
.221	77.3	76.7	.2539
.220	74.1	73.4	.2530
.219	69.9	69.1	.2522
.218	66.6	65.6	.2513
.217*	64.2	62.8	.2504

Table III (cont'd)

Horizontal traverse at X = -.063 in. (α = 75.7°)

Z	t_{expt}	t_{corr}	r_{calc}
in.	°F	°F	in.
.280	100.1	100.1	.2870
.270	99.8	99.8	.2772
.265	99.5	99.5	.2724
.260	98.9	98.9	.2675
.255	95.5	95.3	.2626
.252	91.1	90.9	.2598
.250	87.0	86.8	.2578
.248	82.3	81.9	.2559
.246	76.7	76.1	.2539
.245	73.5	72.9	.2530
.244	70.5	70.0	.2520
.243	67.2	66.5	.2510
.242*	63.6	62.2	.2500

Horizontal traverse at X = 0 in. (α = 90.0°)

Z	t_{expt}	t_{corr}	r_{calc}
in.	°F	°F	in.
.301	100.1	100.1	
.291	99.8	99.8	
.281	99.5	99.5	
.271	96.3	96.3	
.266	92.0	91.8	
.263	87.9	87.7	r = z
.261	84.4	84.1	
.259	80.9	80.6	
.257	77.0	76.7	
.256	74.7	74.3	
.255	73.2	72.8	
.254	71.4	70.9	
.253	69.3	68.8	
.252	67.8	67.4	
.251	66.0	65.4	
.250*	63.9	62.9	

Table III (cont'd)

Horizontal traverse at X = .062 in. (α = 104.1°)

Z in.	t_{expt} °F	t_{corr} °F	r_{calc} in.
.310	100.1	100.1	
.300	99.8	99.8	
.290	99.5	99.5	
.285	98.9	98.9	
.280	97.5	97.5	
.275	94.3	94.2	
.270	89.7	89.5	
.268	87.7	87.5	
.266	85.4	85.1	
.264	82.9	82.7	
.262	80.6	80.3	
.260	78.2	78.0	
.258	76.7	76.6	
.256	75.0	74.8	
.254	73.2	73.0	
.252	71.4	71.1	.2595
.250	69.9	69.6	.2576
.248	68.7	68.4	.2556
.246	67.5	66.2	.2537
.244	65.7	65.3	.2518
.242*	64.2	63.7	.2500

Horizontal traverse at X = .125 in. (α = 119.4°)

Z in.	t_{expt} °F	t_{corr} °F	r_{calc} in.
.321	100.1	100.1	
.311	99.8	99.8	
.301	99.5	99.5	
.291	97.8	97.8	
.286	96.1	96.0	
.281	93.2	93.0	
.276	89.4	89.2	
.271	85.6	85.4	
.266	82.9	82.8	
.261	81.5	81.4	
.256	81.8	81.7	
.251	82.6	82.6	
.246	82.9	82.9	
.241	82.9	82.9	
.231	79.4	79.2	
.226	75.5	75.2	.2583
.221	70.5	70.0	.2539
.219	68.4	67.8	.2522
.217	65.4	64.8	.2504
.2165*	64.5	63.8	.2500

Table III (cont'd)

Horizontal traverse at X = .187 in. (α = 137.1°)

Z in.	t_{expt} °F	t_{corr} °F	r_{calc} in.
.323	100.1	100.1	
.313	99.5	99.5	
.303	98.7	98.7	
.293	95.8	95.8	
.288	93.7	93.7	
.283	91.1	91.0	
.278	89.4	89.2	
.273	87.7	87.6	
.268	86.5	86.4	
.263	86.1	86.2	
.253	87.3	87.3	
.243	87.7	87.7	
.233	87.9	87.9	
.223	87.3	87.2	
.213	86.2	86.1	
.203	84.7	84.6	
.193	81.5	81.3	
.183	77.0	76.7	
.178	74.7	74.3	.2582
.173	70.8	70.8	.25475
.171	69.3	68.8	.2534
.169	67.8	67.3	.25205
.167	66.3	65.7	.2507
.166*	65.7	65.1	.2500

Horizontal traverse at X = .250 in.

Z in.	t_{expt} °F
.340	100.1
.330	99.8
.320	99.5
.310	98.7
.300	97.2
.290	94.6
.285	92.9
.280	91.7
.270	89.7
.260	89.1
.250	89.7
.240	90.0
.230	90.5
.220	90.8
.200	91.1
.180	91.4
.160	91.4
.140	91.7
.120	91.7
.110	91.4
.100	91.4
.090	90.8
.080	90.0
.070	88.8

Table III (cont'd)

Horizontal traverse at X = .375 in.		Horizontal traverse at X = .500 in.		Horizontal traverse at X = .625 in.	
Z in.	t_{expt} °F	Z in.	t_{expt} °F	Z in.	t_{expt} °F
.390	100.1	.390	100.1	.390	100.1
.365	99.8	.365	99.8	.365	99.8
.340	99.5	.340	99.5	.340	99.5
.315	98.4	.315	98.4	.315	98.7
.290	95.5	.290	96.6	.290	97.8
.265	92.6	.265	94.9	.265	96.6
.240	92.0	.240	93.7	.240	95.8
.215	92.3	.215	93.2	.215	94.9
.190	92.9	.190	93.2	.190	94.3
.165	92.9	.165	93.4	.165	94.3
.140	93.1	.140	93.4	.140	94.3
.115	93.4	.115	93.4	.115	94.3
.090	93.4	.090	93.7	.090	94.3
.065	93.4	.065	93.7	.065	94.3

Table IV

Measurements of Temperature Distribution - Test 109

Vertical traverse below sphere at Z = 0 in. ($\alpha = 0^{\circ}$)

X	t_{expt}	t_{corr}	r_{calc}
in.	°F	°F	in.
-.274	100.1	100.1	
-.269	100.4	100.4	
-.264	101.8	101.8	
-.261	105.2	105.3	M =
-.259	110.1	110.4	"
-.257	118.9	120.0	"
-.256	124.5	125.7	
-.255	130.3	132.0	
-.254	136.9	138.9	
-.253	145.3	147.9	
-.252	153.9	156.3	
-.251	160.8	162.5	
-.2505*	164.0	166.0	

Vertical traverse above sphere at Z = 0 in. ($\alpha = 180.0^{\circ}$)

X	t_{expt}	r_{calc}
in.	°F	in.
.374	113.8	
.371	114.1	
.361	114.1	
.351	114.1	M =
.341	114.1	"
.321	114.1	"
.301	114.6	
.291	115.2	
.281	116.3	
.271	118.6	
.266	122.9	
.263	127.5	
.261	131.4	
.259	136.3	
.257	144.2	
.256	147.5	
.255	151.5	
.254	155.5	
.253	159.9	
.252	162.9	
.251	165.3	
.250*	167.1	

*Indicates surface point.

Table IV (cont'd)

Horizontal traverse at X = -.251 in. (α = 10.4°)

Z	t_{expt}	t_{corr}	r_{calc}
in.	°F	°F	in.
.096	100.1	100.1	.2687
.086	100.7	100.7	.2653
.076	103.0	103.0	.2623
.066	112.1	112.9	.2595
.061	116.0	116.9	.2583
.056	120.5	121.4	.2572
.051	126.4	127.6	.2561
.046	134.1	135.8	.2552
.041	139.3	141.0	.2543
.036	144.5	146.1	.2536
.031	149.3	151.6	.2529
.026	156.6	159.5	.2523

Horizontal traverse at X = -.189 in. (α = 42.1°)

Z	t_{expt}	t_{corr}	r_{calc}
in.	°F	°F	in.
.195	100.1	100.1	.2716
.190	100.4	100.4	.2680
.185	101.3	101.3	.2645
.180	105.0	105.1	.2610
.177	110.1	110.4	.2589
.175	114.9	115.3	.2576
.173	121.4	122.0	.2562
.172	125.3	126.0	.25555
.171	129.2	130.0	.2549
.170	134.4	135.4	.2542
.169	139.9	141.0	.25355
.168	145.3	146.5	.2529
.167	149.6	151.0	.2522
.166	155.0	156.5	.25155
.165	160.3	162.3	.2509
.164*	163.7	166.4	.2502

Table IV (cont'd)

Horizontal traverse at X = -.126 in. (α = 60.4°)

Z	t_{expt}	t_{corr}	r_{calc}
in.	°F	°F	in.
.246	100.1	100.1	.2764
.236	101.0	101.0	.2675
.231	105.3	105.5	.2631
.228	111.8	112.1	.2605
.226	118.3	118.7	.2587
.224	126.4	127.0	.2570
.223	131.4	132.1	.2561
.222	135.2	136.1	.2552
.221	140.7	141.7	.2544
.220	146.9	148.0	.2535
.219	153.4	154.7	.2527
.218	159.5	161.0	.2518
.217	164.5	165.8	.2509
.216*	168.1	170.2	.2500

Horizontal traverse at X = -.064 in. (α = 75.5°)

Z	t_{expt}	t_{corr}	r_{calc}
in.	°F	°F	in.
.271	100.1	100.1	.2785
.266	100.7	100.7	.2736
.261	102.4	102.4	.2687
.258	105.0	105.0	.2658
.256	108.4	108.6	.2639
.254	112.7	112.9	.2619
.252	119.1	119.6	.2600
.251	123.6	124.2	.2590
.250	127.8	128.4	.2581
.249	132.5	133.1	.2571
.248	136.9	137.4	.2561
.247	142.1	142.7	.2552
.246	146.9	147.8	.2542
.245	152.6	153.6	.2533
.244	157.6	158.8	.2523
.243	162.9	164.0	.2513
.242*	168.4	170.9	.2503

Table IV (cont'd)

Horizontal traverse at X = -.001 in. (α = 90.0°)

Z in.	t_{expt} °F	t_{corr} °F	r_{calc} in.
.286	100.1	100.1	
.276	101.5	101.5	
.271	105.0	105.1	
.266	113.5	113.7	
.264	118.0	118.1	
.262	124.7	125.0	
.260	132.5	133.0	
.259	136.3	136.9	
.258	139.9	140.5	
.257	143.7	144.2	
.256	148.0	148.5	
.255	151.0	151.4	
.254	154.4	154.8	
.253	157.9	158.4	
.252	161.6	162.3	
.251	164.5	165.3	
.2495*	169.7	171.5	

Z = r

Horizontal traverse at X = .061 in. (α = 103.8°)

Z in.	t_{expt} °F	t_{corr} °F	r_{calc} in.
.296	100.1	100.1	
.286	100.7	100.7	
.281	101.8	101.8	
.276	105.0	105.1	
.271	110.7	110.9	
.268	116.3	116.5	
.266	120.3	120.5	
.264	124.5	124.7	
.262	129.2	129.5	
.260	134.4	134.7	
.258	138.8	139.1	
.256	143.4	143.7	
.254	148.3	148.6	
.252	152.8	153.3	.2592
.251	155.0	155.5	.2583
.250	157.1	157.7	.2573
.249	158.9	159.6	.25635
.248	160.5	161.1	.2554
.247	162.4	163.0	.2544
.246	163.7	164.3	.253$\frac{45}{}$
.245	165.3	165.9	.2525
.244	166.8	167.4	.2515
.243	168.4	169.0	.2506
.242*	170.0	170.8	.2496

Table IV (cont'd)

Horizontal traverse at X = .124 in. (α = 119.1°)

Z in.	t_{expt} °F	t_{corr} °F	r_{calc} in.
.307	100.1	100.1	
.297	100.4	100.4	
.287	101.3	101.3	
.282	103.0	103.0	
.277	106.1	106.1	
.272	111.0	111.0	
.267	118.0	118.1	
.262	126.7	126.8	
.259	131.4	131.5	
.257	134.7	134.8	
.252	141.0	141.2	
.247	145.3	145.5	
.242	148.5	148.7	
.237	151.5	151.6	
.232	154.2	154.4	
.227	158.7	159.0	.2587
.222	164.0	164.4	.2543
.219	167.9	168.5	.2517
.218	169.2	169.9	.2508
.217*	170.5	171.2	.2500

Horizontal traverse at X = .186 in. (α = 136.7°)

Z in.	t_{expt} °F	t_{corr} °F	r_{calc} in.
.306	100.1	100.1	
.296	100.4	100.4	
.286	101.5	101.5	
.276	105.3	105.3	
.271	109.0	109.0	
.266	114.1	114.1	
.261	119.1	119.2	
.256	125.0	125.1	
.251	129.4	129.6	
.246	132.8	132.8	
.241	134.7	134.8	
.236	135.2	135.2	
.226	134.1	134.1	
.216	132.2	132.2	
.206	132.8	132.8	
.196	136.1	136.2	
.191	140.4	140.8	
.186	145.0	145.5	
.181	150.2	150.7	.2595
.176	156.6	157.2	.2561
.171	163.4	164.3	.2527
.170	165.0	165.9	.2520
.169	166.6	167.5	.2513
.168	168.1	169.2	.2506
.167*	169.5	170.5	.2500

Table IV (cont'd)

Horizontal traverse at X = .249 in. (α = 167.5°)

Z	t_{expt}	r_{calc}
in.	°F	in.
.306	100.1	
.296	100.4	
.286	101.3	
.276	103.8	
.271	105.8	
.266	109.0	
.256	116.3	
.246	122.9	
.236	127.2	
.226	128.3	
.216	127.5	
.206	125.8	
.196	124.7	
.186	122.9	
.176	122.8	
.166	122.5	
.156	122.5	
.146	122.5	
.126	123.9	
.116	125.0	
.106	126.9	
.096	129.7	
.086	133.3	
.076	138.2	.2603
.066	146.4	.2576
.061	150.2	.2564
.056	153.6	.2553
.051	157.4	.2542
.046	161.3	.2532
.041	164.0	.2524
.039	165.0	.2520

Horizontal traverse at X = .374 in.

Z	t_{expt}
in.	°F
.316	100.1
.291	100.4
.266	102.7
.241	109.8
.216	118.0
.191	121.1
.166	119.4
.141	117.7
.116	116.0
.091	114.9
.066	114.4
.041	114.1
.016	113.8
.003	113.8

Table IV (cont'd)

Horizontal traverse at X = .499in.

Z in.	t_{expt} °F
.316	100.1
.291	100.4
.266	101.0
.256	101.8
.246	102.4
.236	103.8
.216	107.0
.191	110.7
.166	114.1
.141	115.2
.116	115.5
.091	114.9
.066	114.4
.041	113.8
.016	113.8
-.009	113.8

Horizontal traverse at X = .624 in.

Z in.	t_{expt} °F
.316	100.1
.291	100.4
.266	100.7
.241	101.5
.216	102.7
.191	104.7
.166	106.4
.141	108.1
.116	109.5
.091	110.4
.066	111.0
.041	111.2
.016	111.2
-.009	111.2

Table V

Measurements of Temperature Distribution - Test 110

Vertical traverse below sphere at Z = 0 in. ($\alpha = 0^{\circ}$)

X	t_{expt}	t_{corr}	r_{calc}
in.	°F	°F	in.
-.278	100.1	100.1	
-.273	100.7	100.7	
-.268	103.0	103.0	
-.265	106.4	106.4	
-.263	110.1	110.1	M
-.261	115.2	115.2	=
-.260	118.9	119.2	R
-.259	122.2	123.2	
-.258	126.4	127.5	
-.257	130.8	132.2	
-.256	135.0	136.3	
-.255	139.9	141.2	
-.254	145.6	147.2	
-.253	152.0	154.1	
-.252	158.4	160.6	
-.251	164.5	167.3	
-.2505*	166.1	169.1	

Vertical traverse above sphere at Z = 0 in. ($\alpha = 180.0^{\circ}$)

X	t_{expt}	r_{calc}
in.	°F	in.
.374	120.5	
.357	120.5	
.337	120.5	
.327	121.1	
.317	121.4	
.307	121.4	M = R
.297	122.5	
.287	124.2	
.277	125.8	
.267	135.0	
.264	140.4	
.259	145.8	
.257	149.9	
.255	154.7	
.253	160.1	
.252	162.4	
.251	165.3	
.250*	167.4	

*Indicates surface point.

Table V (cont'd)

Horizontal traverse at X = -.251 in. (α = 10.4°)

Z in.	t_{expt} °F	t_{corr} °F	r_{calc} in.
.111	100.1	100.1	.27445
.101	100.7	100.7	.2706
.096	101.5	101.5	.2687
.091	102.7	102.7	.2669
.086	104.7	104.8	.2653
.081	107.5	107.9	.2637
.076	111.2	111.8	.2623
.071	116.0	116.8	.26085
.066	121.7	122.6	.2595
.061	127.5	128.7	.2583
.056	133.6	135.0	.2572
.051	138.8	140.3	.2561
.046	143.1	144.6	.2552
.041	147.5	148.9	.2543
.036	151.2	152.8	.2536
.033	153.6	155.3	.2532
.031	154.7	156.4	.2529
.029	156.0	157.8	.2527
.027	157.4	159.2	.25245
.025	158.7	160.6	.25225
.023	160.0	162.0	.25205
.021	161.3	163.4	.2519
.019	161.9	163.9	.2517
.017	162.4	164.3	.2516

Horizontal traverse at X = -.189 in. (α = 42.1°)

Z in.	t_{expt} °F	t_{corr} °F	r_{calc} in.
.210	100.1	100.1	.2825
.200	100.4	100.4	.2752
.190	102.7	102.7	.2680
.185	107.0	107.1	.2645
.180	115.5	115.8	.2610
.178	120.3	120.8	.2596
.176	125.8	126.6	.25825
.174	132.2	133.1	.2569
.172	139.3	140.4	.2555
.170	147.5	148.9	.2542
.169	151.0	152.3	.25355
.168	154.4	155.8	.2529
.167	157.4	158.6	.2522
.166	160.5	161.7	.25155
.165	164.0	165.5	.2509
.164*	167.1	169.0	.2502

Table V (cont'd)

Horizontal traverse at X = -.126 in. (α = 60.4°)

Z in.	t_{expt} °F	t_{corr} °F	r_{calc} in.
.251	100.1	100.1	.2809
.241	102.1	102.1	.27195
.236	106.1	106.5	.2675
.233	111.0	111.4	.2649
.231	115.2	115.5	.2631
.229	120.0	120.4	.2614
.227	126.1	126.7	.2596
.225	133.3	134.0	.2579
.224	137.4	138.2	.2570
.223	141.2	142.2	.2561
.222	145.6	146.7	.2552
.221	149.9	150.9	.2544
.220	153.9	154.8	.2535
.219	157.9	158.8	.2527
.218	161.6	162.6	.2518
.217	165.3	166.4	.2509
.216*	168.4	170.0	.2500

Horizontal traverse at X = -.064 in. (α = 75.5°)

Z in.	t_{expt} °F	t_{corr} °F	r_{calc} in.
.281	100.1	100.1	.2882
.271	101.0	101.0	.2785
.266	103.3	103.3	.2736
.263	106.4	106.5	.2707
.261	108.7	108.8	.2687
.259	112.1	112.3	.2668
.257	116.6	116.9	.2649
.255	121.7	122.1	.2629
.253	127.5	127.9	.2610
.251	134.7	135.2	.2590
.250	138.0	138.4	.2581
.249	141.2	141.8	.2571
.248	145.0	145.6	.2561
.247	149.1	149.7	.2552
.246	152.8	153.5	.2542
.245	156.8	157.6	.2533
.244	160.8	161.7	.2523
.243	164.0	165.1	.2513
.242*	168.7	170.5	.2503

Table V (cont'd)

Horizontal traverse at X = -.001 in. (α = 90.0°)

Z	t_{expt}	t_{corr}	r_{calc}
in.	°F	°F	in.
.302	100.1	100.1	
.292	100.4	100.4	
.282	102.7	102.7	
.277	106.1	106.1	
.274	109.8	109.9	
.272	112.7	112.8	
.270	116.6	116.8	
.268	120.5	120.8	
.266	125.8	126.1	
.264	130.8	131.1	
.262	136.6	137.0	
.260	142.3	142.8	
.258	148.0	148.5	
.256	154.2	154.7	
.255	157.1	157.6	
.254	159.7	160.3	
.253	162.4	162.9	
.252	164.5	165.0	
.251	166.8	167.5	
.250*	170.2	171.4	

Horizontal traverse at X = .061 in. (α = 103.8°)

Z	t_{expt}	t_{corr}	r_{calc}
in.	°F	°F	in.
.302	100.1	100.1	
.292	101.3	101.3	
.282	105.5	105.6	
.277	110.4	110.6	
.272	117.2	117.5	
.267	125.6	125.9	
.264	131.4	131.8	
.262	135.8	136.1	
.260	139.3	139.7	
.258	143.1	143.6	
.256	147.7	148.2	
.254	151.5	151.9	
.252	155.2	155.7	.2592
.250	158.7	159.2	.2573
.249	160.3	160.8	.25635
.248	161.6	162.1	.2554
.247	163.2	163.7	.2544
.246	164.7	165.3	.25345
.245	166.1	166.6	.2525
.244	167.6	168.2	.2515
.243	169.2	169.8	.2506
.242*	170.8	171.5	.2496

Table V (cont'd)

Horizontal traverse at X = .124 in. (α = 119.1°)

Z	t_{expt}	t_{corr}	r_{calc}
in.	°F	°F	in.
.313	100.1	100.1	
.303	100.4	100.4	
.293	101.8	101.8	
.288	103.3	103.3	
.283	105.5	105.5	
.278	109.3	109.3	
.273	114.0	114.0	
.268	120.3	120.3	
.265	123.9	124.0	
.263	126.4	126.6	
.258	133.0	133.3	
.253	139.3	139.6	
.248	145.6	145.9	
.243	151.2	151.6	
.238	156.3	156.7	
.233	160.3	160.6	
.231	161.9	162.2	
.229	163.2	163.5	.2604
.227	164.5	164.8	.2587
.225	165.8	166.1	.2569
.223	167.4	167.7	.25515
.222	168.1	168.5	.2543
.221	168.7	169.0	.25345
.220	169.2	169.6	.2526
.219	170.0	170.4	.2517
.218	170.8	171.1	.2508
.217*	171.3	171.6	.2500

Horizontal traverse at X = .186 in. (α = 136.7°)

Z	t_{expt}	t_{corr}	r_{calc}
in.	°F	°F	in.
.311	100.1	100.1	
.301	100.4	100.4	
.291	101.5	101.5	
.281	104.1	104.1	
.276	106.1	106.2	
.271	109.8	109.9	
.266	113.8	113.9	
.261	118.0	118.1	
.256	122.9	123.1	
.251	128.1	128.3	
.246	133.0	133.3	
.241	137.4	137.7	
.236	141.0	141.2	
.231	143.7	143.9	
.226	145.6	145.7	
.221	145.8	145.8	
.211	147.4	147.4	
.201	150.2	150.3	
.196	151.5	151.6	
.191	153.4	153.5	
.186	156.3	156.5	
.181	159.2	159.5	.2595
.176	162.4	162.8	.2561
.171	165.5	166.0	.2527
.169	167.4	167.9	.2513
.168	168.1	168.7	.2506
.167*	169.2	169.7	.2500

Table V (cont'd)

Horizontal traverse at X = .249 in. (α = 167.5°)

Z in.	t_{expt} °F	r_{calc} in.
.311	100.1	
.301	100.4	
.291	101.0	
.281	102.7	
.271	105.8	
.261	111.5	
.251	118.3	
.241	125.8	
.231	131.7	
.221	135.5	
.211	136.9	
.201	136.6	
.181	134.7	
.161	133.6	
.141	133.6	
.121	136.3	
.111	138.8	
.101	141.2	
.091	144.0	
.081	147.5	
.071	151.5	.2589
.061	155.2	.2564
.051	159.2	.2542
.046	161.1	.2532
.041	162.9	.2524
.036	165.0	.2516
.031	166.8	.2509
.029	167.1	.2507

Horizontal traverse X = .374 in.

Z in.	t_{expt} °F
.311	100.1
.286	100.7
.261	103.3
.241	109.3
.221	116.9
.201	123.9
.181	127.2
.161	126.9
.136	125.2
.111	123.9
.086	121.9
.061	121.1
.036	120.8
.011	120.5
.004	120.5

Table V (cont'd)

Horizontal traverse at X = .499 in.

Z	t_{expt}
in.	°F
.311	100.1
.286	100.4
.261	101.3
.236	103.3
.211	107.5
.186	112.9
.161	117.5
.136	120.0
.111	120.5
.086	120.5
.061	120.0
.036	119.4
.011	119.1
-.014	119.1

Horizontal traverse at X = .624 in.

Z	t_{expt}
in.	°F
.286	100.1
.261	100.7
.236	101.5
.211	103.3
.186	105.3
.161	108.1
.136	110.7
.111	112.9
.086	114.1
.061	115.2
.036	115.5
.011	115.5
-.014	115.5

Table VI

Physical Properties of Air and n-Heptane

Property	Unit	°F	Value	Reference
Air*				
Thermal conductivity	$Btu/(ft^2)(sec)(^\circ F/ft)$	32	3.89×10^{-6}	(19,23)
		70	4.14	
		100	4.34	
		130	4.54	
		212	5.11	
Thermometric conductivity	ft^2/sec	70	$.230 \times 10^{-3}$	(23)
		100	.254	
		130	.280	
Kinematic viscosity	ft^2/sec	70	$.164 \times 10^{-3}$	(23)
		100	.181	
		130	.198	
n-Heptane (vapor)				
Thermal conductivity	$Btu/(ft^2)(sec)(^\circ F/ft)$	212	2.86×10^{-6}	(19)
		392	3.11	
n-Heptane (liquid)				
Thermal conductivity	$Btu/(ft^2)(sec)(^\circ F/ft)$	86	22.5×10^{-6}	(19)
		140	21.9	
Isobaric heat capacity	$Btu/(lb)(^\circ F)$	53.3	.520	(6)
		80.3	.537	
		98.3	.547	
Latent heat of vaporization	Btu/lb	77.0	156.8	(27)
		209.2	136.0	

*Dry air at standard atmospheric pressure.

Table VII

Experimental Results for Local Thermal Flux

Angular Position α degree	Surface Temperature t_s °F	Radial Temperature Gradient at Surface $\left(\frac{\partial t}{\partial n}\right)_{n=0}$ °F/ft	Local Thermal Flux $-\dot{q}$ Btu/(ft^2)(sec)	Thermal Transfer Coefficient h Btu/(ft^2)(sec)(°F)	Nusselt Number Nu	$\frac{Nu}{\sqrt{Re}}$
Test 107						
0	61.6	44.7×10^3	.182	4.74×10^{-3}	48.4	1.06
11.5	(61.6)	46.5	.190	4.93	50.3	1.10
42.5	61.5	42.2	.172	4.46	45.4	.990
60.6	62.5	38.6	.157	4.19	42.8	.935
75.7	62.0	30.8	.126	3.31	33.8	.738
90.0	63.7	15.1	.0622	1.71	17.3	.380
104.1	65.2	8.73	.0359	1.03	10.5	.230
119.4	63.4	11.4	.0468	1.27	12.9	.282
137.1	64.2	12.9	.0528	1.47	15.0	.328
Test 108						
0	62.4	56.2×10^3	.230	6.09×10^{-3}	62.2	.957
11.5	(62.4)	55.9	.228	6.06	61.8	.951
42.5	62.6	54.0	.222	5.92	60.1	.924
60.6	62.8	48.9	.201	5.40	54.7	.842
75.7	62.1	41.9	.171	4.51	46.0	.708
90.0	62.8	23.4	.0964	2.57	26.1	.401
104.1	63.7	11.4	.0468	1.29	13.0	.201
119.4	63.8	19.1	.0786	2.17	22.0	.339
137.1	65.1	13.2	.0541	1.54	15.7	.241

( ) Interpolated Value.

Table VII (cont'd)

Angular Position α degree	Surface Temperature t_s °F	Radial Temperature Gradient at Surface $-\left(\frac{\partial t}{\partial n}\right)_{n=o}$ °F/ft	Local Thermal Flux $\mathring{q}$ Btu/(ft^2)(sec)	Thermal Transfer Coefficient h Btu/(ft^2)(sec)(°F)	Nusselt Number ηu	$\frac{\eta u}{\sqrt{Re}}$
Test 109						
0	165.9	92.2×10^3	.443	6.73×10^{-3}	58.3	1.05
10.4	(166.0)	95.6	.459	6.97	60.5	1.09
42.1	166.4	92.4	.444	6.69	58.1	1.05
60.4	170.2	80.7	.390	5.57	48.0	.870
75.5	170.8	69.4	.336	4.74	40.9	.741
90.0	171.4	43.1	.208	2.92	25.2	.456
103.8	170.7	19.8	.0956	1.35	11.7	.211
119.1	171.2	18.9	.0915	1.29	11.1	.201
136.7	170.5	27.8	.134	1.91	16.4	.298
167.5	(167.4)	41.9	.201	2.99	26.0	.470
180.0	167.1	40.2	.193	2.89	25.0	.452
Test 110						
0	169.1	70.8×10^3	.340	4.93×10^{-3}	42.8	1.08
10.4	(169.1)	71.5	.344	4.98	43.2	1.11
42.1	168.9	62.8	.302	4.38	38.0	.973
60.4	170.0	54.7	.265	3.79	32.6	.836
75.5	170.4	48.1	.232	3.30	28.5	.730
90.0	171.4	31.8	.154	2.16	18.6	.477
103.8	171.5	19.4	.0939	1.31	11.3	.291
119.1	171.6	9.45	.0457	.639	5.51	.145
136.7	169.7	16.3	.0790	1.13	9.77	.250
167.5	(167.4)	29.7	.143	2.12	18.4	.469
180.0	167.3	30.7	.147	2.19	19.0	.485

Table VIII

Measured and Integrated Gross Convective Thermal Transfer

Values in Btu/sec x 10^3

Test No.	Measured				Integrated	
	$\dot{m}(H_g - H_\ell)$ Enthalpy Change	$\Sigma k_i A_i \frac{\partial t}{\partial x}$ Conduction through Feed-tube	$\dot{Q}_r$ Radiation Correction	$\dot{Q}$ Convection	$\dot{Q}$ Convection	% Diff.
107	.544	-.003	-.033	-.508	-.519	-2.2
108	.772	-.003	-.036	-.733	-.686	6.4
109	-	-	-	1.53	1.39	9.2
110	-	-	-	1.09	.967	11.3

Table IX

Experimental Displacement Thickness of the Thermal Boundary Layer

Values in ft.

α degree	Test Number 107	108	109	110
0	$.45 \times 10^{-3}$	$.39 \times 10^{-3}$	$.42 \times 10^{-3}$	$.57 \times 10^{-3}$
11	.48	.39	.44	.59
42	.53	.42	.42	.61
61	.61	.50	.53	.72
76	.75	.55	.59	.81
90	1.15	.88	.82	1.15

Table X

Experimental and Smoothed Values of $\delta_t^* \sqrt{\frac{U}{D\nu_s}}$

α degree	Test Number 107	108	109	110	Smoothed
0	.50	.61	.56	.54	.55
11	.53	.61	.58	.55	.56
42	.58	.65	.56	.57	.61
61	.67	.78	.72	.68	.69
76	.82	.86	.78	.76	.81
90	1.27	1.37	1.09	1.08	1.20

Table XI

Experimental and Correlated Local Thermal Flux

Values in Btu/(ft^2)(sec)

	Test Number							
	107		108		109		110	
α degree	Expt	Correlated	Expt	Correlated	Expt	Correlated	Expt	Correlated
0	.182	.183	.230	.256	.443	.460	.340	.326
11	.190	.179	.228	.248	.459	.438	.344	.321
42	.172	.167	.222	.230	.444	.402	.302	.296
61	.157	.141	.201	.201	.390	.379	.265	.267
76	.126	.123	.171	.173	.336	.326	.232	.230
90	.062	.080	.096	.115	.208	.230	.154	.156

PART II.

TEMPERATURE GRADIENTS IN TURBULENT GAS STREAMS

MEASUREMENT OF TEMPERATURE, ENERGY AND PRESSURE GRADIENTS

Investigation of Thermal Transfer **I&EC—April 1953**

A detailed knowledge of the distribution of temperature, thermal flux, and the pressure gradients associated with the turbulent flow of fluids is of importance in creating a background of experimental facts from which it is possible to predict the transfer characteristics for a particular physical situation.

Special methods and equipment employed in the measurement and control of temperature and thermal flux in an investigation of thermal transfer in turbulent gas streams are described. Measurements of the thermal flux and the pressure gradient are presented as a function of the imposed temperature distribution and macroscopic flow rate. They extend from gross velocities of 10 to 90 feet per second and to average temperature gradients as high as 1000° F. per foot.

The results represent a contribution to the knowledge of the shear and thermal flux associated with the nonisothermal flow of air between parallel plates. As expected, the thermal transfer coefficients for nonuniform transfer are larger than those obtained in this work under conditions of uniform transfer.

Reprinted from INDUSTRIAL AND ENGINEERING CHEMISTRY, Vol. 45, Page 864, April 1953

ENGINEERING AND PROCESS DEVELOPMENT

Temperature Gradients in Turbulent Gas Streams

Measurement of Temperature, Energy, and Pressure Gradients

W. G. SCHLINGER, N. T. HSU, S. D. CAVERS[1], AND B. H. SAGE

California Institute of Technology, Pasadena, Calif.

THERMAL flux and shear at the boundaries of a two-dimensional stream must be known in order to determine values of the eddy conductivity and eddy viscosity as a function of relative position in the flow channel. In addition, the distribution of velocity, thermal flux, and temperature within the body of the stream must be established. The present discussion is concerned with the measurements of temperature, thermal flux, and shear in a uniform, steady air stream. In this discussion, the term "uniform flow" implies that properties of the fluid and conditions of flow remain unchanged along the length of the channel.

The measurement and control of temperature offer problems of wide scientific and industrial interest. The basic information concerning the measurement of this undefined concept (*4, 13*) has been reviewed and assembled in a systematic form (*1*). No attempt is made here to enlarge or improve upon the basic methods of measurement. The equipment utilized in the determination of values of eddy conductivity and eddy viscosity (*18*) under conditions of steady, uniform flow has been described (*6*), and the results are available (*28–31*). In measurements of this type it is desirable to establish the temperature gradient in the vicinity of the solid boundary of the stream as well as in the turbulent core. The attainment of steady conditions requires careful attention to the control of temperature, thermal flux, and rate of flow. Measurement of the temperature of such a flowing stream with stationary instruments is not in itself a simple problem.

The arrangement of the apparatus (*6*) is shown schematically in Figure 1.

Essentially it involved a circulating air stream at *A* which passed between two parallel plates, *B* and *C*, each maintained at substantially uniform temperature by the longitudinal circulation of oil in ducts *D* and *E*. The channel where measurements were made was 11 inches in width, 0.75 inch in height, and 13 feet in length. The air stream was circulated by means of the blower, *F*, driven by a variable-speed motor. A refrigeration coil, *G*, and electric heaters, *H*, were provided to remove or supply energy at a steady rate. After passing the Venturi meter and its approach section, *I*, the air flowed through the control heater, *J*, and a grid-type resistance thermometer, *K*. After passing through a calming section and a set of screens at *L*, the air reentered the channel at *A*. The oil circulating systems, not shown in Figure 1, for the closed ducts, *D* and *E*, included axial-flow pumps, refrigeration coils, and electric heaters. These heaters supplied energy at a steady rate. Control was established by small grid-type heaters mounted in the oil circuit.

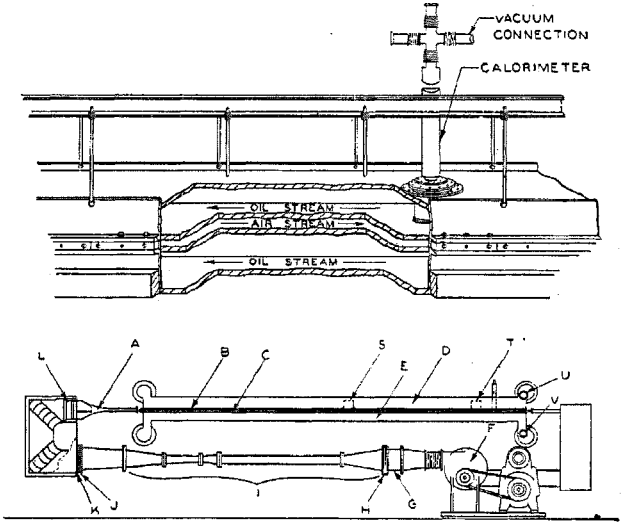

Figure 1. Schematic Arrangement of Flow Channel

[1] Present address, University of Saskatchewan, Saskatoon, Saskatchewan, Canada.

Arrangements were provided for traversing the channel by means of a mechanical gear which has been described (*6*). Thermocouples were provided in the upper and lower copper plates to establish the temperature at the boundary of the air stream. The temperature of the circulating oil was determined by means of strain-free resistance thermometers (*24, 25*). The thermal flux measurements normal to the flowing air stream were made at points *S* and *T* of Figure 1. The calorimeters employed to determine the thermal flux were located 8.3 and 12.7 feet downstream from the converging entrance section. The stream was substantially uniform in its properties and along the direction of flow the flux from plate to plate was not measurably different at these two points. Some minor variations in flux existed near the entrance and at the edges of the channel as a result of the thermal flow through the vertical walls.

Temperature Measurements

The temperature of the air stream was determined by means of the small resistance thermometer shown in Figure 2.

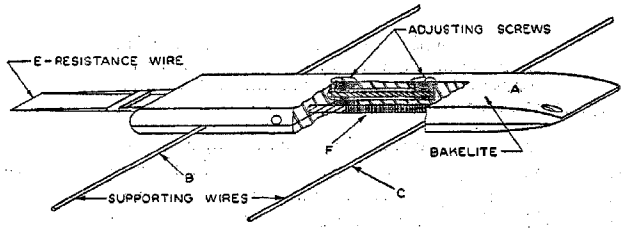

Figure 2. Support for Resistance Thermometer

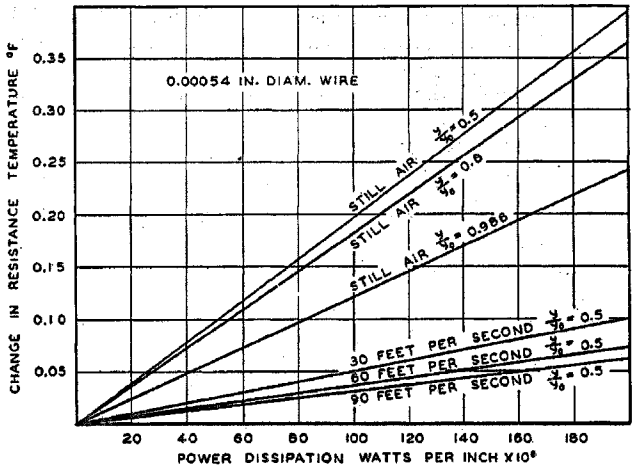

Figure 3. Temperature Change of 0.5-Mil Platinum Wire as Function of Power Dissipation

The assembly, *A*, was constructed of phenolic resin and was mounted on two steel wires, *B* and *C*. Each was stressed at a total tension of approximately 200 pounds. The wires formed a support for the thermometer which was relatively free from vibration at air velocities up to 100 feet per second. Two hardened steel needles were mounted in the plastic member, *A*, and supported the resistance wire, *E*. As shown in the cutaway section, *F*, provision was made for adjustment of the position of the end of one of the needles. This adjustment permitted the resistance thermometer to be arranged parallel to the wires, *B* and *C*. Dual platinum leads of No. 40 B. and S. gage wire were brought through *A* along the surface of the needles and served as the electrical leads to the 0.5-mil platinum thermometer which was mounted transverse to the stream. These leads were soldered to the fine wire by conventional microtechniques. The two No. 40 B. and S. gage platinum wire leads along each needle were insulated from the needle and each other by thin layers of lacquer. The platinum lead wires were also attached to *B* and *C* by means of lacquer, and a junction between the platinum and copper leads was made in a thermally insulated container outside the flow channel.

A current of 2.97×10^{-3} ampere was permitted to flow through the circuit and the electromotive force was measured by means of a White-type potentiometer with an uncertainty of about 0.2 microvolt. The current flowing was determined by measurement of the voltage across a standard resistance. Under these conditions corresponding to an energy dissipation of 4.85×10^{-5} watt, the average temperature of the wire in still air was approximately 0.3° F. above that of its surroundings. The magnitude of this inference was determined by measuring the resistance temperature of the wire as a function of thermal transfer from it under a number of conditions of flow. For point velocities above 10 feet per second the position in the flowing stream did not materially difluence the thermal transfer. However, at low velocities the thermal transfer was no longer a single-valued function of the point velocity but was influenced by the position in the flow channel.

Figure 3 presents data for the change in resistance temperature of a 0.00054-inch platinum wire as a function of power dissipation for several different positions in the channel. The data shown represent critically chosen values based upon present measurements and information correlated by McAdams (*21*). The present data for the center of the channel were in fair agreement with his correlations, which were used to establish the behavior in the center of the conduit shown in Figure 3. At velocities in excess of 100 feet per second the rise in the resistance temperature of the wire above the adiabatic wire temperature was less than 0.05° F. for a power dissipation of 129.3×10^{-6} watt per inch. This dissipation was employed in nearly all of the measurements. The detailed results of the experimental measurements of thermal transfer from small wires, which were made in the course of establishing the corrections shown in Figure 3, are available (*33*).

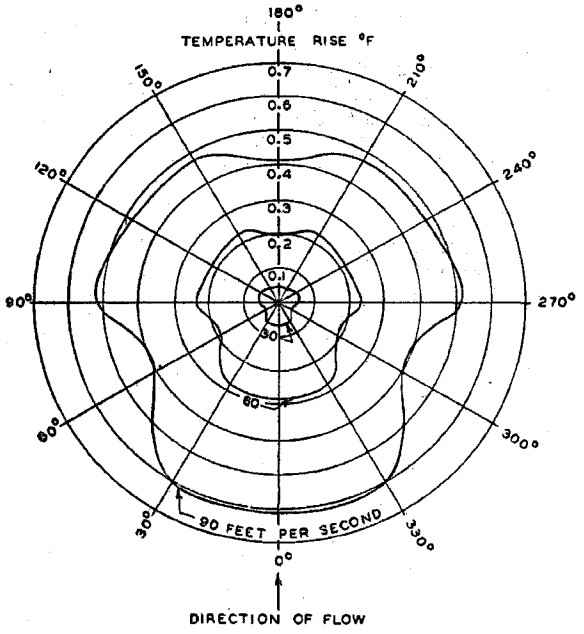

Figure 4. Estimated Temperature Distribution around an Adiabatic Wire in a Turbulent Air Stream

At relatively high velocities the impact temperature (*3, 8*) becomes important. Thermodynamically, the stagnation temperature, T_s, may be computed from the following expression:

$$T_s = T + \Delta T_s = T + \int_P^{P_s} \left(\frac{\partial T}{\partial P}\right)_s dP \backsimeq T + \frac{bT^*}{C_P} \ln \frac{P_s}{P} \backsimeq T + \frac{u^2}{2gC_P} \quad (1)$$

The second equality applies only to a perfect gas. The impact or stagnation temperature may not be realized at any point on the surface of the thermometer.

Figure 4 presents the estimated temperature distribution around a cylinder under the conditions of flow (*12*) encountered in

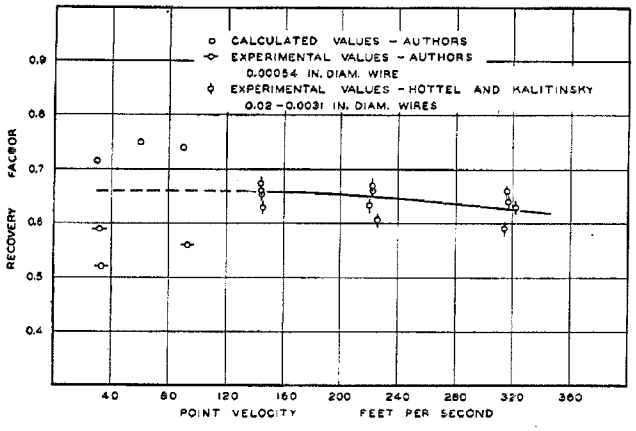

Figure 5. Recovery Factors for Small Wires Mounted Transverse to a Low Velocity Air Stream

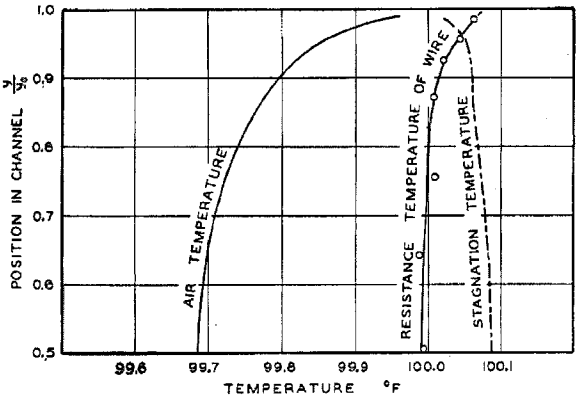

Figure 6. Temperature Distribution in an Adiabatic Air Stream

the channel. This distribution was based upon the existence of a laminar boundary layer around the wire and the behavior predicted for a flat plate (*10*) at that element of the surface of the wire parallel to the direction of flow. Such an assumption is open to question, but affords a simple means of estimating the temperature of the inner surface of the boundary layer at two points on the surface of the wire when there is no net thermal transfer from the wire.

The temperature on the side of the cylinder away from the oncoming stream was estimated by application of Equation 1 to the pressure distribution given by Goldstein (*12*) for the flow conditions within the channel. Likewise, the temperature of the wire at the side exposed to the oncoming stream was estimated by application of Equation 1 to the pressure distribution given by Goldstein, using the stagnation pressure as the constant of integration. These temperatures were corrected for the estimated variation in thermal transfer coefficient that existed around the wire. The results of these calculations are presented in Figure 4. The average temperature around the wire is a function of both the Prandtl number of the fluid and the Reynolds number of the flow about the wire as suggested by Eckert (*8*). The temperature distributions shown in Figure 4, which include a first-order correction of the thermal transfers to and from the wire, do not take into consideration the effect of the thermal conductivity of the wire in other than a semiquantitative fashion. However, these estimates of temperature distribution serve to illustrate the importance of flow conditions upon measurements of the temperature of a moving air stream.

For present purposes it is convenient to utilize the recovery factor concept (*3*) to determine the actual temperature of the flowing gas from the resistance of a small wire located transversely to the stream. This factor is defined conveniently in terms of the resistance temperature of the wire, the impact temperature as described by Equation 1, and the thermodynamic temperature of the gas in the stream. It may be established from

$$\xi = \frac{T_w - T}{T_s - T} \qquad (2)$$

Earlier studies (*5, 8, 9, 11, 14, 17, 23*) with air yielded recovery factors varying from 0.62 to nearly unity. More recently Hottel and Kalitinsky (*16*) measured the recovery factors for air with several sizes of circular wire at velocities from 140 to 320 feet per second. An average value of 0.66 was obtained for the lower velocities, which appeared to be nearly independent of wire size. The data of Hottel and Kalitinsky (*16*) appear to vary at the lower velocities from 0.62 to approximately 0.69. The recommended value is somewhat smaller than 0.69, which was obtained from Eckert's measurements for small wires at a velocity of 100 feet per second (*8, 9*). For longitudinally mounted wires agreement (*9, 22*) was obtained with the values predicted for a flat plate by Emmons and Brainerd (*10*). McAdams and coworkers (*22*) determined the recovery factor within Lucite tubes and obtained values varying between 0.875 and 0.905, which agreed reasonably well with predictions of Emmons and Brainerd, Polhausen (*32*), and Eckert and Weise (*9*), who estimated that the recovery factors for a flat plate should be the square root of the Prandtl number.

A series of confirmatory experimental measurements was made in order to ascertain whether the recovery factor at low velocities for air as measured by Hottel and Kalitinsky (*16*) was followed by the 0.5-mil platinum wire used in these investigations. The temperature of the air was carefully determined at L of Figure 1 and compared with the resistance temperature of the 0.5-mil wire. The temperature of this wire was determined as a function of the electrical energy added for each set of flow conditions and the temperature corresponding to no energy addition was employed as the adiabatic wire temperature. The detailed experimental data and the characteristics of the wire are available (*33*). These data were employed in establishing the ultimate corrections to be applied to measurements of the temperature of the air stream.

Figure 5 shows the measured recovery factor as a function of point velocity normal to the 0.5-mil wire as determined from these data under such conditions that the temperature of the channel wall corresponded to that of an adiabatic boundary (*22*). In this instance the predictions of Emmons and Brainerd (*10*) were used to establish the proper temperature for oil baths D and E of Figure 1 in order to obtain adiabatic conditions of flow. The equipment shown in Figure 1 is not as satisfactory for the measurement of recovery factors as that used by Hottel and Kalitinsky (*16*), but the results are in fair agreement with their data. As a matter of interest, recovery factor values calculated from the average temperature of the laminar boundary around the wire shown in Figure 4 have been included as points in Figure 5. The agreement between the predicted values and those measured experimentally is satisfactory for present purposes, where an uncertainty of 10% in the recovery factor corresponds to not more than 0.06° F. in the measured air temperature. For this investigation a recovery factor of 0.66 was employed (*16*).

As a second check upon the accuracy of gas temperature measurements, the temperature of the 0.5-mil platinum wire was measured as a function of position under conditions of substantially uniform adiabatic flow and at a wall temperature of 100° F. The results of these measurements are shown in Figure 6. For comparison, the stagnation temperature and the air temperature established from a recovery factor of 0.66 have been presented along with the adiabatic resistance temperature. The agreement of the air temperature at the wall with the adiabatic wall temperature of 100° F. is satisfactory.

McAdams and coworkers (*22*) have summarized corrections to the temperature measurements of gases arising from radiant transfers. For the conditions encountered in these studies the temperature difference between the resistance thermometer and the walls is small and in all cases the temperature of one wall is

above and the other is below that of the thermometer. For these reasons the maximum correction for radiant transfer at point velocities above 10 feet per second was about 0.01° F. and has been neglected here.

On the basis of the foregoing discussion it is possible to prepare an over-all correction for the resistance temperature of a platinum wire as a function of point stream velocity for several different energy dissipations. Figure 7 presents the difference in temperature between the 0.5-mil platinum wire as measured by its electrical resistance and that of the air stream as a function of the point velocity with power dissipation as a parameter. It is apparent that for power dissipations of practical utility the temperature difference reaches a minimum. Such behavior occurs because the correction is made up of the temperature rise resulting from the energy addition to the wire, required to measure its resistance, which decreases with increase in velocity and of a second term which increases rapidly with point velocity resulting from impact temperature rise.

The data of Figure 7 are based upon experiment, assuming a constant recovery factor of 0.66 (*16*), and correlated thermal transfer coefficient (*22*). They describe with reasonable accuracy the effect of air flow around small wires at velocities below 100 feet per second. There is still need for further experimental work upon the recovery factors of small wires at low velocity, if the temperature of the gas stream is to be determined with accuracy. The insert to Figure 7 shows the magnitude of the effect of position in the channel upon the behavior of the thermometer. All the curves in the main body of the figure apply to the center of the stream. Under such circumstances with a low convective transfer coefficient, radiation becomes important even at low temperatures. The problem of gas-temperature measurement becomes increasingly difficult as greater precision is desired. It is believed that the corrections of Figure 7 are known with sufficient accuracy to establish the temperature of the air stream relative to the resistance temperature of the wire within 0.01° F. for velocities less than 50 feet per second and within 0.05° F. for velocities between 50 and 100 feet per second.

From the corrections of Figure 7 the calibration of the resistance thermometer shown in Figure 2 was not difficult. It was carried out in still air by bringing the upper and lower plates, *B* and *C*, of Figure 1 to the desired temperature as indicated from the readings of resistance thermometers located at *U* and *V*. When all these thermometers were immersed in an agitated oil bath, they were compared with the resistance of an instrument calibrated by the National Bureau of Standards. It is believed that the temperatures of the oil baths were known relative to the international platinum scale (*1*) with an uncertainty of not more than 0.01° F. Thus the corrections in Figure 7 control the accuracy with which the temperature of the air stream was known, except for the gradual shift in the calibration of the small wire with time.

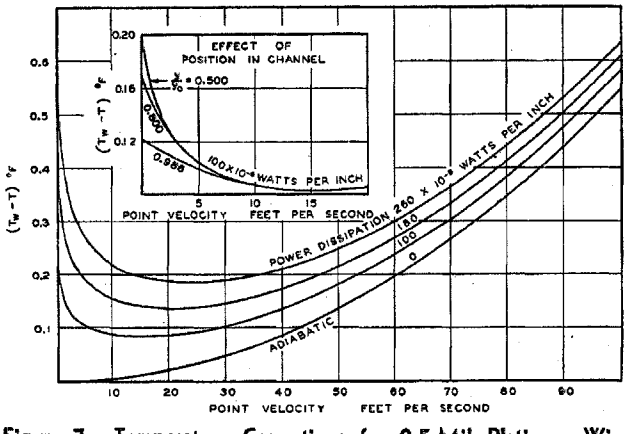

Figure 7. Temperature Corrections for 0.5-Mil Platinum Wire in a Turbulent Air Stream

The copper plates, *B* and *C* of Figure 1, showed little temperature difference along their length. Copper-constantan thermocouples of the multilead type, constructed from No. 36 B. and S. gage wire, were used to determine the surface temperatures. These thermocouples were located within 0.031 inch of the inner surface of each of the plates. The cold junctions of the thermocouples were located in an agitated ice bath at an average distance of approximately 10 feet from the points at which the temperatures were measured. A White-type double potentiometer with 10,000-microvolt range was employed to measure the electromotive force of these thermocouples. It is believed that the uncertainty in measuring the temperature of the plate surfaces was less than 0.01° F. These thermocouples were calibrated in place under quiescent conditions by the use of the resistance thermometers in the circulating oil baths. These thermometers were of the glass case, helium-filled, strain-free, four-lead type similar to those developed by the National Bureau of Standards (*1*, *24*). Mueller-type bridges were employed for the measurement of their resistance. A fixed low current was employed in the bridge circuit, so that the rise in temperature of the wire above the helium surrounding it was a reproducible function of temperature. The leads connecting the bridges to the resistance thermometers were of the four-lead type and were of No. 12 B. and S. gage copper wire except within the glass case of the thermometer. Without temperature control of the room in which the equipment was placed, significant changes in lead resistance were experienced. However, the conventional interchange of connections compensated the variation in the resistance of these relatively heavy leads. The arrangement of the temperature-measuring equipment which was located in a single temperature-controlled space has been presented (*6*).

Measurement of Thermal Flux

The equipment shown schematically in Figure 1 was so operated that there were very small temperature gradients in the direction of flow (*6*). For this reason substantially uniform thermal transfers to the flowing stream were realized when the temperatures of the upper and lower plates were maintained at different values. It was desired to determine the thermal flux through the stream under a variety of flow conditions and temperature gradients.

In order to make such measurements, two calorimeters were located in the upper plate along the axis of the channel (*6*) and are identified by points *S* and *T* of Figure 1. In principle, each calorimeter consisted of an isolated circular section of the upper plate approximately 3.25 inches in diameter and an electric heater located in the isolated section. The electrical energy necessary to maintain the section at the same temperature as the upper plate was determined. Precautions were taken to prevent thermal losses from the upper side of the isolated section, so that the energy added to the calorimeter corresponded, with but small correction, to that transferred to the flowing stream.

Figure 8 presents a sectional view of the calorimeter that was used (*6*). The associated adiabatic vacuum jacket and radiation shields are included in this figure.

The upper wall of the flow channel is shown at *A* and the thermocouple wells utilized to determine the average upper plate temperature in the vicinity of the calorimeter are indicated at *B*. The isolated circular section, *C*, was provided with a flat spiral type of recessed electrical heater at *D* which was covered by a second copper plate, *E*, provided with cooling coils, *F*. The temperature of the isolated section was determined by a thermocouple located in the well, *G*, whereas the temperature difference between the adjacent upper wall and the isolated section, *C*, was established from a four-junction couple located in wells such as *H* and *B*. The vacuum jacket, *J*, was attached to the isolated section as indicated in the insert of Figure 8. A serrated surface, *K*, was employed to decrease the contact between the upper wall and the isolated section. The entire jacket was assembled with silver solder, except for two joints which were made between brass sections with soft solder to facilitate final assembly. Stainless steel was employed in many parts of the equipment in order to obtain low thermal conductivity and to permit the use of thin sections because of the high tensile strength of this material. A series of gold-plated radiation shields was installed above the isolated section, *C* at *L*, and offset openings were provided in these shields for the electrical leads and tubing to carry the coolant.

Table I. Measurements of Thermal Flux

Test No.	Reynolds No.	Position[a], Feet	Plate Separation, Foot	Plate Temperature, ° F. Upper	Lower	Thermal Flux × 10², B.T.U./(Sq. Ft.)(Sec.) Gross	Net	Nusselt No.
74	19,830	12.5	0.0598	99.98	100.01	0.22	0.00	...
		8.1	0.0574	99.99	99.99	0.23	−0.01	...
76	18,070	12.5	0.0598	99.95	100.01	0.19	0.01	...
		8.1	0.0574	99.96	99.99	0.20	0.00	...
78	17,720	12.5	0.0598	114.82	114.87	0.26	0.02	...
		8.1	0 0574	114.83	114.83	0.24	−0.04	...
79	18,360	12.5	0.0599	114.60	85.30	22.81	22.57	42.53
		8.1	0.0574	114.59	85.53	22.32	22.08	40.20
80	17,080	12.5	0.0599	130.02	130.05	0.48	−0.09	...
		8.1	0.0574	130.00	130.01	0.56	−0.02	...
81	18,250	12 5	0.0598	129.20	70.60	44.94	44.72	42.06
		8.1	0.0574	129.16	71.10	44.59	44.37	40.43
87	35,500	12.5	0.0599	130.16	69.48	76.61	76.14	69.27
		8.1	0.0576	130.14	70.23	77.13	76.66	67.93
88	51,790	12.5	0.0599	130.10	130.06	1.93	0.00	...
		8.1	0.0576	130.08	130.00	2.12	−0.00	...
89	55,350	12.5	0.0599	130.03	69.54	106.10	105.26	96.07
		8.1	0.0576	129.99	70.42	106.97	106.13	94.58
91	9,670	12 5	0.0599	129.99	69.76	25.96	25.84	23.69
		8.1	0.0576	129.96	70.23	26.53	26.41	23.47
93	36,730	12.5	0.0599	114.87	114.89	0.70	0.04	...
		8.1	0.0576	114.86	114 86	0.63	−0.06	...
94	38,760	12.5	0.0599	115.02	84.87	40.17	39.65	72 60
		8.1	0.0576	115.01	85.11	40.54	40.02	71.05
156	18,940	12.5	0.0601	130.00	130.01	0.70	0.10	...
		8.1	0.0580	130.00	130.00	0.55	−0.06	...
156	6,630	12.5	0.0601	130.02	130.01	0.32	0.11	...
		8.1	0.0580	130.01	129.99	0.24	0.02	...
157	6,550	12.5	0.0601	130.01	69.85	17.72	17.64	16.24
		8 1	0.0580	129.96	70.12	18.57	18.49	16.52
158	18,580	12.5	0.0601	130.05	69.71	43 06	42.83	39 32
		8.1	0.0580	129.95	70.12	44.18	43.95	39.27

[a] Distance downstream measured from end of converging section.

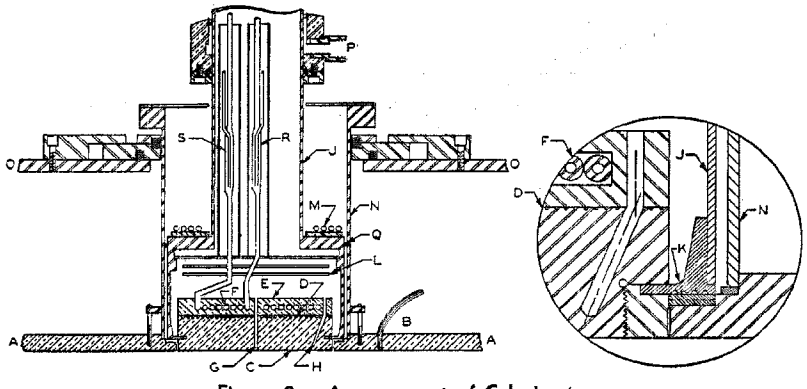

Figure 8. Arrangement of Calorimeter

A small auxiliary heater and a set of cooling coils were provided at M in order to decrease the temperature gradient along the vacuum jacket wall, J, in the vicinity of its junction with the isolated section. Differential thermocouples were provided to indicate the temperature gradients in the wall of the vacuum jackets from the auxiliary heater, M, to its junction with the isolated section, C. A rubber seal at Q prevented the flow of air into or out of the working section as a result of small static pressure differences between the flow channel and the atmosphere of the laboratory. An outer jacket, N, was installed to avoid contact of the oil bath with the vacuum jacket. Provision was made for the relative movement of the calorimeter and the cover plate of the oil bath, as has been described (*6*). The type of construction shown in Figure 8 was necessary because the upper plate, A, was constructed of copper and the oil bath cover, O, was of steel. Thus, relative motion between the two surfaces was obtained as a result of change in temperature. Provision was made at P for the circulation of oil from the oil bath around the vacuum jacket in order to avoid temperature gradients in the jacket. This arrangement also permitted the upper part of the jacket to be cooled, allowing the use of wax seals at the point at which the electric leads emerged from the vacuum jacket. Small electric heaters were provided to bring the temperature of leads R and S in the upper part of the jackets to the temperature of the isolated section.

The upper part of the vacuum jacket, J in Figure 8, was connected directly to an oil diffusion pump and a mechanical fore pump. Conventional compensated bellows were employed to permit the lateral movement of the calorimeter relative to the diffusion pump as shown in Figure 1. Refrigeration equipment was provided to cool the oil circulating through the isolated section, C, of Figure 8 when the upper plate was operating below the temperature of the lower plates. The temperature of the oil entering and leaving the section was determined by copper-constantan thermocouples introduced into the thin-walled stainless steel tubes at points R and S. The quantity of oil introduced was determined from the change in pressure through a flow circuit not shown in Figure 8. The cooling unit was calibrated by determining the electrical energy necessary to maintain section C at a constant temperature with known temperatures and temperature differences between R and S for a fixed rate of flow of oil through coils F.

A pressure somewhat below 0.2 micron was obtained during operation and the temperature of C was brought within 0.005° F. of plate A. Suitable adjustments to the heater and cooling coils at M were made to yield a negligible temperature gradient in the vacuum jacket, J, near its attachment to the isolated section, C. The energy from the heater, D required to maintain section C at the temperature of the upper plate was taken as the flux leaving plate A when corrected for small miscellaneous losses determined by direct calibration.

The thermal losses from the calorimeter were established under substantially isothermal quiescent conditions in the channel. The energy required to maintain the isolated section, C, at a series of temperatures above that of jacket J and plate A of Figure 8 was established The total miscellaneous transfers at a temperature difference of 0.01° F. between plate C and its surroundings by radiation and by conduction at the junction shown in the insert of Figure 8 were not more than 2% of the total transfer across the channel at a bulk air velocity of approximately 10 feet per second with a temperature difference of 10° F. between the plates shown in Figure 1.

Average values of the thermal conductivity of air as measured with the calorimeter under quiescent conditions were in fair agreement with critically chosen values (*28*) after appropriate corrections were made for the effects of humidity (*15*). The point temperature gradients in the air below the calorimeter were not constant and variations of as much as 10% were encountered near the upper and lower plates. The reason for this anomalous behavior is not clear at present. An average value of 4.16×10^{-6} B.t.u./(sec.) (° F.) (feet) was obtained for dry air at 100° F. when utilizing the corrections for humidity established by Hirschfelder *et al.* (*15*). This value is not believed to be an improvement over the critically chosen value (*28*) of 4.34×10^{-6} B.t.u./(sec.) (° F.) (feet) based upon earlier experimental work directed specifically to measurements of the thermal conductivity of air.

From measurements with the calorimeters described, the thermal flux was established as a function of conditions of flow. However, the physical situation was markedly different from that normally encountered in nonuniform, thermal transfer (*21*). Nevertheless, it is possible to utilize the conventional Nusselt number (*27*) for the purpose of correlating the measurements that have been obtained. They do not bear any direct relation-

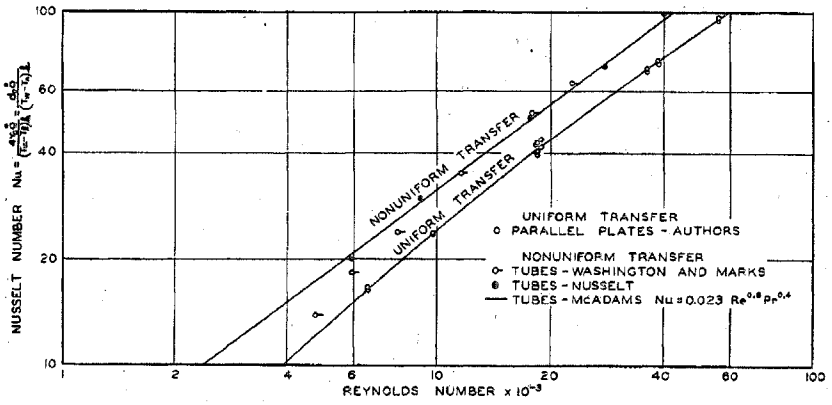

Figure 9. Influence of Reynolds Number upon Nusselt Number

Table II. Dimensionless Characteristics of Thermal Transfer and Shear for Air Flowing between Parallel Plates[a]

Reynolds No.	Nusselt No.	Friction Factor × 10³	Maximum Velocity Feet/Sec.
5,000	12.56	8.92	9.45
10,000	24.38	7.90	18.20
15,000	34.36	7.41	26.85
20,000	43.45	6.96	35.65
25,000	51.88	6.58	44.40
30,000	59.84	6.34	53.15
40,000	74.82	5.93	70.65
50,000	88.72	5.60	88.25
60,000	101.40	5.34	105.85

[a] Data of this table were obtained in a rectangular flow channel with a plate separation of 0.06 foot.

ship to existing correlations (*21*). Under the present circumstances the Nusselt number is defined by

$$Nu = \frac{8r_h\mathring{Q}}{(T_u - T_l)k} = \frac{4y_0\mathring{Q}}{(T_u - T_l)k} \quad (3)$$

The characteristic temperature difference has been taken as one half that between the two plates and the characteristic length as four times their hydraulic radius. The value of thermal conductivity was taken as that for air at the temperature at the midpoint of the channel. The Nusselt number was used to describe the present experimental data and is shown in Figure 9. It was lower than values predicted for nonuniform thermal transfer.

As a matter of interest the following relationship proposed by McAdams (*21*) for nonuniform thermal transfer

$$Nu = 0.023\ Re^{0.8}\ Pr^{0.4} \quad (4)$$

was included in Figure 9 along with the present measurements. In addition, the data of Washington and Marks (*35*) and Nusselt (*27*) have been included for comparison. The correlations of Norris and Streid (*26*) did not appear applicable to this comparison and were not employed. In the case of the present experimental data, the Reynolds number was computed in the following way:

$$Re = \frac{2}{\nu^*}\int_0^{y^0} u\,dy = \frac{2y_0u}{\nu^*} = \frac{4r_hu}{\nu^*} \quad (5)$$

The viscosity of air (*28*) was based upon the measurements of Kellström (*19*) corrected for the effect of water as suggested by Hirschfelder (*15*). No attempt was made to reconcile the marked differences between the Nusselt numbers obtained from the present data and those which apply to nonuniform conditions of transfer. The standard deviation of the Nusselt number for the present experimental data shown in Figure 9 from the smooth curve is 1.04.

Table I includes experimental values of the thermal flux, plate temperatures, and plate separation together with the corresponding Reynolds numbers. Smoothed values of the Nusselt number are recorded in a part of Table II. The maximum point velocities presented in this table were obtained from the experimental measurements and afford a somewhat more direct comparison with the experimental data than may be realized from the Reynolds criterion. These data are not directly applicable to nonuniform thermal transfer and the marked differences between the present data and the correlation of McAdams (*21*) are to be expected.

Shear

The pressure gradient within the flow channel used in this work (*6*) was measured for a variety of flow conditions. The experimental results are recorded in Table III. It is convenient to define the friction factor (*2*) in the following way:

$$f = \frac{y_0g}{\sigma U^2}\frac{dP}{dX} = \frac{2T_0g}{\sigma U^2} \quad (6)$$

The data of Table III are presented in Figure 10 in terms of this factor as a function of Reynolds number which was evaluated from Equation 5. The standard deviation of the experimental measurements was 0.00036. The data of Table III and of Figure 10 were corrected for the small variations (*33*) in the separation of the plates (*6*), so that the results might represent more nearly the behavior in uniform flow. These corrections were made on the basis of the change in kinetic energy of the stream as a whole and in no case amounted to more than 0.01 of the pressure gradient recorded in Table III. The variation in temperature across the flow channel did not influence the measured pressure gradient significantly, although it did result in dissymmetry in the velocity distribution (*29*).

The generalization of Nikuradse (*25*) for friction in smooth tubes may be expressed in the following way:

$$\frac{1}{\sqrt{f}} = 4.0 \log (Re\sqrt{f}) - 0.4 \quad (7)$$

The correlation of Drew and Genereaux (*7*) for commercial pipe may be written in similar form.

$$\frac{1}{\sqrt{f}} = 3.2 \log (Re\sqrt{f}) + 1.2 \quad (8)$$

Curves for Equations 7 and 8 have been included in Figure 10 and bracket the present measurements except for Reynolds

Table III. Measurement of Pressure Gradient

Test No.	Nominal Plate Temperature, °F. Upper	Lower	Reynolds No.	Plate Separation[a], Foot	Velocity, Feet/Sec. Av.	Max.	Plate Separation[b], Foot Position 1	Position 2	Pressure Gradient[c], Lb./Sq.Ft./Ft. $\frac{\Delta P}{\Delta x}$	$\frac{dP}{dx}$
69	100	100	55,550	0.0601	85.78	97.87	0.0617	0.0583	1.609	1.572
70	100	100	8,510	0.0601	13.21	15.54	0.0615	0.0585	0.0498	0.0520
74	100	100	19,830	0.0606	30.70	35.32	0.0618	0.0584	0.255	0.258
75	100	70	18,100	0.0603	27.45	31.73	0.0620	0.0586	0.228	0.231
76	100	100	18,070	0.0600	28.10	32.34	0.0617	0.0583	0.235	0.235
78	115	115	17,720	0.0604	28.60	32.99	0.0618	0.0586	0.237	0.242
79	115	85	18,370	0.0606	28.20	32.56	0.0618	0.0587	0.239	0.245
80	130	130	17,080	0.0603	28.90	33.27	0.0617	0.0582	0.241	0.242
81	130	70	18,250	0.0604	28.10	32.31	0.0618	0.0583	0.239	0.241
87	130	70	35,500	0.0602	54.50	62.32	0.0617	0.0587	0.770	0.775
88	130	130	51,790	0.0602	87.40	99.67	0.0616	0.0583	1.703	1.690
89	130	70	55,350	0.0606	85.40	97.27	0.0618	0.0587	1.642	1.646
90	130	130	9,040	0.0601	15.39	18.12	0.0618	0.0584	0.0730	0.0752
91	130	70	9,670	0.0607	14.90	17.60	0.0615	0.0587	0.0719	0.0746
93	115	115	36,730	0.0604	59.00	67.31	0.0613	0.0587	0.778	0.787
94	115	85	38,760	0.0607	58.93	67.24	0.0611	0.0586	0.802	0.809
157	130	70	6,550	0.0608	10.00	12.10	0.0616	0.0590	0.0314	0.0330
158	130	70	18,580	0.0608	28.42	32.82	0.0616	0.0590	0.226	0.234

[a] Plate separation at a position 13 feet downstream from converging section where maximum velocity was determined from pitot tube measurements

[b] Plate separation expressed in feet for positions 1 and 2 which are 1.5 and 8.0 feet downstream from end of converging section.

[c] Pressure gradient corrected for variation in plate separation.

numbers below 7000, where the present data indicate a slightly lower friction factor than would be predicted from Equation 7. The experimental measurements of Nikuradse (*25*) for water flowing in tubes varying between 0.394 and 1.97 inches in diameter have been included in Figure 10 for comparison with the present measurements for air flowing between parallel plates. The agreement is within the uncertainty of measurement of the small pressure gradients experienced in the present work. Reichardt's measurements of the flow of air between parallel plates (*34*) were not well adapted to the evaluation of the friction factor shown in Figure 10.

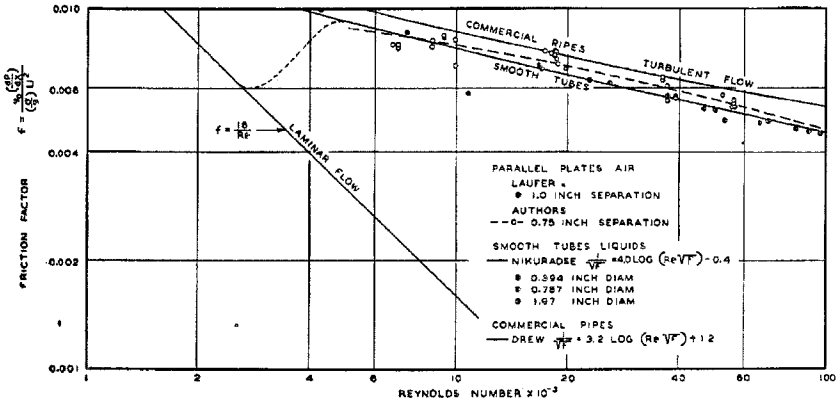

Figure 10. Variation of Friction Factor with Reynolds Number

The friction factor obtained by Laufer (*20*) for the flow of air between parallel plates with 1-inch separation has been depicted in Figure 10. The point shown indicates a lower factor than was obtained in the present measurements or reported by Nikuradse (*25*) for the flow of water in tubes. The data of Laufer which were reported in terms of the maximum velocity were converted to the basis of Figure 10 by the use of generalized velocity distributions. Not more than 2% uncertainty was introduced by this change in basis.

Acknowledgment

The assistance of H. H. Reamer in connection with the construction and operation of the equipment is acknowledged. W. N. Lacey reviewed the manuscript and Evelyn Anderson assisted in its preparation in final form. Betty Kendall, D. B. Wilford, and Kazuhiko Sato contributed to the preparation of the data.

Nomenclature

b = specific gas constant
C_P = isobaric heat capacity, B.t.u. per (pound) (° F.)
d = differential operator
d_0 = diameter of circular conduit, feet
f = Fanning friction factor
g = acceleration of gravity, feet per square second
k = thermal conductivity, B.t.u. per (second) (feet) (° F.)
ln = natural logarithm
log = common logarithm
Nu = Nusselt number
P = pressure, pounds per square foot
Pr = molecular Prandtl number
$\dot{Q}$ = thermal flux, B.t.u. per (square foot) (second)
Re = Reynolds number
r_h = hydraulic radius, feet
S = entropy, B.t.u. per (pound)(° R.)
T = thermodynamic temperature, ° R.
U = gross velocity, feet per second
u = velocity at a point, feet per second
x = distance downstream, feet
y = vertical distance in channel, feet
y_0 = total height of channel, feet
Δ = difference in
∂ = partial differential operator
ν = kinematic viscosity, square feet per second
σ = specific weight, pounds per cubic foot
τ_0 = shear at wall, pounds per square foot
ξ = recovery factor

Superscript

* = average

Subscripts

l = lower plate
s = stagnation
u = upper plate
w = wire

Literature Cited

(1) Am. Inst. Physics, "Temperature, Its Measurement and Control," New York, Reinhold Publishing Corp., 1941.
(2) Bakhmeteff, B. A., "Mechanics of Turbulent Flow," Princeton, N. J., Princeton University Press, 1941.
(3) Batho, C., *J. Inst. Civil Engrs.*, 174, 317–31 (1907–8).
(4) Bridgman, P. W., "The Logic of Modern Physics," pp. 117–18, New York, Macmillan Co., 1938.
(5) Brun, E., and Vernotte, P., *Compt. rend.*, 194, 594–6 (1932).
(6) Corcoran, W. H., Page, F., Jr., Schlinger, W. G., and Sage, B. H., IND. ENG. CHEM., 44, 410–19 (1952).
(7) Drew, J. B., and Genereaux, R. P., *Trans. Am. Inst. Chem. Engrs.*, 32, 15–19 (1936).
(8) Eckert, E., *Z. ver. deut. Ing.*, 84, 813–17 (1940); Natl. Advisory Comm. Aeronaut., *Tech. Mem.* 983 (1941).
(9) Eckert, E., and Weise, W., *Forsch. Gebiet. Ingenieurw.*, 12, 40–50 (1941); Natl. Advisory Comm. Aeronaut., *Tech. Mem.* 1000 (1941).
(10) Emmons, H. W., and Brainerd, J. G., *Trans. Am. Soc. Mech. Engrs.*, 63, A105-10 (1941).
(11) Franz, A., "Jahrbuch 1938 deutscher Luftfahrtforschung," Vol. II, pp. 215–18; Natl. Advisory Comm. Aeronaut., *Tech. Mem.* 953 (1940).
(12) Goldstein, S., "Modern Developments in Fluid Dynamics," Vols. I and II, London, Oxford University Press, 1938.
(13) Goranson, R. W., "Thermodynamic Relations in Multicomponent Systems," p. 9, Carnegie Institution of Washington, 1930.
(14) Hartmann, W., *Forsch. Gebiet. Ingenieurw.*, 10, supplement, *Forschungsheft*, No. 397 (1939).
(15) Hirschfelder, J. O., Bird, R. B., and Spotz, E. L., *Trans. Am. Soc. Mech. Engrs.*, 71, 921–37 (1949).
(16) Hottel, H. C., and Kalitinsky, A., *J. Appl. Mech.*, 12, A25–32 (1945).
(17) Joukowsky, V., *Tech. Phys. U.S.S.R.*, 5, 968–94 (1938).
(18) von Kármán, Th., *Trans. Am. Soc. Mech. Engrs.*, 61, 705–10 (1939).
(19) Kellström, G., *Phil. Mag.*, 23, 7th series, 313–38 (1937).
(20) Laufer, J., Natl. Advisory Comm. Aeronaut., *Tech. Note* 2123 (1950).
(21) McAdams, W. H., "Heat Transmission," New York, McGraw-Hill Book Co., 1942.
(22) McAdams, W. H., Nicolai, L. A., and Kennan, J. H., *Trans. Am. Inst. Chem. Engrs.*, 42, 907–25 (1946).
(23) Meissner, W., *Forsch. Gebiet. Ingenieurw.*, 9, 213–18 (1938).
(24) Meyers, C. H., *Bur. Standards J. Research*, 9, 807 (1932).
(25) Nikuradse, J., *Forsch. Gebiet. Ingenieurw.*, 4, supplement, *Forschungsheft*, No. 361 (1933).
(26) Norris, R. H., and Streid, D. C., *Trans. Am. Soc. Mech. Engrs.*, 62, 525–33 (1940).
(27) Nusselt, W., *Forschungsheft*, 53, 1750–808 (1905).
(28) Page, F., Jr., Corcoran, W. H., Schlinger, W. G., and Sage, B. H., Am. Doc. Inst., *Doc.* 3293 (1951).
(29) Page, F., Jr., Corcoran, W. H., Schlinger, W. G., and Sage, B. H., IND. ENG. CHEM., 44, 419–24 (1952).
(30) Page, F., Jr., Schlinger, W. G., Breaux, D. K., and Sage, B. H., Am. Doc. Inst., *Doc.* 3294 (1952).
(31) Page, F., Jr., Schlinger, W. G., Breaux, D. K., and Sage, B. H., IND. ENG. CHEM., 44, 424–30 (1952).
(32) Polhausen, E., *Z. angew. Math. u. Mech.*, 1, 115–21 (1921).
(33) Reamer, H. H., Cavers, S. D., and Sage, B. H., Am. Doc. Inst., *Doc.* 3713 (1952).
(34) Reichardt, R., *Z. angew. Math. u. Mech.*, 20, (6), 297–328 (1940); Natl. Advisory Comm. Aeronaut., *Tech. Mem.* 1047 (1943).
(35) Washington, L., and Marks, W. M., IND. ENG. CHEM., 29, 337–45 (1937).

RECEIVED for review August 22, 1952. ACCEPTED December 22, 1952. For material supplementary to this article order Document 3713 from the American Documentation Institute, % Library of Congress, Washington 25, D. C., remitting $1.00 for microfilm (images 1 inch high on standard 35-mm. motion picture film) or $2.25 for photocopies (6 × 8 inches) readable without optical aid.

PART III.

TEMPERATURE GRADIENTS IN TURBULENT GAS STREAMS

BEHAVIOR NEAR BOUNDARY IN TWO-DIMENSIONAL FLOW

Temperature Gradients in Turbulent Gas Streams

BEHAVIOR NEAR BOUNDARY IN TWO-DIMENSIONAL FLOW

S. D. CAVERS[1], N. T. HSU, W. G. SCHLINGER, AND B. H. SAGE

California Institute of Technology, Pasadena, Calif.

AN UNDERSTANDING of turbulence is one of the more important problems in the field of engineering science today. Most of the scientific efforts on the problem have been directed to measurements of the transfer of momentum and the associated determinations of velocity as a function of position in a flowing stream. The magnitude and extent of these investigations prevent any systematic review of the subject in this discussion, and for an appraisal of the present understanding of turbulence the reader is referred to standard works in the field of fluid mechanics (*1*).

Comparable investigations have not been made in the field of thermal transfer. In many instances the experimental techniques are simpler and permit a more accurate appraisal of transfer phenomena than can be obtained readily from the studies of the transport of momentum. Prandtl (*14*) and Reynolds (*16*) indicated the basic characteristics of convective thermal transfer when considered directly analogous to the transfer of momentum. The work of Kármán (*9*) outlined the principal relationships associated with the concepts of eddy viscosity and eddy conductivity which afford a useful although empirical evaluation of the effects of turbulence in streams during momentum and thermal transfer.

Boelter and coworkers (*2*) carried forward the analogy of thermal and momentum transfer. These calculations were predicated upon the Reynolds analogy which is equivalent to an equality of the eddy conductivity and eddy viscosity. Experimental measurements (*5, 11, 13*) have indicated that for a Prandtl number near unity the ratio of eddy conductivity to eddy viscosity does not approach unity except possibly at high Reynolds numbers. The relationship of eddy conductivity and eddy viscosity is complex even under conditions of steady uniform flow particularly in the transition region between turbulent and laminar flow. It is difficult to establish experimentally the relationship of these quantities in the transition region since they both approach zero as the boundary of the turbulent region is reached.

It is the purpose of the present discussion to report the results of a series of investigations of the temperature gradients near the wall of a steady uniform air stream flowing between parallel plates. The results were obtained over a period of nearly 3 years and serve to establish the eddy conductivity for the steady uniform flow of air with an accuracy sufficient for many industrial needs. It has been shown that such data not only are of utility in calculations on steady uniform streams but also can be used for predicting the temperature distribution under conditions of nonuniform thermal transfer (*4, 17*).

Eddy Viscosity and Eddy Conductivity Equations Are Established for Transition Region

The total conductivity may be described by the following expression:

$$\epsilon_c = \epsilon_c + \kappa = \frac{\mathring{Q}}{C_p \sigma} \frac{dy}{dt} \tag{1}$$

Correspondingly, the total viscosity may be defined by

$$\epsilon_m = \epsilon_m + \nu = \frac{\tau g}{\sigma} \frac{dy}{du} \tag{2}$$

The terms in Equations 1 and 2 are defined by the following expressions:

$$\kappa = \frac{k}{C_p \sigma} \tag{3}$$

$$\nu = \frac{\eta g}{\sigma} \tag{4}$$

$$\tau = -\left(\frac{y_0}{2} - y\right) \frac{dP}{dx} \tag{5}$$

Equation 5 applies only to situations involving uniform flow. A combination of Equations 1, 2, and 5 yields the following expression for the ratio of the total conductivity to the total viscosity:

$$\underline{\mathrm{Pr}} = \frac{\epsilon_m}{\epsilon_c} = \frac{C_p \tau_0 g l}{\mathring{Q} l_0} \frac{dt}{du} \tag{6}$$

This dimensionless quantity, $\underline{\mathrm{Pr}}$, has been defined as the total Prandtl num-

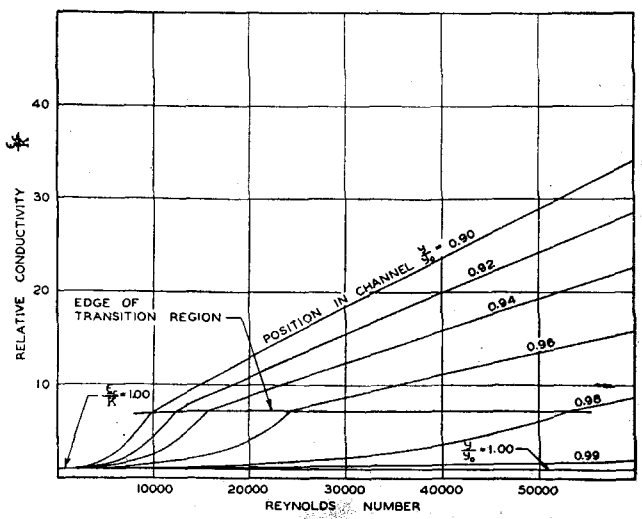

Figure 1. Ratio of Total to Molecular Conductivity on Basis of Reynolds Analogy

[1] Present address, University of Saskatchewan, Saskatoon, Canada.

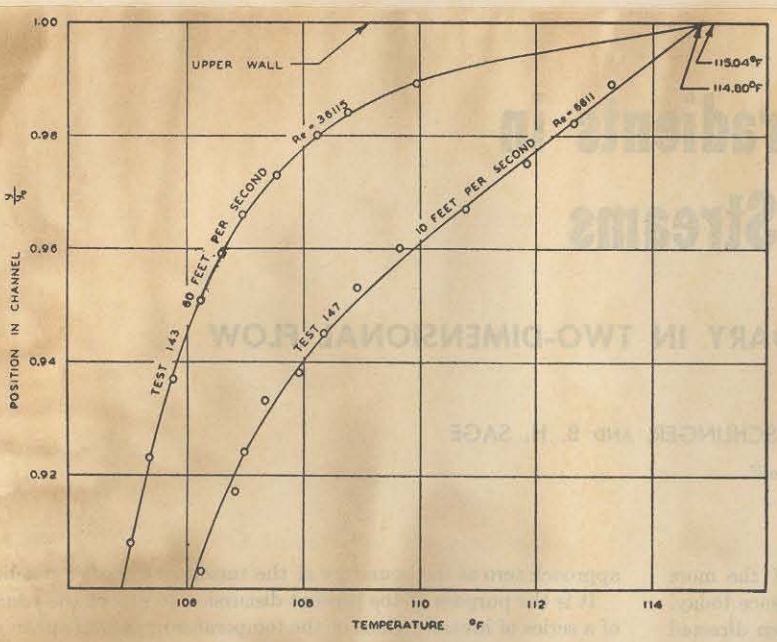

Figure 2. Temperature Distribution near Wall for Tests 143 and 147

ber. Correspondingly, the eddy Prandtl number, Pr_ϵ, may be defined as

$$\mathrm{Pr}_\epsilon = \frac{\epsilon_m}{\epsilon_c} = \underline{\mathrm{Pr}}\left(1 + \frac{\kappa}{\epsilon_c}\right) - \frac{\nu}{\epsilon_c} \qquad (7)$$

In order to predict the thermal transfer in a steadily flowing stream a knowledge of the velocity distribution as well as the variation of eddy conductivity with position is necessary. In the main body of such a stream it has been found as a fair approximation (*1*, *10*) that the flow conditions may be described in terms of two parameters. The distance parameter y^+ is defined by

$$y^+ = \frac{y_d}{\nu}\sqrt{\frac{\tau_0 g}{\sigma}} \qquad (8)$$

The velocity parameter u^+ may be associated with the flow condition in the following way:

$$u^+ = u\sqrt{\frac{\sigma}{\tau_0 g}} \qquad (9)$$

As a rough approximation it has been found that u^+ is a single-valued function of y^+. On the basis of this approximation it may be shown (*5*, *17*) that the ratio of total viscosity to kinematic viscosity in the main body of the stream may be established from

$$\frac{\epsilon_m}{\nu} = \frac{0.4}{\nu}\sqrt{\frac{\tau_0 g}{\sigma}}\left(1 - \frac{l}{l_0}\right) l \qquad (10)$$

Near the wall in the transition region the situation is somewhat more complex but the ratio of total viscosity to kinematic viscosity may be approximated (*5*, *7*, *17*) at a given temperature from

$$\frac{\epsilon_m}{\nu} = \frac{\epsilon_m + \nu}{\nu} = \frac{l}{l_0}\cosh^2\left[0.0695\left(\frac{l_0 - l}{\nu}\right)\sqrt{\frac{\tau_0 g}{\sigma}}\right] \qquad (11)$$

If the Reynolds analogy (*9*, *14*) is followed, Equations 10 and 11 assume the forms

$$\frac{\epsilon_c}{\kappa} = \frac{\epsilon_c + \kappa}{\kappa} = 1 + \left\{\frac{0.4\,l}{\kappa}\sqrt{\frac{\tau_0 g}{\sigma}}\left(1 \frac{l}{l_0}\right)\right\} \cdot \frac{\nu}{\kappa} \qquad (12)$$

$$\frac{\epsilon_c}{\kappa} = \frac{\epsilon_c + \kappa}{\kappa} = 1 + \left\{\frac{l}{l_0}\cosh^2\left[0.0695\left(\frac{l_0 - l}{\nu}\right)\sqrt{\frac{\tau_0 g}{\sigma}}\right]\right\} \cdot \frac{\nu}{\kappa} - \frac{\nu}{\kappa} \qquad (13)$$

The point in the flowing stream where these expressions yield identical values of $\frac{\epsilon_c}{\kappa}$ corresponds to the inner edge of the transition region. Equations 12 and 13 are based on the assumption of equality of the eddy conductivity and eddy viscosity in accordance with the Reynolds analogy. The values of $d\left(\frac{\epsilon_c}{\kappa}\right)/dy^+$ from Equations 12 and 13 are not equal when the values of relative conductivity from the two equations are the same. The edge of the transition region is taken as a value of y^+ of 26.6 (*17*).

Figure 1 shows the ratio of total to molecular conductivity on the basis of the Reynolds analogy utilizing Equations 12 and 13. It has been shown that the relative conductivity is a single-valued function of Reynolds number and position in the channel (*17*). Experimental measurements have been made to determine the extent to which the assumption of the Reynolds analogy is true and to establish with some certainty the actual values of the tem

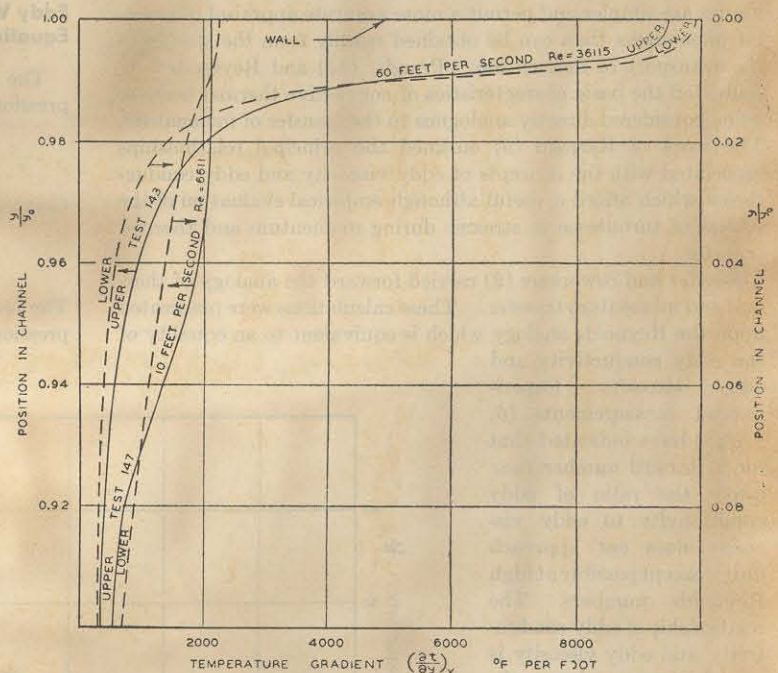

Figure 3. Temperature Gradients Near Wall for Tests 143 and 147

perature distribution and the eddy conductivity near the edge of a uniform turbulently flowing air stream. The data of Figure 1 disregard any influence of temperature distribution upon the eddy properties or the thermometric conductivity.

Temperature Gradient Was Imposed on Air Stream for Temperature Distribution Measurements

The equipment employed in these investigations has been

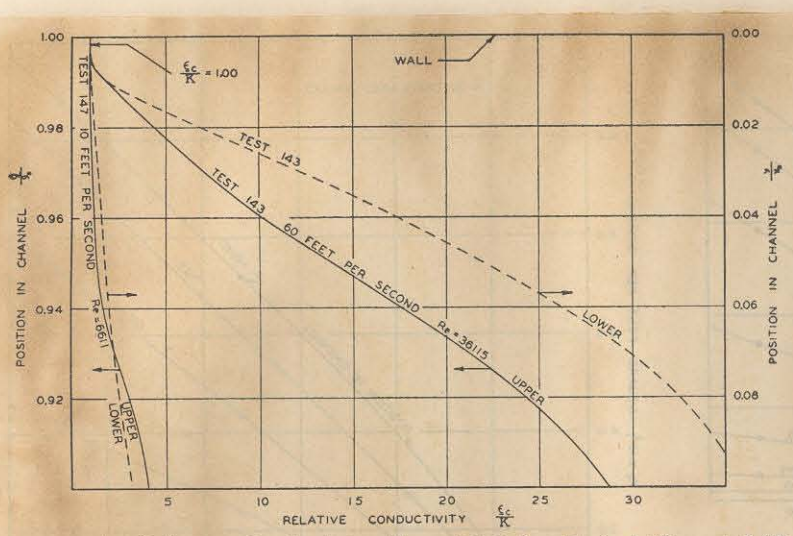

Figure 4. Relative Conductivity Near Wall for Tests 143 and 147

described in detail (*5*). It consisted of two parallel copper plates between which air was permitted to flow under steady uniform conditions. The temperatures of the two plates were maintained at constant but different values, thus imposing a temperature gradient upon the air stream. The thermal flux and temperature distribution in the stream were measured by methods which have been discussed (*5, 18*). The temperatures were known with a standard error of not more than 0.05° F. and the thermal flux was established with a standard error of 0.5%. The determinations of the errors were based upon a careful evaluation of the precision and accuracy of the numerous basic measurements used in obtaining these eddy quantities (*5, 15, 18*).

Earlier studies of the velocity distribution (*13*) indicated that there was a systematic trend in the relationship of the velocity parameter u^+ (*1, 14*) to the distance parameter y^+ with Reynolds number. Graphical correlations of velocity distribution (*13*) and shear (*18*) based upon experiment were used throughout this discussion in establishing the eddy viscosity in the stream. Likewise, the thermal flux was based upon a correlation (*18*) of individual measurements with the flow conditions. Values obtained from this correlation were utilized rather than the directly measured quantities because of the increased accuracy with which the thermal flux could be established from the statistical correlations employed (*18*) in relating it to the conditions of flow.

At the wall the temperature gradient was established from the following expression:

$$\left[\frac{dt}{dy}\right]_{y=0, y_0} = \frac{\mathring{Q}}{\kappa C_p \sigma} \qquad (14)$$

The properties of air required in the solution of Equation 14 were obtained from a recent critical review (*10*). Corrections were made for the effect of humidity upon the thermal conductivity, heat capacity, and specific weight in accordance with the assumption of ideal solutions and statistical mechanical estimates as to the effect of water upon the thermal conductivity of air (*7*).

Since the wall temperatures were known and the temperature of the air stream was measured to within 0.004 inch of the wall, the following equation could be applied effectively where A was some point in the stream near the wall in question:

$$t_w = \int_{y=A}^{y=0, y_0} \left(\frac{dt}{dy}\right) dy + (t)_{y=A} \qquad (15)$$

It was found advantageous to apply Equation 15 to the flowing stream at values of y/y_0 from 0.1 to the lower wall and from 0.9 to the upper wall by graphical iterative techniques. No difficulty was experienced in obtaining agreement between the experimental data and Equation 15 within 0.01° F. which was much less than the standard error of temperature measurements. Near the wall the error in establishing the position of the wire exceeded the uncertainty in measuring the air temperature.

Temperature Gradients and Eddy Conductivities Were Obtained from Experimental Data

The experimental measurements, which were made with particular emphasis upon the flow conditions near the wall, are recorded in Table I. Figure 2 illustrates the temperature distributions obtained for tests 143 and 147. These data include only values of y/y_0 greater than 0.9 and represent the behavior near the upper wall. The smoothed curves shown in this figure were based upon the iterative application of Equation 15. The corresponding values of temperature gradients are shown in Figure 3. In this instance the behavior near both the upper and lower walls was included so that the differences could be shown. The temperature gradients near the upper wall were determined in greater detail than those near the lower boundary of the flowing stream. However, the differences between the upper and lower walls are several times the experimental uncertainty and may be due to the vorticity (*19, 20*) in the stream amplifying the effect of dif-

Table I. Experimental Conditions

Quantity	Test Numbers									
	60[a]	61[a]	140	141	143	144	145	146	147	148
Distance between plates, foot	0.05725	0.05708	0.05758	0.05825	0.05825	0.05750	0.05750	0.05815	0.05833	0.05833
Traverse location[b], feet	12.5	12.5	8.1	12.5	12.5	8.1	8.1	12.5	12.5	8.1
Incoming air temp., ° F.	100.0	100.0	100.0	100.0	100.0	100.0	100.0	100.0	100.0	100.0
Upper plate temp., ° F.	114.98	85.29	114.96	115.04	115.04	114.95	115.04	115.07	114.88	114.87
Lower plate temp., ° F.	85.31	114.49	85.03	84.82	84.85	85.03	85.15	85.53	85.04	85.10
Gross velocity, ft./sec.	13.1	12.6	30.0	30.0	57.6	60.2	91.3	86.8	10.4	9.8
Maximum velocity, ft./sec.	15.2	14.9	34.9	34.8	66.8	68.6	104.0	98.8	12.6	11.8
Reynolds No.	8122	7754	18578	18821	36115	37528	56689	54680	6611	6069
Pressure gradient[c], lb./cu. ft.	−0.0515	−0.0488	−0.2517	−0.2453	−0.7759	−0.8215	−1.685	−1.514	−0.0331	−0.0293
Thermal flux, B.t.u./(sq. ft.) (sec.)	0.0113	0.0107	0.0242	0.0243	0.0411	0.0421	0.0558	0.0537	0.00934	0.00901
Wt. fraction water	0.0115	0.0145	0.0110	0.0129	0.0095	0.0109	0.0110	0.0089	0.0087	0.0096
Pressure at traverse location, lb./sq. inch	14.374	14.308	14.260	14.285	14.286	14.389	14.332	14.378	14.319	14.337

[a] Tests 60 and 61 were made to investigate in a preliminary fashion the effect of inverting the temperature gradient.
[b] Traverse location measured from end of converging section.
[c] Pressure gradient is average of change in static pressure over 4-foot length of working section approximately 10 feet downstream from the end of the converging section. It is measured with the traversing mechanism downstream from the static taps. No significant change with time was observed. The values recorded were correlated with data obtained at other flow conditions.

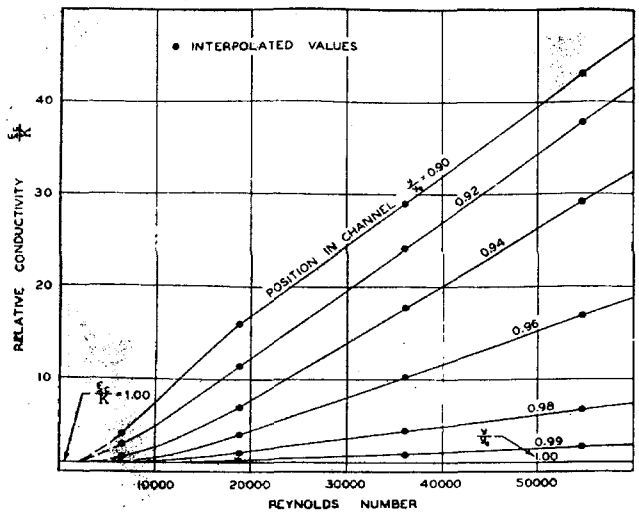

Figure 5. Effect of Reynolds Number upon Relative Conductivity

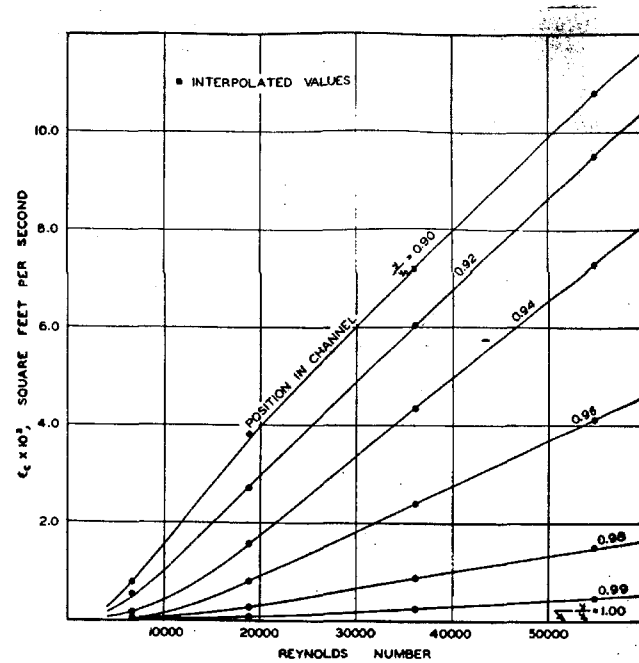

Figure 6. Eddy Conductivity Near the Boundary of a Turbulent Air Stream

ferences in molecular properties which result from variations in temperature between the walls.

Experimental measurements associated with the flow conditions in Table I are available (*8*) along with the corresponding smoothed values of temperature gradients and temperatures obtained from the iterative solution of Equation 15. A sample of the latter tabulation constitutes Table II which also includes eddy properties derived from each traverse. The data of Table II were not smoothed with respect to the conditions of flow and represent the results obtained for a single rate of flow and temperature difference. The information available in Table II is similar to that obtained in earlier studies (*10, 12*) which were focused upon the conditions of flow near the center of the channel. Relative conductivities, $\frac{\epsilon_e}{\kappa}$, near the upper and lower walls for test 143 at a gross velocity of 60 feet per second and for test 147 at a gross velocity of 10 feet per second are depicted in Figure 4. Differences in the relative conductivity between the upper and lower walls are evident for both velocities. Near the lower wall there is a more rapid increase in the relative conductivity with position than near the upper wall.

The influence of Reynolds number upon the relative conductivity is shown in Figure 5. In this instance only the behavior near the upper wall was included. Except at Reynolds numbers below 17,000 there is nearly a linear variation in the relative conductivity with this variable. The calculated relative conductivities were interpolated to even values of y/y_0 as indicated in the figure. Similar behavior was found near the lower wall. If it is assumed that Equations 10 and 11 described the eddy viscosity satisfactorily in the region near the wall, a comparison of Figures 1 and 5 indicates a large deviation from the Reynolds analogy.

As a result of the influence of temperature upon the molecular properties it appears desirable to present the results in terms of eddy conductivity. This quantity was smoothed with respect to conditions of flow described in Table I and these values are recorded in Table III. Some difference exists between the present data and the earlier results (*11, 13*). Because of the refinements employed in the present investigation and the emphasis placed upon the behavior near the wall, the data of Table III are to be preferred. The standard deviation of the data of this table from experimental measurements (*8*) was less than 0.03 square feet per second.

Figure 6 illustrates the effect of Reynolds number upon the eddy conductivity and the influence is similar to that shown in Figure 5 for the relative conductivity. There is substantially a linear change in the eddy conductivity with Reynolds number at values of this variable greater than 17,000. Figure 7 depicts the effect of position in the channel upon the eddy conductivity and these data represent smoothed values based upon all the experimental conditions described in Table I. The detailed effect of position upon the eddy conductivity for values of y/y_0 greater than 0.99 or less than 0.01 is uncertain.

Figures 4 through 7 serve to illustrate the effect of position and Reynolds number upon the relative and eddy conductivities. The greater part of the resistance to thermal transfer from a boundary to a turbulently flowing stream is usually encountered within the part of the stream described in these figures.

Total Prandtl Number. The relation of the eddy conductivity to the eddy viscosity has been considered by many investigators. As indicated earlier, Kármán (*9*) clarified the earlier discussion and Boelter and coworkers (*2*) carried the analysis of thermal transfer on the basis of the Reynolds analogy to its logi-

Table II. Sample of Experimental Temperature Measurements

(Test 141—velocity 30 feet/sec.)

y/y_0	Temp., ° F.	y/y_0	Temp., ° F.
0.987	111.92	0.482	99.26
0.987	111.54	0.439	98.38
0.983	110.52	0.396	97.69
0.983	110.99	0.353	97.14
0.976	119.59		
0.968	108.54	0.310	96.46
0.961	107.94	0.268	95.91
0.954	107.36	0.225	95.36
0.947	106.96	0.182	94.86
0.940	106.54	0.139	94.29
		0.117	93.99
0.933	106.25	0.0958	93.63
0.924	106.03	0.0815	93.25
0.918	105.82	0.0672	92.93
0.904	105.28	0.0529	92.60
0.890	105.17		
0.876	104.90	0.0458	92.47
0.847	104.12	0.0386	91.82
0.804	103.66	0.0315	91.49
0.761	103.05	0.0315	91.68
0.718	102.61	0.0243	91.11
		0.0243	91.35
0.675	101.99	0.0172	89.81
0.632	101.36	0.0172	90.24
0.589	100.77	0.0172	90.78
0.546	100.11	0.0100	89.18
0.504	99.29	0.0100	89.01
0.482	99.05		

Table III. Eddy Conductivities near Upper Wall

y/y_0	Reynolds No. × 10^{-3} 5.0	7.5	10.0	12.5	15.0	17.5	20.0	25.0	30.0	35.0	40.0	45.0	50.0	55.0	60.0
	Eddy Conductivities, Square Feet/Second × 10^3														
0.90	0.41	0.98	1.55	2.15	2.78	3.37	3.95	5.01	5.99	6.96	7.96	8.92	9.90	10.80	11.70
0.92	0.26	0.58	1.01	1.50	2.00	2.45	2.94	3.91	4.86	5.82	6.75	7.69	8.62	9.56	10.48
0.94	0.09	0.22	0.42	0.67	0.98	1.33	1.72	2.54	3.34	4.15	4.95	5.75	6.54	7.33	8.15
0.96	0.01	0.06	0.16	0.30	0.48	0.68	0.90	1.35	1.81	2.28	2.74	3.21	3.68	4.15	4.62
0.98	0.00	0.02	0.06	0.12	0.17	0.24	0.31	0.48	0.68	0.86	1.02	1.18	1.34	1.50	1.66
0.99	0.00	0.01	0.02	0.03	0.04	0.08	0.10	0.14	0.18	0.24	0.28	0.34	0.39	0.46	0.55
1.00	0.00	0.00	0.00	0.00	0.00	0.00	0.00	0.00	0.00	0.00	0.00	0.00	0.00	0.00	0.00

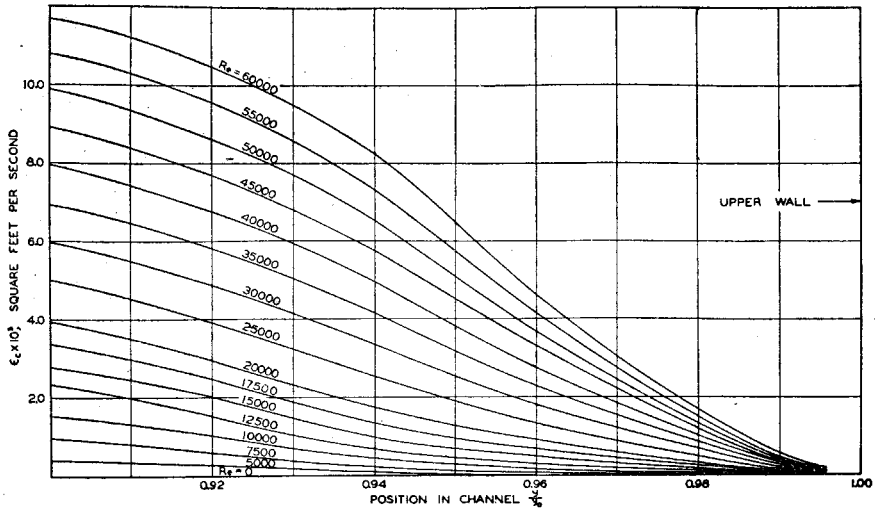

Figure 7. Effect of Position in Channel upon Eddy Conductivity Near Upper Wall

cal conclusion. The assumption of equality of the eddy properties is not justified by experiment (*11, 13*). Figure 8 shows the total conductivity and total viscosity as a function of position in the flow channel. The total viscosities were obtained from experimental measurements made in the present channel at an earlier date (*11, 13*) with somewhat different plate separation and calculated from a correlation (*4, 17*) of velocity distribution given by Equation 11 which was based upon a suggestion of Rannie as described by Dunn (*6*). It is apparent that the detailed knowledge of the total viscosity is not sufficient to determine with certainty the variation in the total Prandtl number defined by Equation 6. However, it appears that the total Prandtl number approaches the molecular Prandtl number, Pr_m, in a simple fashion (*11, 13*) as the wall is reached. The change in the molecular Prandtl number with position was small in comparison with the effects of flow conditions upon the total Prandtl number in the present investigation.

Eddy Conductivity Correlated with Momentum Transfer and Location in Stream Allow Prediction of Thermal Transfer

The variation in the relative conductivity in the transition and turbulent regions near the wall was set forth on the basis of the Reynolds analogy in Equations 12 and 13. If it is assumed that the molecular Prandtl number is unity, these expressions may be rewritten,

$$\frac{\epsilon_c l_0}{\kappa l} = \cosh^2 By^+ \qquad (16)$$

$$\frac{\epsilon_c l_0}{\kappa l} = C + Dy^+ \qquad (17)$$

In order for Equations 16 and 17 to yield a continuous variation in the relative conductivity from the wall through the transition region it is necessary at a given value of the distance parameter $^+$ that the relative conductivity be equal from Equations 16 and 17. Figure 9 shows the experimental values of the relative conductivity as a function of the distance parameter for the upper and lower walls. By means of least squares techniques (*3*) Equation 17 has been fitted to the experimental data shown in Figure 9. The coefficient in Equation 16 was determined from the required point of intersection.

The coefficients of these expressions yield different values for the rate of change of the relative conductivity with the distance parameter at values of the latter quantity of 26.7. In Equation 18 the behavior for values of y^+ less than 26.7 is given for the upper wall.

$$\frac{\epsilon_c l_0}{\kappa l} = \cosh^2 (0.0597\ y^+) \qquad (18)$$

Equation 19 gives similar information for values of y^+ greater than 26.7.

$$\frac{\epsilon_c l_0}{\kappa l} = 0.392\ y^+ - 3.88 \qquad (19)$$

The foregoing expressions yield a standard deviation from the smoothed experimental data shown in Figure 9 of 0.527.

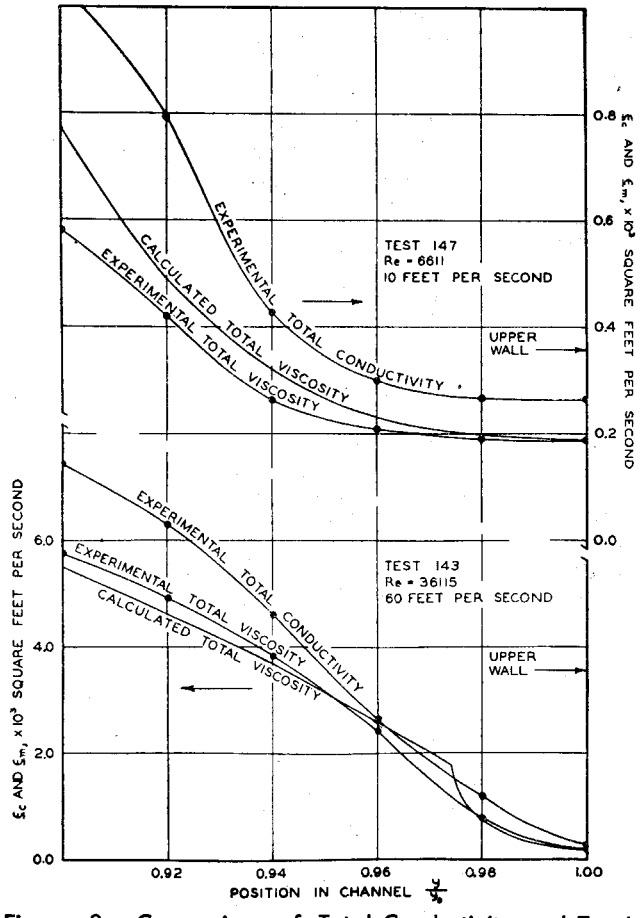

Figure 8. Comparison of Total Conductivity and Total Viscosity

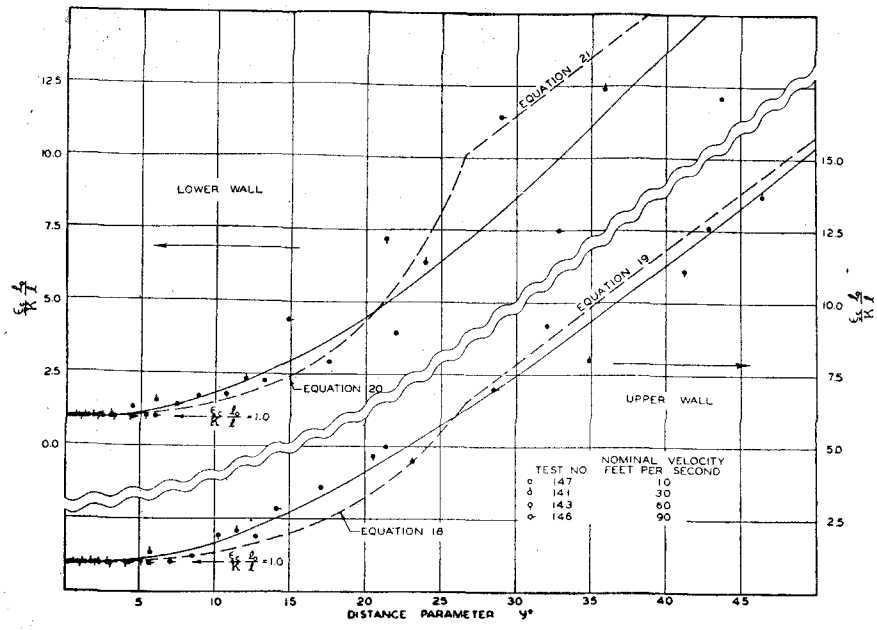

Figure 9. Effect of Distance Parameter upon Relative Conductivity

Similar information is presented in Equations 20 and 21 for the behavior near the lower wall. Equation 20 applies at values of y^+ less than 26.7 and Equation 21 for greater values.

$$\frac{\epsilon_c l_0}{\kappa l} = \cosh^2 (0.0683\ y^+) \qquad (20)$$

$$\frac{\epsilon_c l_0}{\kappa l} = 0.406\ y^+ - 0.722 \qquad (21)$$

In this instance an over-all standard deviation from experiment of 1.318 was obtained. In determining the constants only experimental measurements for values of y^+ less than 200 were employed. The difference in behavior at the upper and lower walls is evident from a comparison of Equations 18 with 20 and 19 with 21. The latter equations are shown as dotted curves in Figure 9. The magnitude of these differences is several times the standard error of measurement.

Smooth full curves were drawn through the data of Figure 9 based upon experimental behavior at values of y^+ as large as 500. The standard deviation of the smooth curve from the data near the upper wall was 0.327 and for the data near the lower wall was 1.165. These measures of agreement indicated that it would be possible to fit the experimental data more closely with a single-valued nonlinear functional relation than by Equations 18 through 21. Table IV records values of the ordinate of Figure 9 as a function of y^+ for the upper and lower walls.

Figure 10 shows the averages of the values of the relative conductivity for the upper and lower walls. The data include the present measurements together with similar information from earlier studies (*12*, *13*). A smooth curve was drawn through these averaged experimental data which yielded a standard deviation of 0.608 from the points shown. Smoothed values of the averages from Figure 10 have been included in Table IV.

Until further information is available concerning the asymmetric behavior encountered in this experimental program, it is recommended that the average values recorded in Table IV be employed except for flow between horizontal parallel plates where the present experimental data are directly applicable. It is surprising that such a simple correlation yielded a single-valued relationship of the relative conductivity to the distance parameter with a fair approximation.

Acknowledgment

H. H. Reamer contributed material to the experimental program. Betty Kendall aided greatly in the preparation of the data in a form suitable for publication. W. H. Corcoran reviewed the manuscript.

Nomenclature

A, B, C, D = constants
cosh = hyperbolic cosine
C_p = isobaric heat capacity, B.t.u./(pound)(°F.)
d = differential operator
g = acceleration of gravity, feet/square second
k = thermal conductivity, B.t.u./(second)(feet)(°F.)
l = distance from center line, feet
l_0 = distance from center line to wall, feet
P = pressure, pounds/square foot
$\mathring{Q}$ = thermal flux, B.t.u./(square foot)(second)
t = temperature, °F.
u = point velocity, feet/second
x = downstream distance, feet
y = distance from lower wall, feet
y_d = distance from nearer wall, feet
y_0 = separation between plates, feet
ϵ_c = eddy conductivity, square feet/second
ϵ_c = total conductivity, $\epsilon_c + \kappa$, square feet/second
ϵ_m = eddy viscosity, square feet/second
ϵ_m = total viscosity, $\epsilon_m + \nu$, square feet/second

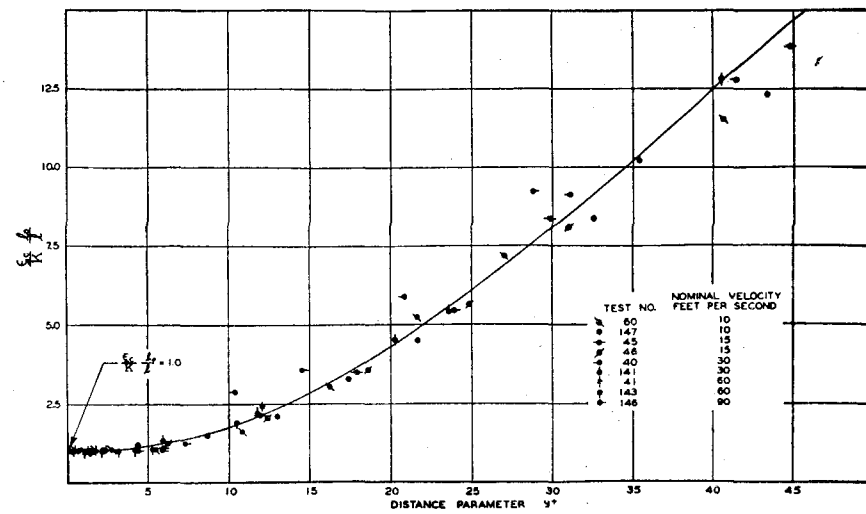

Figure 10. Effect of Distance Parameter upon Average Relative Conductivity

Table IV. Smoothed Values of Relative Conductivity

y^+	$\frac{\epsilon d\theta}{\kappa dl}$ Lower wall[a]	Upper wall[a]	Average[b]
0.00	1.00	1.00	1.00
2.00	1.00	1.00	1.00
4.00	1.09	1.11	1.10
6.00	1.26	1.20	1.24
8.00	1.52	1.39	1.46
10.00	1.86	1.67	1.77
12.00	2.26	2.04	2.15
14.00	2.73	2.48	2.59
16.00	3.25	2.97	3.11
18.00	3.83	3.54	3.68
20.00	4.48	4.13	4.32
22.00	5.20	4.76	4.98
24.00	6.00	5.40	5.73
26.00	6.85	6.07	6.48
28.00	7.72	6.75	7.25
30.00	8.65	7.46	8.05
32.00	9.59	8.19	8.90
34.00	10.58	8.95	9.77
36.00	11.60	9.70	10.66
38.00	12.62	10.50	11.56
40.00	13.64	11.27	12.46
42.00	14.66	12.04	13.36
44.00	15.66	12.85	14.26
46.00	16.70	13.66	15.10
48.00	17.75	14.53	15.95
50.00	18.70	15.38	16.77
Standard deviations	1.165	0.327	0.566[a] 0.608[b]

[a] Based upon present measurements.
[b] Based upon present and earlier data.

η = absolute viscosity, pound second/square foot
κ = thermometric conductivity, square feet/second
ν = kinematic viscosity, square feet/second
σ = specific weight, pounds/cubic foot
τ = shear, pounds/square foot
τ_0 = shear at wall, pounds/square foot

Dimensionless parameters

Pr_m = molecular Prandtl number ν/κ
$\underline{Pr}$ = total Prandtl number $\epsilon_m/\underline{\epsilon_e}$
Pr_e = eddy Prandtl number ϵ_m/ϵ_e
Re = Reynolds number $2y_0\nu/\nu$
u^+ = velocity parameter (Equation 9)
y^+ = distance parameter (Equation 8)

Subscript

w = wall

Literature Cited

(1) Bakhmeteff, B. A., "The Mechanics of Turbulent Flow," Princeton, N. J., Princeton University Press, 1941.
(2) Boelter, L. M. K., Martinelli, R. C., and Jonassen, F., *Trans. Am. Soc. Mech. Engrs.*, **63**, 447–55 (1941).
(3) Brough, H. W., Schlinger, W. G., and Sage, B. H., IND. ENG. CHEM., **43**, 2442–6 (1951).
(4) Connell, W. R., Schlinger, W. G., and Sage, B. H., Washington, D. C., Am. Doc. Inst., *Doc.* **3657** (1952).
(5) Corcoran, W. H., Page, F., Jr., Schlinger, W. G., and Sage, B. H., IND. ENG. CHEM., **44**, 410–19 (1952).
(6) Dunn, L. G., Powell, W. G., and Seifert, H. S., "Heat-Transfer Studies Relating to Rocket Power-Plant Development," Third Anglo-American Aeronautical Conference 1951, Published by The Royal Aeronautical Society.
(7) Hirschfelder, J. O., Bird, R. B., and Spotz, E. L., *Trans. Am. Soc. Mech. Engrs.*, **71**, 921–37 (1949).
(8) Hsu, N. T., Kendall, B. H., Schlinger, W. G., and Sage, B. H., Washington, D. C., Am. Doc. Inst., *Doc.* **3906** (1952).
(9) Kármán, Th. von, *Trans. Am. Soc. Mech. Engrs.*, **61**, 705–10 (1939).
(10) Page, F., Jr., Corcoran, W. H., Schlinger, W. G., and Sage, B. H., Washington, D. C., Am. Doc. Inst., *Doc.* **3293** (1950).
(11) Page, F., Jr., Corcoran, W. H., Schlinger, W. G., and Sage, B. H., IND. ENG. CHEM., **44**, 419–24 (1952).
(12) Page, F., Jr., Schlinger, W. G., Breaux, D. K., and Sage, B. H., Washington, D. C., Am. Doc. Inst., *Doc.* **3294** (1951).
(13) Page, F., Jr., Schlinger, W. G., Breaux, D. K., and Sage, B. H., IND. ENG. CHEM., **44**, 424–30 (1952).
(14) Prandtl, L., *Phys. Z.*, **29**, 487–9 (1928).
(15) Reamer, H. H., Wilford, D. B., and Sage, B. H., Washington, D. C., Am. Doc. Inst., *Doc.* 3713 (1952).
(16) Reynolds, O., *Proc. Manchester Lit. and Philos. Society*, **14**, 7 (1874); "Papers on Mechanical and Physical Subjects," Vol. I, pp. 81–5, Cambridge (1890).
(17) Schlinger, W. G., Berry, V. J., Mason, J. L., and Sage, B. H., IND. ENG. CHEM., **45**, 662–6 (1953).
(18) Schlinger, W. G., Hsu, N. T., Cavers, S. D., and Sage, B. H., *Ibid.*, **45**, 864–70 (1953).
(19) Taylor, G. I., *Phil. Trans.*, **A223**, 289–343 (1923).
(20) Taylor, G. I., *Proc. Roy. Soc. (London)*, **A135**, 85–700 (1932).

RECEIVED for review February 6, 1953. ACCEPTED July 24, 1953. Material supplementary to this article has been deposited as Document 3906 with the ADI Auxiliary Publications Project, Photoduplication Service, Library of Congress, Washington 25, D. C. Copies may be secured by citing the document numbers and by remitting $2.50 each for photoprints or $1.75 each for 35-mm. microfilm. Advance payment is required. Make checks or money orders payable to Chief, Photoduplication Service, Library of Congress.

The region near the boundary of a turbulently flowing fluid accounts for the greater part of the resistance to thermal transfer to or from the stream. An understanding of the influence of conditions of flow upon the temperature distribution near the boundary of turbulently flowing streams is required in order to permit the recent advances in fluid mechanics to be applied to the prediction of thermal transfer in steady flow.

The detailed temperature distribution near the boundary of a turbulent air stream flowing between parallel plates was measured at gross velocities from 10 to 90 feet per second and for average temperature gradients as high as 1000° F. per foot. The corresponding value of thermal flux was determined directly, and from these primary measurements the temperature gradient and eddy conductivity were established as a function of flow conditions.

The eddy conductivity was correlated with the position in the stream and the gross conditions of flow. The measurements permit estimation of the thermal transfer to a turbulently flowing air stream in conduits of large radius to be made with accuracy adequate for some engineering purposes for a variety of uniform and nonuniform conditions of thermal transfer.

PROPOSITIONS

1. In the evaporation of non-spherical drops, the shape effect can be correlated in terms of the relative contribution of the leading and trailing surfaces of the drops.

2. When there is a temperature difference between a sphere and an air stream flowing over its surface, the radial temperature distribution within the laminar thermal boundary layer is analytically similar and is expressed by a modified form of the Blasius function which is the theoretical velocity distribution for laminar boundary layer flow over a flat plate.

3. In the use of a 'hot-wire' for the measurement of the velocity distribution in a two-dimensional channel, a refinement in the calibration would be to include the effect of local fluctuations on the convective thermal transfer from the wire as the magnitude of the fluctuations varies with the position in the channel.

4. When fused tricalcium phosphate fertilizer is produced by the defluorination of rock phosphate, the liberated fluorine is wasted through the stack as hydrogen fluoride. (Hignett and Hubbuch, Ind. and Eng. Chem., 38, 1208, 1946). It is proposed that hydrogen fluoride be recovered as sodium fluoride which is useful as insecticide and preservative of wood-pulp.

5. Systematic investigations of the relation between crystal size and the rate of cooling of a silicate melt will contribute valuable information toward the solution of many geological problems. So

far, the only experimental study of this nature was carried out by Winkler (Mineral. Mag., 28, 557, 1949) for the crystallization of nepheline from a synthetic silicate melt.

6. Recent study (Clayton, Ph. D. Thesis, C.I.T., 1955) shows that information on oxygen isotope abundances in mineral pairs can be used to establish the temperature of crystallization. This isotopic method should provide an excellent check on the accuracy of the simple 'decrepitation method' for the determination of crystallization temperature of minerals with liquid inclusions.

7. It is proposed that test models, made by molding glass around a metal network of known geometric arrangement and then dissolving the metal, be used in porous media studies.

8. By placing a 'hot-wire' type element at an appropriate distance from a boiling surface and observing the frequency of the fluctuations picked up by the sensing element, one can distinquish between nucleate and film type boiling without visual observation.

9. For flow over the surface of a cylinder the velocity distribution is given by (i) the potential solution for the region away from the surface and (ii) the boundary-layer solution in the region close to the surface. A discontinuity in the velocity distribution results in the attempt to combine the two solutions by superimposition or direct attachment. There is need for experimental data to establish the manner in which the two solutions should be combined to describe the complete velocity field.

10. In a country like Burma where rice, timber and petroleum are the leading products, effort should be devoted to develope better uses for rice husk and saw dust which are currently burned as fuel.